

**The Utility of B-mode Ultrasound for the Diagnosis of
Motor Neurone Disease:**

Automated Detection and Analysis of Muscle Twitches in
Ultrasound Images of Motor Neurone Disease Affected
Participants and Healthy Controls

Kate Bibbings

PhD 2017

**The Utility of B-mode Ultrasound for the Diagnosis of
Motor Neurone Disease:**

Automated Detection and Analysis of Muscle Twitches in
Ultrasound Images of Motor Neurone Disease Affected
Participants and Healthy Controls

Kate Bibbings

A thesis submitted in partial fulfilment of the requirements of
the Manchester Metropolitan University for the degree of
Doctor of Philosophy

School of Healthcare Science
the Manchester Metropolitan University
in Collaboration with Royal Preston Hospital

2017

Abstract

Motor Neurone Disease (MND) is a progressive, neurodegenerative disease, for which there is no known cure. Electromyography (EMG) is the standard technique for the detection of diagnostic indicators, such as fasciculations (twitches). Ultrasound (US) imaging may provide a more sensitive alternative to EMG for detection of fasciculations. However, only one computational technique has previously been applied to image sequences to provide an objective measure of fasciculation occurrence. The work presented here therefore describes the development and evaluation of a new computational approach, based on foreground detection using a mixture of Gaussians (GMM). In addition, the only other computational analysis approach available, which is based on feature tracking and mutual information analysis (KLT/MI) was further evaluated.

Two data sets were used to evaluate the computational approaches. The first data set had previously been collected and comprised US images from medial gastrocnemius (MG) and biceps brachii (BB) from healthy ($n = 20$) and MND affected ($n = 5$) participants. The second data set comprised simultaneously recorded US images and intramuscular EMG from five muscles (medial gastrocnemius (MG), biceps brachii (BB), rectus femoris (RF), trapezius (TRAP), rectus abdominis (RA) and thoracic paraspinal (TP)) of healthy ($n = 20$) and MND affected ($n = 20$) participants. Accuracy of the approaches for fasciculation detection was evaluated against two measures of ground-truth: i) manual identification; ii)

intramuscular EMG. Accuracy was defined as the area under the receiver operator curve and comparisons made between the performance of GMM and KLT/MI.

Initial analysis was completed on the large limb muscles, MG and BB. The GMM had better accuracy than the KLT/MI when compared against operator identifications as the ground truth signal (88 – 94 % vs. 82 – 90 %). When EMG was used as the ground truth the GMM again had higher accuracy (81 – 88 % vs. 70 – 79 %). This thesis has shown a GMM computational analysis can detect fasciculations across a wide range of muscles and also can be used for the characterisation of fasciculations as they appear in ultrasound images, with significant differences being found between the healthy and MND affected participant groups. It has provided a foundation from which to build, with suggestions for future work being collecting images of stimulated twitches in a wide range of muscles for further characterisation and also a larger scale study prior to an official diagnosis being made to determine sensitivity and specificity values for this method as a diagnostic test.

Acknowledgements

First and foremost I would like to thank the patients and care staff at Preston Royal Hospital (with special mention to Dr Nick Combes, Pauline Callagher and Wendy Bennett). Without them this piece of research could not have been conducted. I would also like to extend my gratitude to the Motor Neurone Disease Association who have provided the funding for this project and the local Manchester and Cheshire branches who have provided valuable insight as well as their time as participants or an audience for our research. I would also like to thank the supervisory team from Manchester Metropolitan University; Dr Emma Hodson-Tole, Dr Peter Harding and Professor Ian Loram, as well as my fellow PhD students; Maria, Elisabetta, Diego, Amy and Suzi and other research staff; Greg, Ryan, Steve, Stu and Alex.

I would like to offer special thanks to the friends and members of my family who have supported me throughout my PhD and the rest of my academic career, especially to Mam, Dad, Nannas and Grandads who were also participants for the healthy data set, and to Ruth, Daniel, Rachel, Jade and Stuart.

Glossary

Aponeurosis White fibrous tissue, which resembles a flattened tendon which holds muscles together.

Atrophy The decrease in muscle mass.

Attenuation The reduction in amplitude of the ultrasound wave as it passes through different medium.

Biceps Brachii The superficial muscle in the upper arm.

Electromyography: A method for the detection of electrical activity within skeletal muscle tissue. This technique can be conducted from the surface of the skin or from within the muscle using a needle or fine wire electrodes.

Fasciculation A relatively large scale, involuntary muscle twitch.

Fibrillation A small scale, involuntary muscle twitch caused by the loss of a muscle fibres connection with it innervating axon.

Lower Motor Neuron Motor Neurons control voluntary movement, acting as an intermediary between the brain and the skeletal muscles.

Medical Gastrocnemius The medial head of the superficial muscle in the lower leg.

Motor Neurone Disease A progressive, neurodegenerative disease which involves degeneration of both the upper and lower motor neurons.

Motor Unit A group of muscle fibres which are innervated by the same motor neuron.

Myocytes A muscle fibre

Positive Sharps Wave A roundish fruit

Rectus Abdominis The strap shaped muscles located at the front of the abdomen.

Rectus Femoris A superficial muscle in the upper leg that forms part of the quadriceps.

Thoracic Paraspinals The thoracic region of a number of muscles that run the length of the spine.

Trapezius A large muscle located superficially, around the back and shoulder.

Ultrasound: Soundwaves with frequencies above 20 000 hertz. Properties of these waves can be used to produce images which can be used for medical purposes such as the visualisation of internal organs.

Upper Motor Neuron Motor neurons that originate in the brain and connect and carry motor information to the lower motor neurons.

Contents

1	Introduction	13
1.0.1	Research Aims	16
1.0.2	Overview of Thesis	17
1.0.3	Contributions to Knowledge	19
2	Review of Literature I: Muscle Physiology, Motor Neurone Disease and Imaging Techniques	20
2.1	Motor Neurone Disease: Symptoms and Diagnosis	20
2.1.1	Clinical Diagnostic Criteria for Motor Neurone Disease	20
2.1.2	Fasciculations, Fibrillations and positive sharp waves	24
2.2	Integration of Skeletal Muscle with the Nervous System	29
2.2.1	Action Potential Generation	30
2.2.2	Skeletal Muscle: Normative Structure and Function	32
2.2.3	Anatomy of Skeletal Muscles and Muscle Architecture	33
2.2.4	Contraction Generation	36
2.3	Applications of Ultrasound Imaging to Neuromuscular Disease Diagnosis	38
2.3.1	Imaging Skeletal Muscle	38

2.3.2	Imaging of Myogenic and Neurgenic Pathologies . . .	40
2.3.3	Ultrasound Imaging and Motor Neurone Disease . . .	42
2.4	Principles of Ultrasound Imaging Physics	45
2.4.1	Overview of Ultrasound Imaging	45
2.4.2	Interactions between Ultrasound and Tissue	47
2.4.3	Frequency and Wavelength	51
2.5	Summary	52
3	Review of Literature II: Computational Motion Analysis of Images	53
3.1	Feature Tracking using Kanade Lucas Tomasi Analysis . . .	55
3.2	Optical Flow Analysis	60
3.3	Foreground Detection Analysis	64
3.4	Summary	67
4	Ultrasound Image-based Motion Analysis Techniques for the Detection of Muscle Fasciculations: Comparison of Computational Analyses with Manual Identifications	69
4.1	Introduction	69
4.2	Methods	73
4.3	Results	78
4.4	Discussion	79
4.5	Conclusion	83
5	Ultrasound Image-based Motion Analysis Techniques for the Detection of Muscle Fasciculations: Comparison with Intramuscular Electromyography	84

5.1	Introduction	84
5.2	Methods	88
5.3	Results	97
5.4	Discussion	101
5.5	Conclusion	103
6	Application of Foreground Detection Analysis to Additional Muscles	105
6.1	Introduction	105
6.2	Methods	110
6.3	Results	115
6.4	Discussion	118
6.5	Conclusion	120
7	Comparison of Fasciculation Characteristics in Motor Neurone Disease Affected Participants and Healthy Controls	121
7.1	Introduction	121
7.2	Methods	123
7.2.1	Foreground Area Analysis	127
7.2.2	Foreground Object Centroid Analysis	128
7.2.3	Statistical Analysis	129
7.3	Results	133
7.3.1	Twitch Phase Timings	133
7.3.2	Characteristics of Twitch Amplitude	137
7.3.3	Distance between Foreground Object Centroids	141
7.4	Discussion	147

7.5	Conclusion	150
8	Discussion and Conclusions	152
8.0.1	Limitations	158
8.0.2	Conclusion	159
9	Appendices	177
9.1	Appendix 1: Parameterisation Tables for GMM and KLT/MI from Chapter 4	178
9.2	Appendix 2: Parameterisation Tables for GMM and KLT/ MI from Chapter 5	181
9.3	Appendix 3: Parameterisation and Supplimentary Tables for GMM from Chapter 6	187
9.4	Appendix 4: NHS Application for Ethical Approval	195
9.5	Appendix 5: NHS Participant Consent Form	202
9.6	Appendix 6: NHS Participant Information Sheet	203
9.7	Appendix 7: MMU Application for Ethical Approval	206
9.8	Appendix 8: MMU Participant Consent Form	214
9.9	Appendix 9: MMU Participant Information Sheet	215
9.10	Appendix 10: Poster from the MND Association Interna- tional Symposium	217

List of Figures

2.1	Pathway showing diagnostic criteria under the original El Escorial Criteria and with the Awaji Shima recommendations.	23
2.2	Levels of diagnostic certainty for MND and the criteria for each category.	24
2.3	Intramuscular EMG sequence including fasciculation potentials (Left) close up of fasciculation potential in healthy participant (Right)	25
2.4	Intramuscular EMG Sequence including Positive Sharp Waves (1.) and Fibrillation Potentials (2.) Taken from Mills (2005). .	27
2.5	Diagram of the composition of a muscle down to motor unit level and its connections with the motor neurons.	30
2.6	Diagram showing the Neuromuscular Junction	31
2.7	Diagram of striations patterns of muscle fibres (top) and structure of the actin (black) and myosin (grey) filaments (bottom).	34
2.8	Ultrasound image of the Medial Gastrocnemius and Soleus in transverse probe orientation.	39

2.9	Ultrasound image of the Medial Gastrocnemius and Soleus in a Healthy Participant (left) and MND Affected Participant (Right).	42
2.10	Diagram showing the processes involved in ultrasound imaging	46
2.11	Diagram Demonstrating the Absorption of Transmitted waves Waves through a Particular Medium.	48
2.12	Diagram Demonstrating the Transmission and Reflection of Waves when Encountering a Change in Medium.	50
4.1	Examples of ultrasound images collected in each muscle (MG and BB) and each probe orientation (Longitudinal and Transverse), demonstrating the diversity of image content. .	72
4.2	Flowchart showing major steps in the GMM Analysis. . . .	77
4.3	ROC curves of GMM (Blue) and KLT (Red) analysis approaches in BB (Top) and MG (Bottom) in healthy (Left) and patient (Right) populations when compared with the manual identification truth signal.	79
5.1	Overview of Experimental Set-up	91
5.2	Example myoelectric signals showing fasciculation potentials (Top left). Red lines indicate position of fasciculation potentials identified using the describe threshold technique. Two identified potentials are shown in detail on the right. . .	93

5.3	Plot of accuracy calculated by thresholding myoelectric signals by method given in Equation 5.2. Plateau point shown by red line and value of X taken forward to analysis stage shown by green dashed line.	93
5.4	Figure showing comparison of EMG signal (blue), muscle force (red) and frame length (black).	95
5.5	ROC curves of GMM (Blue) and KLT (Red) analysis approaches in BB (Left) and MG (Right) for different probe orientations (Transverse: Solid line, Longitudinal: Dashed line) in healthy (Top) and patient (Bottom) populations when compared with the myoelectric truth signal.	97
6.1	Examples of ultrasound images collected from muscles rectus femoris, rectus abdominis, trapezius and thoracic paraspinals and in both probe orientations (longitudinal and transverse).	107
6.2	GMM signal (red) overlaid with EMG logical signal (blue) and KLT/MI signal (right)	108
6.3	Overview of Muscles Assessed and their Innervation	111
6.4	EMG signal Threshold Calculation for Fasciculation Identification in the Thoracic Paraspinals (top left), Trapezius (top right), Rectus Abdominis (bottom left) ad Rectus Femoris (bottom right) Muscle.	113

6.5	ROC curves of RF (top left), TR (top right), RA (bottom left), TP (bottom right) muscles in longitudinal (blue) and transverse (red) probe orientation for GMM analysis when compared with the myoelectric truth signal.	116
7.1	Example of the process through which individual twitches are extracted from image for further analysis using the one dimensional foreground area signal (Example taken from MG in longitudinal orientation from a MND participant).	124
7.2	Example of how the Euler number of a binary image is calculated; number of foreground objects (white) minus the number of holes (black) ($E_{num} = Obj_f - Obj_b$).	126
7.3	A. Example of peak analysis measures: 1. Peak to peak difference. 2. Maximum peak height. 3. Minimum peak height. B. Example of twitch timing analysis measures: 1. Total twitch time duration. 2. Contraction phase duration. 3. Relaxation phase duration. 4. Inter peak duration.	127
7.4	Example of the total distances (red) and the calculation of x (green) and y (blue) components using k nearest neighbours from foreground object centroids (pink)	129
7.5	Two examples of data distributions successfully transformed (top) and which could not be successfully transformed (bottom)	131
7.6	Boxplots showing comparisons of healthy (H) and MND (M) results for twitch time duration	133

7.7	Boxplots to show comparisons of healthy (H) and MND (M) results for total area of foreground pixels	138
7.8	Boxplots showing total x and y distances between object centroids for healthy and MND affected participant groups in MG and BB.	142
7.9	Boxplots showing mean Euler number of image for twitches from healthy and MND affected participant groups in MG and BB.	143
7.10	3D scatter plot showing total distances between object centroids (x and y components) and Euler number in MG and BB with MND participants in red and healthy participants in blue.	146

List of Tables

2.1	Table showing the variants of MND and their onset and prevalence.	21
4.1	Agreement results for healthy participants (In Percent%) in MG and BB for healthy and MND affected participants. . . .	80
5.1	Area under Curve of ROC Results for Healthy Participants	99
5.2	Number of Trials Taken Forward to Analysis (Healthy Participants)	99
5.3	Area under Curve of ROC Results for Motor Neurone Disease Affected Participants	100
5.4	Number of Trials Taken Foreward to Analysis (MND Affected Participants)	100
5.5	Number of fasciculations detected using GMM in healthy and MND affected participants from BB and MG muscles). .	100
6.1	Number of Trials Taken Forward to Analysis (MND Affected Participants)	115
6.2	Results Table for MND Affected Participants in RF, TR, RA and TP.	117

7.1	Table showing mean and standard deviation values for twitch phase durations (shown in frames/ seconds) in healthy and MND affected participants (1. total twitch time, 2. contraction phase time, 3. relaxation phase time, 4. peak to peak time).	134
7.2	Results from ANOVA Calculations Showing P Values for Muscle, Probe Orientation and Participant Groups for Each of the Four Timing Measures.	135
7.3	Table showing mean and standard deviation values for twitch peak heights in healthy and MND affected participants (1. maximum peak height, 2.minimum peak height, 3. peak height difference) Values are reported as total foreground area as a proportion of the total area (in pixels) of the cropped image.	139
7.4	Results from ANOVA Calculations Showing P Values for Muscle, Probe Orientation and Participant Groups for Each of the Three Peak Amplitude Measures.	140
7.5	Table Showing the Mean and Standard Deviation Values for Total X and Y Distances and Euler Number in Healthy (Top) and MND Affected (Bottom) Participant Groups.	145
7.6	Significance (P values) of total x and y distances between object centroids and object area differences between healthy and MND affected participant groups.)	145

9.1	Number of fasciculations detected using GMM in MND affected (M) and healthy (H) participants from BB and MG muscles (Excluding 7 healthy participants used in parameterisation).	194
-----	--	-----

Chapter 1

Introduction

Motor Neurone Disease (MND) is a progressive, neurodegenerative disease affecting both upper and lower motor neurons to varying degrees. Prevalence in the UK is approximately 2 cases per 100,000 diagnosed every year [1]. For a patient to receive even a "clinically possible" MND diagnosis, either clinical or electrophysiological evidence of both upper and lower motor neurone dysfunction must be found in one region, or lower motor neurone dysfunction in two or more regions. Diagnostic certainty increases as the number of regions symptoms may be found in increases. If such conditions are not met, patients may have to wait for their condition to deteriorate before they reach a level of diagnostic certainty. Currently, diagnosis tends to be based on a combination of the "gold standard" techniques of intramuscular electromyography (EMG) and nerve conduction tests. However, the diagnostic pathway can be lengthy and involve a wide range of other procedures including magnetic resonance imaging and blood tests if MND is not apparent from the outset. Symptoms can be

highly variable between individuals but generally include; muscle weakness, atrophy, spasticity and involuntary muscle twitches [2]. Average life expectancy post diagnosis is 18 to 24 months. There is no known cure and currently, the only treatment routinely used is Riluzole which has been shown to have limited effect, extending life expectancy by approximately 3 months [3].

One of the clinical tools predominantly used in the diagnostic process for neuromuscular disease is intramuscular electromyography (EMG), which is an invasive procedure requiring the insertion needle electrodes into the muscle tissue of the patient. In addition to its invasive nature, EMG has a number of other limitations. For example, it has a small pick up volume (approximately, 1-2 mm in diameter, dependent on needle gauge), which means clinical indicators may be missed if not occurring at the needle tip [4]. Also, due to the invasiveness of the procedure, a trained clinician is required to conduct the assessment, which creates additional cost associated with this method.

A less invasive but more sensitive testing method for detection of involuntary muscle activations would enable improvement in the diagnostic experience for patients through the circumvention of painful testing such as EMG and potentially speed up the time to diagnosis. In addition to this there would be less of a barrier for repeat testing meaning a larger number of longitudinal studies could be carried out, with implications for testing effectiveness of drugs in controlling symptoms associated with neuromuscular disease. B mode ultrasound imaging has been suggested as a possible alternative for the diagnosis of neuromuscular disease [5], [6]. It provides

visualisation of the muscle tissue from the skins surface and has a relatively large field of view.

The majority of studies carried out into the use of ultrasound for non-invasive assessment of muscle tissue focus on the ability of human operators to identify patients with MND. This is achieved from subjective assessment of images, taking into account the structural information, number of involuntary activations, or both. However, there are limitations associated with subjective assessment of images. These include; the time consuming nature of watching video sequences recorded from numerous muscles in numerous patients, the cost involved with hiring individuals with the skills to watch and interpret such images and also that objective assessment of medical images have often shown comparable or improved levels of accuracy to those achieved by subjective, computational analyses [7], [8].

A wide variety of computational analyses have been applied to ultrasound images in order to detect and quantify activation and motion within the muscle tissue. However, this is generally limited to large scale voluntary activations, with only one previous study assessing the viability of computational analysis for the detection of involuntary muscle activations [9]. This study implemented a Kanade Lucas Tomasi tracking algorithm which uses features within images to track motion, coupled with mutual information to provide an identifier of coherent motion within the image, which was hypothesised to correspond to a fasciculation. A number of limitations/ challenges with computational detection of fasciculations were also highlighted, such as the inability of the method to disregard other physiological motion such as blood vessel pulsations which can cause

false positives within the signal.

1.0.1 Research Aims

The main research aim for this thesis is to determine if ultrasound images, through the application of different computer vision algorithms, is an accurate and robust tool for the detection of fasciculations and by extension the possible diagnosis of neuromuscular disease. This will be achieved by comparing the accuracy of computer vision methods to alternative fasciculation detection methods such as human operator identifications and EMG, with spatial and temporal characteristics of twitches being assessed to determine whether they may indicate the presence of underlying pathology within the muscle. This aim will be completed through the achievement of four key objectives which include:

1. The development of an additional computational analysis technique for comparison with the current method of a Kanade Lucas Tomasi (KLT) analysis combined with Mutual Information (MI).
2. The comparison of the KLT and additional analysis techniques to manual identifications and myoelectric signals in both healthy and MND affected participants.
3. The application of one or both techniques to previously untested muscles in MND affected participants.

4. The comparison of spatial and temporal twitch characteristics in both healthy and MND affected participants.

Research Question: Can ultrasound imaging be used to detect small scale muscle activations such as fasciculations in healthy and MND affected participants and are there any quantifiable differences in the characteristics of such activations?

1.0.2 Overview of Thesis

In chapter 2, the first part of the literature review for the thesis is documented. This section of the literature review focuses on the physiological processes that are required to produce contractions within the muscles and how certain pathologies such as MND may affect these processes. It also investigates the role imaging techniques, such as ultrasound can be used to better understand the structure and activation of skeletal muscle and how previous studies have applied it to diagnosis of neuromuscular disease.

Chapter 3 forms the second part of the literature review and introduces a number of computational methods for image analysis such as Kanade Lucas Tomasi tracking, Horn - Schunck optical flow and foreground detection using a mixture of Gaussians. Their potential suitability for motion analysis from ultrasound image sequences is discussed and selection of techniques for use in further chapters is made.

The first experimental chapter, chapter 4, compares the performance of the computational methods selected in chapter 3 (i.e. KLT and GMM)

in comparison to human operator identifications. These methods were applied to previously collected data that was used in the publication Harding et al (2016) [9]. The aim of this chapter was to determine whether the GMM could improve on the performance of the KLT in order to provide a viable alternative to the previously used technique.

Chapter 5 extended the work carried out in chapter 4 by once again comparing the KLT and GMM methods. This chapter compared their performance to a novel EMG truth signal. The aim of this chapter was to determine whether the GMM could provide a valid alternative to the KLT by comparing it to the current gold standard technique for detection of electrophysiological activation.

Chapter 6 aimed to determine the performance of the GMM across a wider range of muscles such as Trapezius, Rectus Femoris, Rectus Abdominis and Thoracic Paraspinals. This was required due to the need for twitches to be identified across a wide range of muscles to diagnose MND.

The final Experimental chapter, chapter 7 aimed to determine whether differences between the health and MND affected participant groups could be found using both spacial and temporal measures taken from ultrasound images. This would indicate whether ultrasound coupled with the GMM could indicate the presence of MND, without the requirement for human analysis of images.

1.0.3 Contributions to Knowledge

This thesis will assess the viability of using computational analyses to detect involuntary muscle activations from ultrasound image sequences that can be an indicator of neuromuscular disease such as MND. It will introduce new methods of analysis and compare performance to the KLT/ MI technique that has previously been used to determine the optimal method and compare to the previously used truth signal (human operator identifications) as well as introducing a new truth signal for comparison (intramuscular EMG). This will allow for conclusions to be drawn as to which technique has superior performance when compared to the truth signals, but also whether these performance levels are within a range that would support use as a diagnostic test. Finally, this thesis will assess whether ultrasound imaging can be used to determine spatial and temporal characteristics of fasciculations and whether these differ between healthy and MND affected participants, yielding preliminary indications as to whether computational analysis of ultrasound images can yield measures that discriminate between healthy and pathological muscle activations.

Chapter 2

Review of Literature I: Muscle Physiology, Motor Neurone Disease and Imaging Techniques

2.1 Motor Neurone Disease: Symptoms and Di- agnosis

2.1.1 Clinical Diagnostic Criteria for Motor Neurone Dis- ease

Motor Neurone Disease (MND) is a neurogenic, degenerative disease affecting upper and lower motor neurons. Symptoms include muscle weakness, atrophy, spasticity and involuntary muscle twitches. The term MND can be used either as an umbrella term for four distinct neuromuscular diseases or exchangeably with the term Amyotrophic Lateral Sclerosis (ALS), as is the case in this thesis. When used as an umbrella term, MND cov-

MND Variant	Symptoms	At Risk Groups	Prevalence
Amyotrophic Lateral Sclerosis	Upper and lower motor neurone involvement.	After the age of 50 (although can be significantly younger in early onset variants).	2 in 100 000
Primary Lateral Sclerosis	Upper motor neurone involvement.	Generally between 30 and 60 (although can be significantly younger in early onset variants).	1 – 6 in 100 000
Progressive Bulbar Palsy	Lower motor neurone involvement in the bulbar region.	After the age of 50 (although can be significantly younger in early onset variants).	1.5 in 100 000
Progressive Muscular Atrophy	Lower motor neurone involvement.	After the age of 50 (although can be significantly younger in early onset variants).	0.24 in 100 000

Table 2.1: Table showing the variants of MND and their onset and prevalence.

ers ALS as well as Primary Lateral Sclerosis (PLS), Progressive Muscular Atrophy (PMA) and Progressive Bulbar Palsy (PBP). PLS is specific to the upper motor neurons and disorders such as Progressive Muscular Atrophy (PMA) and Progressive Bulbar Palsy (PBP) both affect only the lower motor neurons [10] (Table 2.1 [11], [12], [13], [14]).

During the earlier stages of MND, the symptoms present may also overlap with other neurological disorders so the differential diagnosis will aim to rule out mimics out by the body region that they affect. For example upper motor neurone bulbar symptoms could also be explained by brain-stem lesions, mass stroke and demyelinating forms of other degenerative diseases; lower motor neurone bulbar symptoms could be explained by cranial nerve palsies; limb upper motor neurone signs could be explained by cervical myelopathy, cord tumor, hereditary spastic paraparesis, transverse myelopathy and HIV-related myelopathy and limb lower motor neurone signs could be explained by Radiculopathy, plexopathy and neuropathy.

thy [15].

The most effective way to diagnose MND has been a contentious issue over the years leading to a number of different diagnostic criteria being established, as well as additional amendments to those criteria. Initially, guidelines for MND diagnosis were stated in the El Escorial criteria [16]. Currently, recommendations made by the Awaji – Shima Consensus and Airlie House recommendations are used in preference to the El Escorial Criteria (Figure 2.1 and Figure 2.2 [17]), which existed as the previous gold standard for MND diagnosis [17].

One of the primary changes that were suggested in the Awaji – Shima recommendations was the weight given to different types of muscle twitches in the process of diagnosis. Previously greater weight was given to the presence of fibrillations (involuntary activity of fibres) in comparison to fasciculations (involuntary activity of groups of fibres) as an indicator of denervation and therefore MND. However, the updated criteria has allowed equal weighting for fasciculations and fibrillations, meaning a positive diagnosis could be reached on the basis of fasciculations alone.

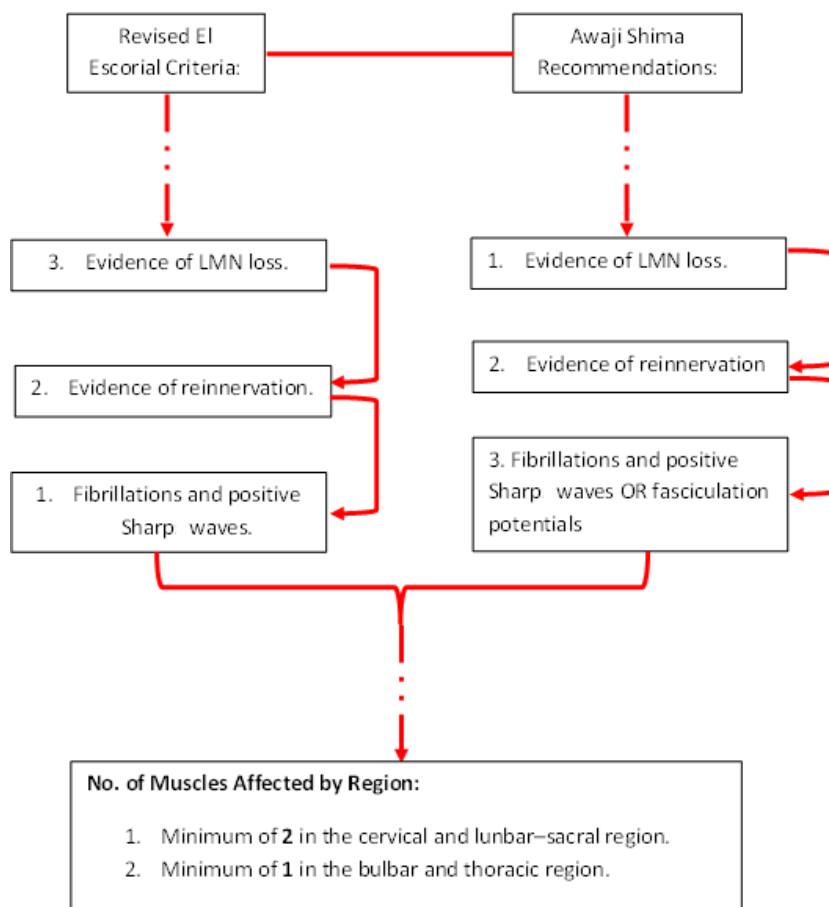


Figure 2.1: Pathway showing diagnostic criteria under the original EI Escorial Criteria and with the Awaji Shima recommendations.

Clinically definite ALS	
Clinical or electrophysiological evidence by the presence of:	
✓	UMN and LMN signs in the bulbar region.
✓	UMN and LMN signs in at least 2 spinal regions.
OR	
✓	UMN and LMN signs in 3 spinal regions.
Clinically probable ALS	
Clinical or electrophysiological evidence by the presence of:	
✓	UMN and LMN signs in at least 2 regions.
✓	Some UMN signs rostral to the above LMN signs.
OR	
✓	Clinical signs of UMN and LMN dysfunction are found in one region.
✓	Electrophysiological signs of LMN loss 2 or more regions.
Clinically possible ALS	
Clinical or electrophysiological evidence by the presence of:	
✓	UMN and LMN dysfunction found only in one region.
OR	
✓	UMN signs alone are found in 2 or more regions.
OR	
✓	LMN signs are found rostral to UMN signs.

Figure 2.2: Levels of diagnostic certainty for MND and the criteria for each category.

2.1.2 Fasciculations, Fibrillations and positive sharp waves

Fasciculations are a type of involuntary muscle twitch. They are localised twitches of individual motor units and occur due to the spontaneous con-

traction and relaxation the motor units within the muscle. If large enough and near enough to the surface, they may be visible to the naked eye [18]. They can occur in healthy individuals, although if they appear with great frequency and are widespread throughout the body, they may also indicate the presence of certain neuropathies, including MND. However, fasciculations are not observed in myopathic disorders [19].

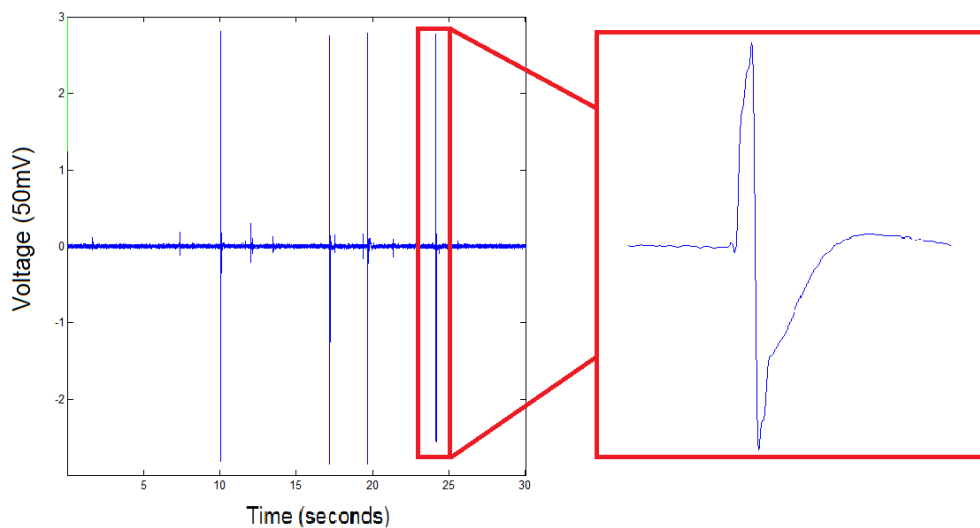


Figure 2.3: Intramuscular EMG sequence including fasciculation potentials (Left) close up of fasciculation potential in healthy participant (Right)

A common tool for the detection of fasciculations of smaller size or from deeper within the muscle is intramuscular EMG. The insertion of a needle up to a few centimeters (depending on needle length) into the muscle tissue allows for action potentials (electrophysiological activations) within the muscle to be recorded. An example of a fasciculation potential can be

seen in Figure 2.3.

As fasciculation potentials can occur in both healthy and pathological muscle tissue, methods to differentiate between the two are required. A number of different characteristics of the fasciculation potentials may be taken into account in order to achieve this. For example, duration of fasciculations can differ between MND sufferers and benign fasciculation syndrome. In the study carried out by Mills [20], it was reported that there was a longer duration fasciculation potentials in benign fasciculation syndrome sufferers, in comparison to MND patients (14.6 ms and 16.9 ms respectively, with a p value of 0.005). In addition to this, the variability of the duration of fasciculations was greater in MND patients and the discharge interval was significantly shorter.

A number of factors can determine whether the fasciculation potential itself arises from pathological origins or not. Complex fasciculation potentials (polyphasic potentials of increased duration and/ or amplitude), along with jitter (an indicator of irregular transmission) and blocking (an indicator of failure in transmission) can all be indicators of MND [21].

Fibrillations are another type of involuntary muscle twitch. In comparison to fasciculations, fibrillations are the reaction of a single muscle fibre when it loses its connection from its innervating axon. They occur on a much smaller scale in comparison to fasciculations and are therefore not visible through the skin [22]. When they occur rhythmically, they indicate that a muscle fibre has lost the connection to its innervating axon. Their origin may be related to the oscillation of the resting membrane potential of the denervated fibres and additional acetylcholine receptors. Unlike

fasciculations, fibrillations may occur in not only neurogenic disorders, but inflammatory and dystrophic muscle diseases [23].

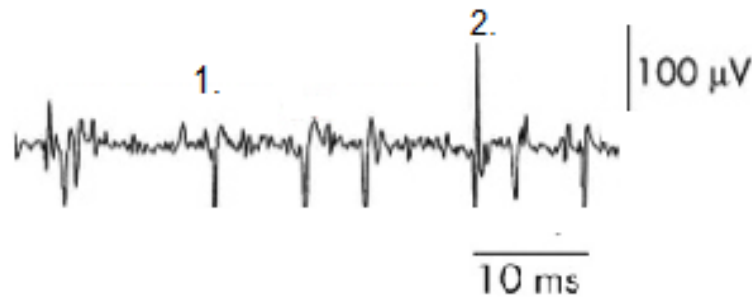


Figure 2.4: Intramuscular EMG Sequence including Positive Sharp Waves (1.) and Fibrillation Potentials (2.) Taken from Mills (2005).

Fibrillation potentials will appear on an electromyogram as much smaller spikes (of amplitudes between 20 and 300 μV in contrast to amplitudes of fasciculations which are between 0.03 and 10 mV), in comparison to fasciculation potentials and will occur over a much shorter time period, lasting less than 5 ms and having a firing rate of between 2 and 20 Hz (see Figure 2.4 [4]). They will be biphasic or triphasic in appearance and can be differentiated from end plate spikes, which are potentials caused by neurotransmitter binding at the neuromuscular junction, by their initial positive direction [24].

Positive Sharp Waves are biphasic potentials with purely positive components, in comparison to the initial negative inflection of fibrillation potentials. They tend to be grouped with fibrillation potentials, as they both represent abnormal firing from damaged nerve or muscle tissue and have

similar amplitudes and short durations [25]. Along side fibrillations, positive sharp waves may also indicate a number of different neuropathic and myopathic disorders and the reasons for their presence varies depending on the pathology. Although, both fibrillation potentials and positive sharp waves tend to be given the same clinical significance and have the same origin, their presence either together or individually may hold different meanings [26]. For example positive sharp waves without fibrillation potentials may be seen following local muscle trauma; and positive sharp waves may be seen alone in some demyelinating polyneuropathies.

Current methods for the diagnosis of MND such as intramuscular EMG are invasive and offer varying levels of certainty in diagnosis. In addition to these points, time to diagnosis tends to be relatively long, with average times of 12 months being reported [27]. The aim of this thesis is to address current challenges in diagnosis and monitoring of MND. Detection of these involuntary activations is typically done using EMG based techniques, in order to fully understand the basis for these techniques and how findings may relate to ultrasound imaging results the following section will discuss the processes that occur between activation of the central nervous system and subsequent contraction of the muscle tissue.

2.2 Integration of Skeletal Muscle with the Nervous System

EMG and ultrasound imaging are two very different methods which both may be used to quantify the "health" of the neuromuscular system. EMG aids in providing insight into the electrophysiological events that produce mechanical activations within the muscle that can be visualised with ultrasound imaging. It is therefore important to understand the mechanisms which underly muscle contraction from the generation of action potentials in the nervous system to the generation of force from the muscle fibres.

Muscle motor units are the muscle fibres that are innervated by the same motor neurone (Figure 2.5). In neuromuscular diseases such as MND, as the muscle degenerates fibres will be denervated from their motor neurone once this occurs the fibre may be re-innervated by a nearby motor neurone and included within a new motor unit. EMG electrodes are used to detect the electrical activity across the muscle membrane during muscle activity this will produce a waveform called a motor unit action potential for each motor unit. During the denervation/ re-innervation process, phenomenon such as complex and combined potentials may be encountered.

In contrast an ultrasound twitch (fasciculation) is the mechanical activation of the muscle produced due to the electrical stimulus provided by the MUAP. This motion of the muscle tissue itself may be viewed using ultrasound imaging techniques due to the changes in shape caused by a twitch and the good temporal resolution of the equipment.

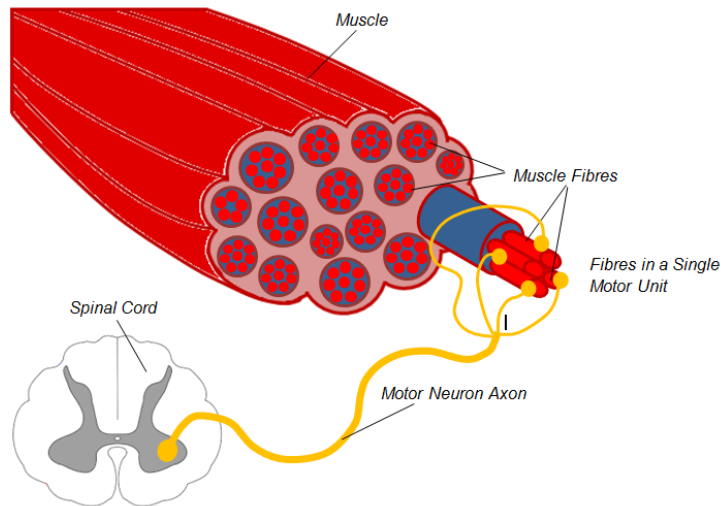


Figure 2.5: Diagram of the composition of a muscle down to motor unit level and its connections with the motor neurons.

2.2.1 Action Potential Generation

The various electrophysiological events laid out in Section 2.1.2, are generally seen as abnormal events occurring due to denervation (although fasciculations can occur in healthy individuals). In the healthy neuromuscular system, muscle contraction is achieved through the transmission of action potentials, down the motor neurons and into the skeletal muscle. Upper motor neurones, originating in the motor cortices of the central nervous system (CNS), interlink with the peripheral nervous system (PNS) and by extension, the muscles through synapses with the α - (lower) motor neurons, originating in the brain stem (head and neck) and spinal cord (rest of the body) [28]. The α - motor neurons extend their axons into the PNS and innervate skeletal muscle fibres directly (Figure 2.5).

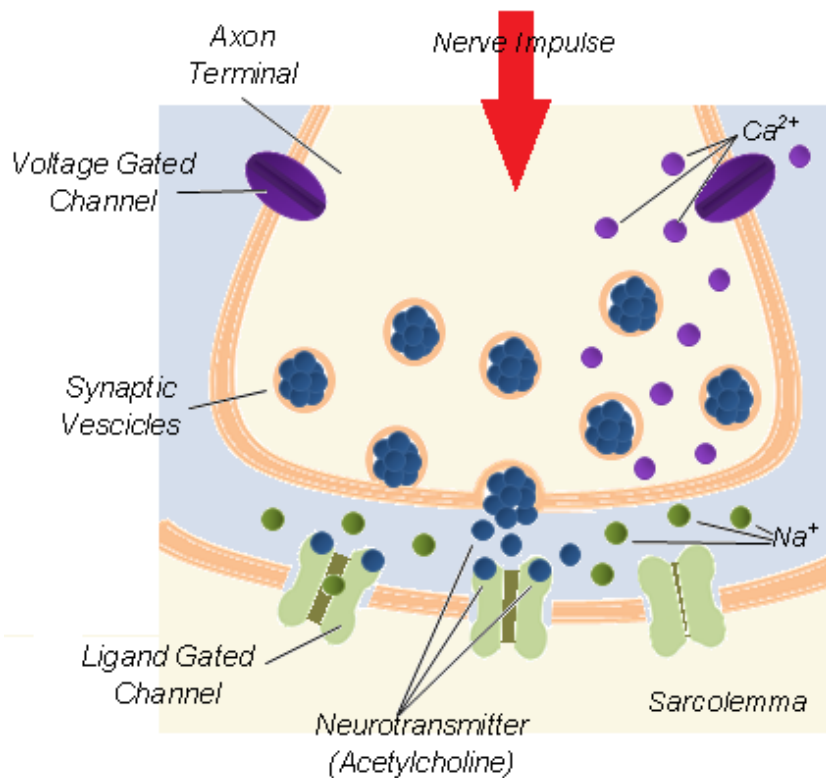


Figure 2.6: Diagram showing the Neuromuscular Junction

Following the generation of an action potential, it will propagate along the motor neurons axon, until it reaches the terminal bouton of the axon. This area, where the motor neuron axon ends and the sarcolemma (cell membrane of the muscle fibre) begins, is called the neuromuscular junction (NMJ) [29], seen in Figure 2.6. The neuromuscular junction is a unique type of chemical synapse, where the transmission of the action potential from the axon to the muscle fibre takes place. The arrival of an action potential causes the opening of voltage-dependent calcium channels and

an influx of Ca^{2+} ions. This creates the conditions for binding of vesicles containing the neurotransmitter Acetylcholine (ACh) to the cell membrane and the release of the ACh into the synaptic cleft. This then binds with acetylcholine receptors on the motor endplate [30]. Activations such as fibrillations and positive sharp waves occur at this stage of transmission if muscle fibres have lost contact with their innervating axon. This causes an increase in ACh receptors on the endplate and causes hyper-excitability at the membrane, causing repetitive, small scale potentials to appear in the EMG signal.

Once transmission has occurred, the action potential generated at the NMJ will propagate along the muscle fibre cell membrane (sarcolemma) and into the networks of T - tubules. This action potential, traveling along the muscle fibre membrane may be detected by the insertion of a needle electrode into the muscle tissue [31] as described in section 2.1.2.

2.2.2 Skeletal Muscle: Normative Structure and Function

Once the action potentials generated in the nervous system reach the motor endplate, the process of force generation will begin. The mechanical activation of the muscle tissue, which can only be inferred from the EMG signals recorded, can be directly visualised using ultrasound imaging. The visualisation of these events and how these events appear within the images can depend on a number of factors such as muscle architecture,

motor unit size and motor unit type. The motor unit size and also number of certain types of motor unit have also been shown to differ between healthy and MND affected populations [32], [33]. An understanding of skeletal muscle structure and function is required in order to determine how healthy and pathological muscle will appear in ultrasound images and how that will correspond to the myoelectric activity of the muscle.

2.2.3 Anatomy of Skeletal Muscles and Muscle Architecture

Within the body, there are 3 different types of muscle: smooth muscle, skeletal muscle and cardiac muscle, each with their own unique structure and functions. Skeletal muscle is a form of striated muscle or muscle that appears striped due to bundles of contractile elements. It is generally under voluntary control and is the specific type of muscle that allows for the locomotion of the human body [34]. The term muscle architecture describes the macroscopic arrangement of muscle fibres relative to the axis of force generation, which contributes to the muscles mechanical function. There are a number of different types of fibre arrangement including parallel, pennate, bipennate and circular [35]. These arrangements, along with fibre length and cross sectional area determine the muscles force production capabilities. Bundles of muscle fibres of varying sizes are known as muscle fascicles and fibres innervated by the same motor neuron are collectively known as motor units (Figure 2.5).

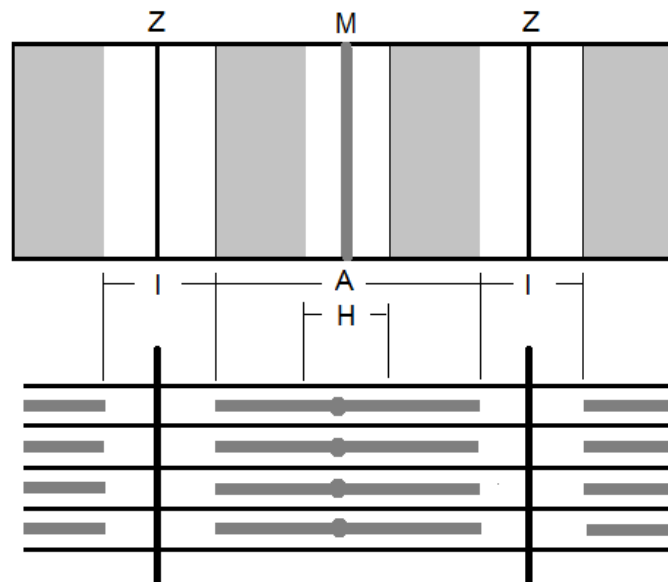


Figure 2.7: Diagram of striations patterns of muscle fibres (top) and structure of the actin (black) and myosin (grey) filaments (bottom).

Muscle fibres, also called myocytes, are the component parts of the motor unit (muscle fibres innervated by a single motor neuron) and contain myofibrils, the long protein cords which are the main contractile elements of the cell [36]. They contain four types of myofilaments which work together to produce muscle contractions. These myofilaments are; thick filaments composed of myosin, thin filaments composed of actin and proteins involved in the regulation of contraction such as tropomyosin, which covers myosin binding sites and troponin, which binds calcium ions revealing the myosin binding sites. These interactions are the basis for force generation and movement of muscle cells [37]. The striation patterns of myofibrils are the result of bands of light and dark colouring (Figure 2.7.

The A bands which are darker and the I bands which are lighter alternate along the length of the myofibril, reflecting the repeating arrangement of strands of thick (myosin) and thin (actin) protein filaments. A dark line, known as the Z line (intersects the I band and forms an anchor point for the actin filaments. At the centre of A band is a lighter area known as the H zone, a region of the myosin filaments devoid of any motor domains. The H zone also often contains a darker line, known as the M line. These bands make up the sarcomere, the functional unit of the myofibril [38].

Physiologically, motor units may be classified into four main groups, each having its own unique characteristics [39]. These groups are: Fast fatigable (FF), fast fatigue resistant (FR), fast intermediate (FI) and slow oxidative (SO). FF motor units produce high forces and fast contraction speeds, but fatigue quickly (over a few seconds). In contrast, FR motor units produce an intermediate force and fast contraction speeds, but are resistant to fatigue. FI units are, as the name suggests, an intermediate between FF and FR and SO produce a low force, slow contraction but they are very resistant to fatigue [40]. For example, in [41] twitch contraction times were assessed in feline ankle extensor muscles. Results reported twitch times of less than 30 msec in both FF and FR motor units, with SO unit types exceeding 40 msec. Whereas the number of motor units in MND affected participants have been shown to decrease by about 80 percent, they were also found to be six times larger than those in healthy participants. In addition to this, during denervation in MND [32], it has been found that the FF were more vulnerable than the SO motor unit types

[33]. These factors may have implications on any analysis of spatial and temporal characteristics of involuntary activations.

2.2.4 Contraction Generation

The physiological actions outlined in section 2.2.1 and 2.2.2 are the instigators for a number of processes that result in the contraction of muscle fibres due to actin and myosin interactions. The mechanical output from these interactions can be visualised using ultrasound imaging, allowing for inferences to be made as to the presence of voluntary or involuntary activations of the muscle without the need for EMG.

The aforementioned interactions are known as the Cross-Bridge cycle and outline the reaction of the muscle tissues to the electrical inputs from the nerve that generate force as output [38]. The actin and myosin proteins introduced in section 1.1 are the filaments that bind together to produce muscle contraction.

There are four stages to the Cross-Bridge cycle. Action potentials reaching the end plate will cause a reaction that releases Ca^{2+} ions into the sarcoplasmic reticulum. The calcium binds to the troponin, changing the configuration and exposing the active site of the actin. This allows the myosin head to attach to the actin and bend to produce a power stroke, which will pull the actin filament. This stage releases ADP and phosphate molecules. An ATP molecule will then bind to the myosin head, causing it to detach. The ATP is then hydrolysed to ADP and phosphate molecules,

returning the process to its initial conditions [42].

The previously mentioned processes allow for small movements between the filaments, but in order to produce a full scale contraction of the muscle, synchronous activations must occur. Contraction of a single fibre will produce a twitch contraction. However, tension must be sustained beyond the fraction of a second generated by a twitch, in order for any meaningful contraction to occur. Therefore, most skeletal muscle contractions in the body are tetanic contractions [43]. Due to the largely different timescales over which an action potential and a muscle twitch can occur (approximately 10 ms and 150 ms in the gastrocnemius muscle respectively [4],[44]), a number of action potentials may stimulate the muscle fibre in the time it takes for a single twitch. This allows for sustained tension within the muscle as long a repeated stimulation of the fibre is maintained. This phenomenon is known as the summation effect and is the reason why full scale muscle contractions are possible [45]. Involuntary activations such as fasciculations do not produce tetanic contractions as they are the product of single action potentials activating single motor units. Therefore within an ultrasound image of a particular muscle, fasciculations will be distinct from large scale voluntary activations as they will produce small scale localised motion of the tissue over relatively short time scales in contrast to larger scale, unified motion produced during tetanic contraction, which will be of longer time duration. Fasciculations and voluntary activations can also be distinguished from an EMG trace. Fasciculations will appear as a single action potential from a single motor unit, in contrast voluntary

contraction will appear as a large number of action potentials from various motor units superimposed onto one another. These signals may be decomposed to pick out the individual motor unit that are contributing to the voluntary activation. This can be done by a number of methods. However, template matching is a popular technique for EMG signal decomposition and is the method used by software such as EMGLab, which matches the shape of each action potential with each different shape belonging to an individual motor unit. Fasciculations would not match with any other action potentials due to them being a single occurrence.

2.3 Applications of Ultrasound Imaging to Neuromuscular Disease Diagnosis

2.3.1 Imaging Skeletal Muscle

A number of imaging modalities can be employed to visualise skeletal muscle *in vivo*. Imaging techniques such as sonography, computed tomography, scintigraphy, radiography, and magnetic resonance imaging (MRI) have allowed for the non-invasive assessment of muscle structure as well as the presence of injury and disease [46].

B-mode ultrasound is a non-invasive imaging modality. It allows for real time acquisition of images of soft tissues within the body using high frequency sound waves. It provides good spatial resolution (especially at

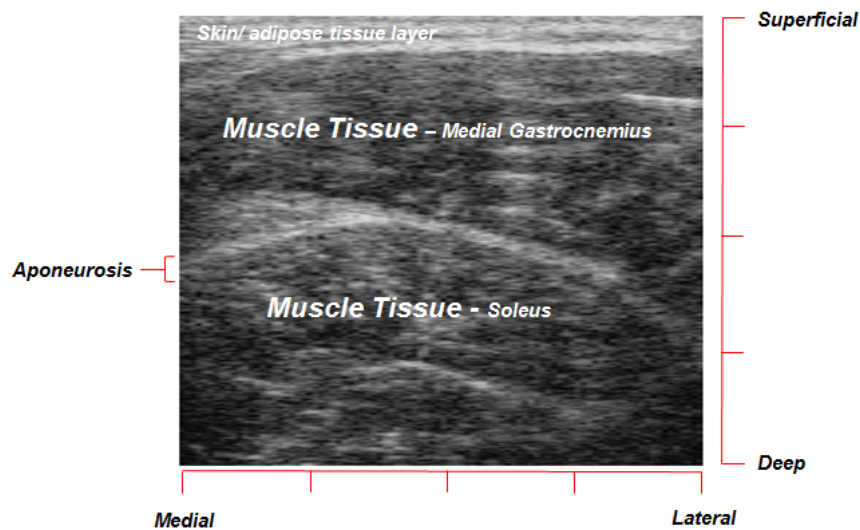


Figure 2.8: Ultrasound image of the Medial Gastrocnemius and Soleus in transverse probe orientation.

higher frequencies), allowing for the collection of structural information, such as muscle thickness [47], fascicle length and pennation angles [48]. However, unlike MRI it provides good temporal resolution (with standard frame rates of between 25 and 100 fps and high frame rate devices collecting up to 10000 fps [49]) and is therefore frequently used in the assessment of dynamic changes in skeletal muscle, within a small field of view which is limited by the size of the transducer [50].

Owing to the differences of the echogenicity of the tissues, muscles can be easily differentiated from fascia and skin, which will appear white (hyperechoic) and bone, which will appear black (anechoic) [51]. They may also be differentiated from each other by aponeuroses (the fascia encasing the muscle) and by the orientation of the fascicles [52]. Such information on density and structure is not only useful in determining and

locating injuries within the muscles but has been used a number of times to accurately distinguish between different types of myogenic and neurogenic diseases [53], [54]. However, some of these disease markers may also be observed in images of aged muscle.

2.3.2 Imaging of Myogenic and Neurgenic Pathologies

Normal aging causes decline within the muscle, such as a loss of skeletal muscle mass and strength. This decline (or sarcopenia) may be coupled with a loss in functional mobility and frailty as individuals age [55]. Morphological changes within the muscle can be viewed using ultrasound. Besides allowing for measurement of muscle thickness and the subcutaneous fat layer, the echo intensity of the muscles within the image can indicate the presence of increased levels of intramuscular fat and fibrous tissue [56].

The atrophy visible in images of aging muscle has a number of underlying causes. As individuals age, the number of fibres and the number of motor units declines [57]. This is due to the denervation of motor units. Some of the fibres within these motor units may be incorporated into remaining motor units. However, those that are not are lost through denervation atrophy [58].

Changes in neurophysiological properties can be noted in muscles during old age and revealed through electromyography. For example factors such as action potential amplitude and duration are significantly increased

with age in myoelectric signals due to the aforementioned denervation/reinnervation process [59].

The presence of different neurogenic and myogenic diseases can also be determined from images acquired using b-mode ultrasound. In the study [53] investigations were carried out into how images of skeletal muscle varied in healthy controls and patients with different myopathies and neuropathies. Results were based on a comparison of a number of measures (density, white-area index and inhomogeneity) taken from the images collected. Density was calculated using an average pixel value from the section of the image selected for analysis and white-area index was quantified by dividing the area of white patches (pixel values greater than 170) by the total area of the image selected for analysis. The inhomogeneity measure was calculated by first applying a Sobel filter to the image, which enhances edges by expressing gradients. This causes an inhomogeneous image to exhibit alternating patches of black and white pixels, which is quantified by dividing the number of white areas by the area of the image selected.

Findings suggested that neuropathies display normal densities and white-area index, but high inhomogeneity levels. In comparison, myopathies had increased densities, with often increased white-area index and sometimes increased inhomogeneity. However, as the age of the healthy participants was increased the distinction between healthy and pathological values decreased, suggesting that the sensitivity/accuracy of this method may be decreased if the age criteria was raised for healthy participants. This may have implications in distinguishing between healthy aging mus-

cle and diseased muscle when applying computer vision techniques to ultrasound images.

2.3.3 Ultrasound Imaging and Motor Neurone Disease

More recently, there have been a number of groups that have been attempting to diagnose specific disorders using ultrasound images of the muscles [60] and [6]. One of these disorders is Motor Neurone Disease.

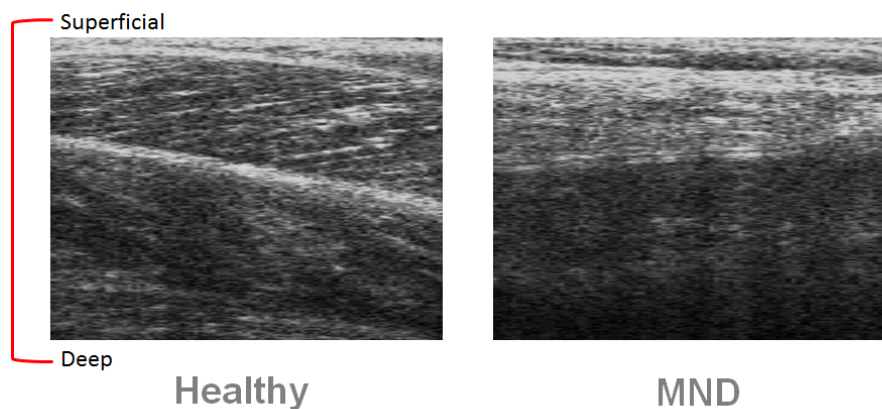


Figure 2.9: Ultrasound image of the Medial Gastrocnemius and Soleus in a Healthy Participant (left) and MND Affected Participant (Right).

The assessment of images, with the aim of forming a diagnosis, tends to be separated into two techniques: using structural information [61], [53] within the images such as muscle thickness (presence of atrophy) and changes in echoicity (infiltration of fatty and fibrous tissues within the muscle) these differences can be seen in Figure 2.9, or information on how the muscle moves [62] such as the presence of fasciculations and fibrillations. As previously mentioned in section 2.1.2, fibrillation detection using

ultrasound, where they appear as small, oscillating movements, has not yet achieved accuracy levels high enough to be considered for clinical diagnostics. In [63] four out of eleven ultrasound images collected gave true positives for fibrillations, with two out of eleven giving true negatives. However, this was only achieved if the fibrillations were firing at a rate of at least 5 Hz. A further study found sensitivity values of 43 - 63% and specificity values of 33-73% in [64]. From this they conclude results do not reaching boundaries that would be acceptable for diagnostic testing.

In contrast to fibrillation detection, ultrasound has been used to detect fasciculations with greater levels of success, achieving sensitivity levels of 96% and specificity levels of 84% respectively, using human operators to determine whether they had observed fasciculations in at least four muscles from 12 muscle groups (including the sternocleidomastoid, biceps brachii, forearm flexors, quadriceps, tibialis anterior and rectus abdominis). [6].

Despite previous studies being able to determine the presence of fasciculation with good sensitivity/ specificity levels, a large number of these are based on subjective assessment of US images by a human operator to determine whether fasciculations are present or absent [6], [65], [5]. A small number of studies have applied motion tracking techniques to determine the presence of small stimulated twitches [66] and then involuntary twitches [9], however, no comparisons have currently been made between these automated techniques and electrophysiological activity within the muscle. In addition to this, only one computer vision technique has

currently been assessed in relation to twitch detection [9], meaning no quantitative comparison of potential twitch detection techniques has yet been carried out.

Additionally, no methods to determine differences between fasciculations as they appear in the images to distinguish between healthy and MND affected participants have been determined, although it is predicted that this may be possible. During the progression of MND, fibres lose their connection to the innervating axon of their original motor unit, the process of re-innervation will occur to include the denervated fibre into a new, nearby motor unit. This will cause the new motor unit to become larger, due to the greater number of fibres contained within it. In relation to EMG signals, motor unit action potentials will be of greater amplitude and increased duration in comparison which are also of increased duration and area (more single fibre action potentials summing) and are also more complex in morphology. Due to the larger number of fibres per motor unit in MND patients, each fasciculation will result in the contraction of a larger number of fibres also. The area of tissue displacement in MND compared to healthy participants could be predicted to:

1. Remain the same due to the reinnervated fibres being adopted by other motor units that are close to the original motor unit, causing additional motion but within the same area.
2. Increase, due to the greater number of fibres contracting during a single fasciculation, which should result in greater force production. This greater force production should cause a greater number of pas-

sive fibres to be displaced by the active fibres, causing a larger area of motion within the image.

2.4 Principles of Ultrasound Imaging Physics

B mode ultrasound imaging may be used to visualise the dynamic processes occurring within the skeletal muscles such as voluntary activations (muscle contractions) and involuntary activations (fasciculations). It may also, due to the emission of sound waves and their interactions with different tissue media, give indications as to the properties of the muscle tissue itself. The following section outlines the principles behind ultrasound imaging and the phenomenon that allow the creation of images as well as problems that may be encountered.

2.4.1 Overview of Ultrasound Imaging

The basis of ultrasound imaging relates to the transmission and reflection of sound waves through various mediums. The rapid vibration of piezoelectric crystals located within the ultrasound transducer produces the high frequency sound waves required for the generation of ultrasound images. The waves produced travel in a longitudinal motion by the compression and expansion of the molecules in the medium. Any reflections of sound waves at boundaries between mediums will be detected by the elements contained within the transducer [67] - see figure 2.10.

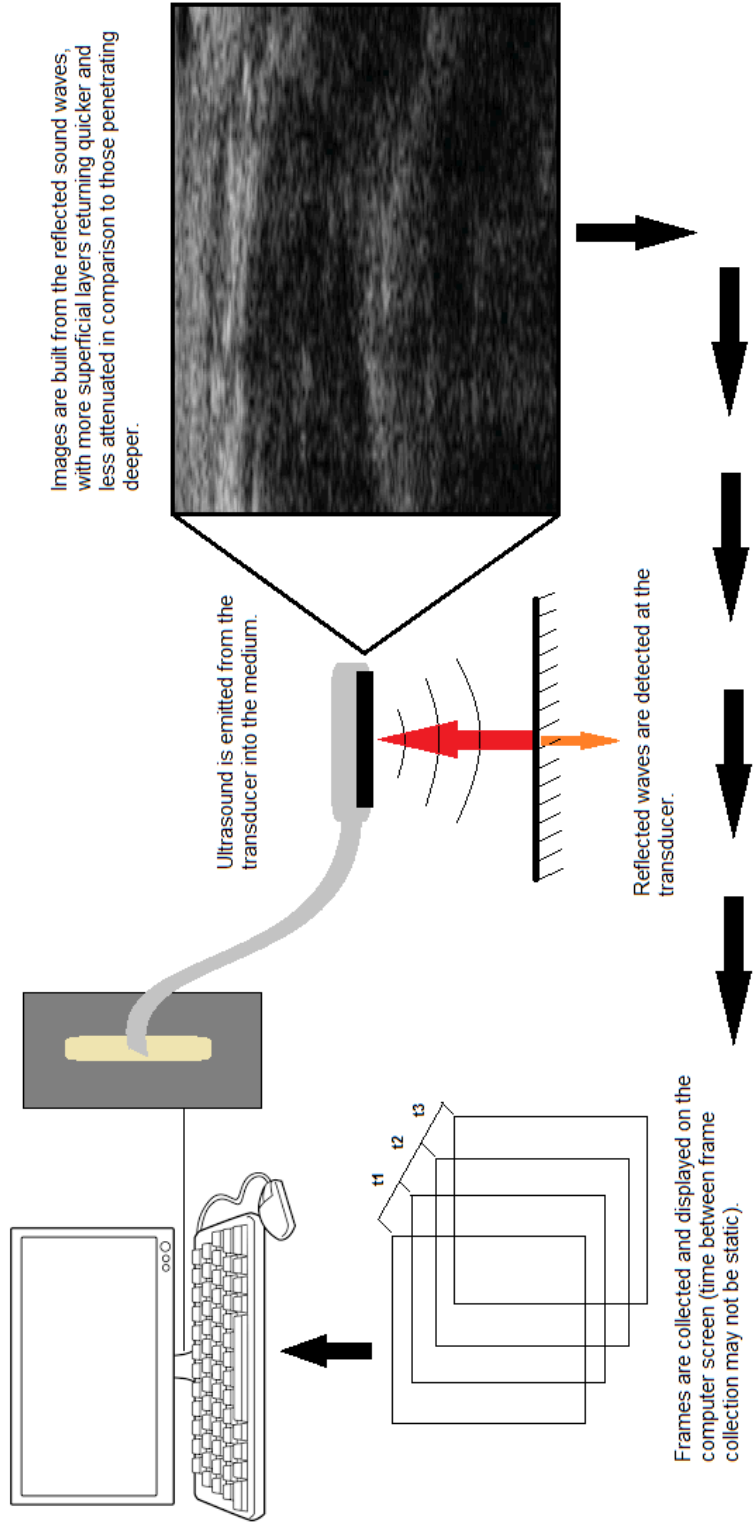


Figure 2.10: Diagram showing the processes involved in ultrasound imaging

2.4.2 Interactions between Ultrasound and Tissue

Attenuation

As ultrasound waves propagate through the tissue, the energy intensity or amplitude of the wave is weakened. This is due to the waves being reflected, refracted, absorbed, scattered or diffracted [68]. The amplitude decay of a tissue can be modelled using the following equation:

$$A = A_0 e^{-\alpha z} \quad (2.1)$$

where α is the attenuation coefficient, A_0 is the unattenuated amplitude and A is the attenuated amplitude once the wave has travelled distance z from the origin.

The attenuation coefficient (α) of a material describes how easily the sound wave can propagate throughout that particular material:

$$\text{Attenuation} = \alpha f \quad (2.2)$$

A small attenuation coefficient (α) indicates that the ultrasound wave will travel through the medium without large losses in intensity, whereas a larger attenuation coefficient indicates that the sound wave intensity is weakened more rapidly. Attenuation is proportional to the square of the sound frequency due to the decrease in penetration with an increase in

frequency [67] and can be calculated through the product of the distance travelled, frequency and attenuation of the medium (Equation 2.4.2).

Absorption

The absorption (conversion of energy in the ultrasound to heat) of that particular tissue will determine the colour of the image, ranging from white images showing maximum reflection of sound waves (e.g. bone) to black images showing vary little reflection (e.g. water). Absorption into the tissue is the greatest contributor to the attenuation of the sound waves (Figure 2.11). It is the conversion of the energy from the sound waves into heat, mainly due to the friction in particles when displaced by the wave [68].

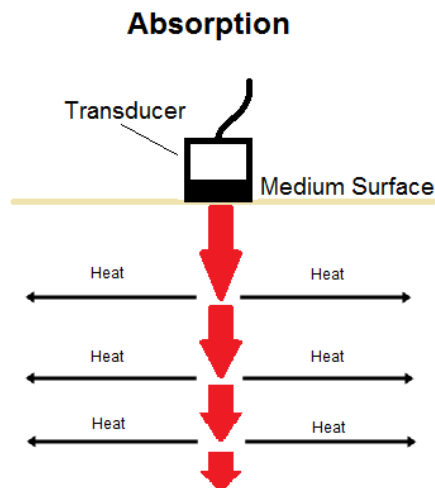
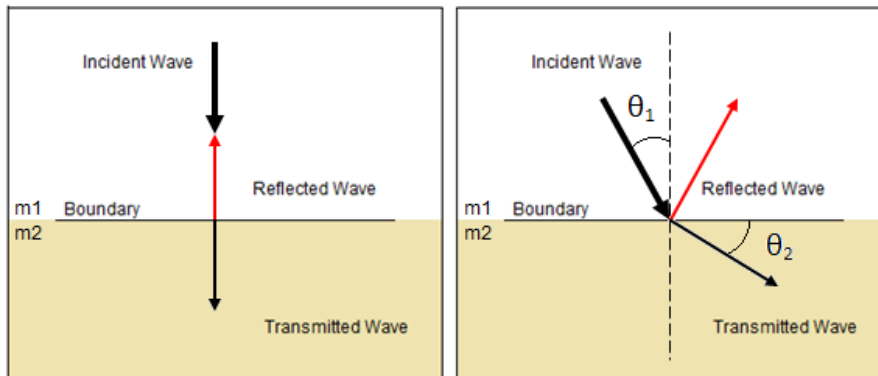


Figure 2.11: Diagram Demonstrating the Absorption of Transmitted waves through a Particular Medium.

Reflection

The theory behind ultrasound imaging is similar to those of optics. Once an ultrasound wave is produced and is released into the body it will propagate throughout the tissue as a pressure wave at approximately 1500 m/s [69]. When a tissue boundary is reached, such as the boundary between soft tissue and a blood vessel, the differing acoustic characteristics of the two mediums will cause some of the wave to be reflected back. Some may travel onwards through the tissue to continue this process until the entire wave has been reflected, transmitted or converted into heat. This enables an image of the area of interest to be constructed. This is demonstrated in Figure 2.12 . The angle at which the wave hits the boundary is the same as the angle it is reflected at [70].

Reflection occurs at the tissue boundaries in the body and this principle is the basis of ultrasound imaging. At a tissue boundary, the characteristics of the material will differ. In relation to ultrasound the most important property of the material to be considered is the Acoustic Impedance. Acoustic Impedance is the opposition to the flow of sound through a material and the difference of Acoustic Impedance at a tissue boundary will determine what percentage of the wave will be reflected and what percentage will carry on through the tissue [71].



θ_1 - Angle of Incidence
 θ_2 - Angle of Refraction

Figure 2.12: Diagram Demonstrating the Transmission and Reflection of Waves when Encountering a Change in Medium.

Refraction and Diffraction

Refraction occurs at boundaries between two materials, due to the difference in velocities of waves within the two mediums. This causes a change in the angle at which the wave is travelling as it either speeds up or slows down on entering the new material (Figure 2.12). This angle can be determined using Snell's Law:

$$n_i \sin \theta_i = n_r \sin \theta_r \quad (2.3)$$

where θ_i and θ_r are the angles of incidence and refraction respectively and n_i and n_r are the refractive indices of each material [72].

2.4.3 Frequency and Wavelength

The frequency and wavelength of the ultrasound waves are highly relevant to medical ultrasound as they determine the depth to which the waves can penetrate and the quality of the image. The frequency of a wave makes reference to the number of cycles of a sound wave per second. Standard ultrasound frequencies range between 1 - 13 MHz, although higher frequencies can be attained [73]. When imaging skeletal muscle 4 - 8 MHz is standard, however, higher frequencies may be required to visualize small muscles such as those in the hands and feet with sufficient detail [74].

The wavelength is the distance a wave travels during one cycle and is inversely proportional to frequency. It is one of the main factors affecting the axial resolution of an image and the scanning depth, due to increased levels of attenuation as the frequency increases [75]. High frequency and small wavelengths produce higher quality images, but cannot penetrate the tissues and are therefore only useful on superficial structures, such as the muscles. This is due to a linearly dependent relationship between frequency and attenuation of the wave (see equation 2.4.2). Low frequency and large wavelengths produce poorer quality images but can be used to image structures at greater depths, such as the liver and kidneys, where the structures are relatively large and less detail is required [68].

2.5 Summary

There are a number of imaging techniques that can visualise muscle tissue non-invasively. However, with the exception of ultrasound imaging, none offer the required levels of spatial and temporal resolution required to capture the transient motion associated with muscle fasciculations. Also the interactions of ultrasound with tissue allow for relatively clear images of muscle structure to be relayed in close to real time, relaying information on muscle size, shape and fibre orientation, as well as tissue composition.

For ultrasound to be a viable method for the diagnosis of MND, it would need to be effective in the identification of certain indicators of the disease. Of these indicators, arguably the most notable are the involuntary activations that occur within the muscles. These activations, when shown to be present across a wide range of muscles and being progressive in nature can warrant a positive MND diagnosis. In contrast to the current diagnostic technique, ultrasound offers a non invasive method to assess fasciculations and possibly other muscle activity. However, current subjective methods of images analysis, such as human operator identifications can be time consuming and highly subjective, indicating that an automated detection method may be superior.

Chapter 3

Review of Literature II:

Computational Motion Analysis of Images

Recent studies into the use of ultrasound imaging to detect involuntary muscle activations have generally been focused on the performance of human operators in this particular task [65], [6]. These studies have yielded good results (accuracy over 80%), however they remain a largely subjective method of analysis. Computational analysis of involuntary muscle activations has also been investigated, however these particular studies are few in number [66], [9]. In [66] the idea of an automated analysis was introduced through the use of a Kanade Lucas Tomasi tracker coupled with mutual information analysis was assessed in relation to the identification of small scale stimulated muscle twitches with a high degree of success. Further from that, a KLT/MI analysis method was implemented for the detection of fasciculations, in [9]. Operator identifications were used as truth

signals for comparison and results reaching 83 - 94% accuracy.

Although the few studies that have investigated the use of computational analysis for fasciculation detection have reached high levels of accuracy, they highlighted a number of limitations such as accuracy reduction in pathological muscle tissue and detection of other physiological motion (such as blood vessels). These limitations are due to how the KLT and the MI operate respectively. The KLT requires well defined corner features to reliably track features from one frame to the next. However, pathologies such as MND appear more homogenous in the ultrasound images compared to the more heterogeneous images that are collected from healthy participants. This causes difficulties associated with finding good corner features to track, likely causing the reported drop in accuracy in the MND affected participants.

The MI is based on differentiating between coherent and random motion within the image, with noise appearing as random motion and fasciculations appearing as coherent motion. However, all physiological motion within the image is coherent and therefore these motions will also appear in the MI signal as a false positive.

Finally, although fasciculations are detected there is no indication whether they are more likely to be healthy or related to some form of neuromuscular disease. Subsequent chapters will explore the possibility of using different image processing methods in order to solve these limitations.

3.1 Feature Tracking using Kanade Lucas Tomasi Analysis

A large number of the recent publications use the Kanade Lucas Tomasi (KLT) tracking method for analysis of both voluntary and involuntary muscle activations [66], [50], [9]. KLT object tracking works through a process of feature selection, feature tracking and feature monitoring. It was initially proposed for image registration purposes (a previously computationally costly endeavour). The technique is generally based on the combined content of three papers, Lucas [76], who set out the general tracking method used, Tomasi [77], who discussed the detection and tracking of feature points and Shi [78], who determined good features to track and how to analyse their persistence and quality through frames.

The Lucas Kanade feature tracking method is based on solving the displacement $(x + \Delta x, y + \Delta y)$ in the image between times t and $t + \Delta t$, where Δt is small. In order to estimate the optical flow, three assumptions are made. Firstly, that the intensities of points will look the same in each frame (brightness constancy constraint - equation 3.1). In addition to this, it is also assumed that points will move coherently with their neighbours (spatial coherency constraint) and that the motion will be small.

Brightness Constancy Constraint:

$$H(x, y, t) = I(x + \Delta x, y + \Delta y, t + \Delta t) \quad (3.1)$$

By calculating a Taylor series approximation of the image signal I (equation 3.1),

$$I(x+\Delta x, y+\Delta y, t+\Delta t) = I(x, y, t) + \frac{\delta I}{\delta x} \Delta x + \frac{\delta I}{\delta y} \Delta y + \frac{\delta I}{\delta t} \Delta t + \text{HigherOrderTerms} \quad (3.2)$$

the first order partial derivatives of the spatial and temporal coordinates can be used to reduce the unknown terms when higher order terms are presumed to be negligible and therefore ignored:

$$I(x + \Delta x, y + \Delta y, t + \Delta t) - I(x, y, t) = I_x \Delta x + I_y \Delta y + I_t \Delta t \quad (3.3)$$

which gives:

$$I_x u + I_y v + I_t = 0 \quad (3.4)$$

based on the assumption that any motion between two frames will be effectively zero.

The above equation 3.1, defines a single local constraint, at a single pixel, on the image. However, there are still two unknowns (u, v). To solve

this, additional equations are needed. The first stage of this solution involves the assumption that within a small neighbourhood area of pixels (p_i) of the point in question, displacement will be locally smooth and consistent between frames. By using a least squares regression model

$$\begin{bmatrix} u \\ v \end{bmatrix} = (A^T A)^{-1} A^T b \quad (3.5)$$

an approximation may be found and by implementing an iterative method, re-introducing the higher order terms previously disregarded. The values can then be refined and more accurate approximations made until convergence.

$$\begin{bmatrix} u \\ v \end{bmatrix} = \begin{bmatrix} \sum_i f(x)(p_i)^2, & \sum_i f(x)(p_i)f(y)(p_i) \\ \sum_i f(y)(p_i)f(x)(p_i), & \sum_i f(y)(p_i)^2 \end{bmatrix}^{-1} \begin{bmatrix} -\sum_i f(x)(p_i)f(t)(p_i) \\ -\sum_i f(y)(p_i)f(t)(p_i) \end{bmatrix} \quad (3.6)$$

Due to the local nature of this method of feature tracking, the method will fail if the motion is larger than the predefined neighbourhood area. This can be solved by applying the analysis at a number of pyramid levels. By decreasing the resolution of the image, windows containing the same number of pixels will account for larger areas. This coarse to fine method enables the detection of larger displacements within the image.

The feature selection criteria used during the implementation of a KLT tracker was determined in Tomasi and Kande (1991) [77]. Features are

selected based on whether they have significant change in intensities in both the x and y directions (corner features). This selection criteria is used to solve what is known as the aperture problem [79]. The aperture problem occurs when motion is viewed through a small aperture (such as the pixel neighbourhood used in Lucas Kanade optical flow calculations) in this case, motion of edges cannot be determined unambiguously, therefore corner features must be used.

By analyzing the eigenvalues of A, it can be determine whether the area of the image in question has the correct characteristics to be a 'good feature'. By selecting only corner features, the aperture problem is solved. This is because, at corners motion it easy to detect along both the horizontal and vertical axes. A corner feature is represented by

$$A = \begin{bmatrix} \sum_i f(x)(p_i)^2, & \sum_i f(x)(p_i)f(y)(p_i) \\ \sum_i f(y)(p_i)f(x)(p_i), & \sum_i f(y)(p_i)^2 \end{bmatrix} = \begin{bmatrix} \lambda_1 & 0 \\ 0 & \lambda_2 \end{bmatrix} \quad (3.7)$$

where A represents the sum of gradients in relation to the x and y coordinates within the window. There will be two eigenvalues (λ_1, λ_2) whose magnitudes represent the type of point. If both eigenvalues have large positive values, then the feature in question is a corner point. Selection criteria is based on whether the values of the eigenvalues associated with the feature point are greater than a predefined threshold:

$$\min(\lambda_1, \lambda_2) > \lambda \quad (3.8)$$

The KLT is a widely used method for analysis of motion in images and

is regularly applied to ultrasound images of skeletal muscle. However, in complex physiological systems and when using imaging modalities prone to noise it exhibits a number of limitations. For example fasciculations may be difficult to distinguish from the background noise due to their small scale. Also, as there is no way to differentiate between fasciculations and other physiological motion which may occur in the image. Additionally, the KLT needs image heterogeneity (i.e. good corner features) to perform well which, due to changes in muscle structure in neuropathies, may be reduced. To improve the accuracy of the technique, mutual information is used as an additional stage in the analysis to improve results; this method is expanded on in the below section.

Mutual Information for the Interpretation of the KLT Analysis Outputs

Using the above feature selection process and applying the Lucas - Kanade method of optical flow, motion between frames may be determined. In order to interpret these values and determine the presence of muscle twitches, the statistical process of mutual information was proposed to enable the differentiation of twitches, noise and other motion within the images [66].

Mutual information is a measure of the mutual dependence of two variables, X and Y (equation 3.9).

$$MI(X; Y) = \sum_{y \in Y} \sum_{x \in X} p(x, y) \log\left(\frac{p(x, y)}{p(x)p(y)}\right) \quad (3.9)$$

Where $P(x,y)$ is the joint probability distribution of X and Y , and $P(x)$ and $P(y)$ are the individual probability distributions of X and Y . In [9] it was hypothesised that the magnitude of the MI signal represents the likelihood of that US image transition containing a muscle twitch. High mutual information indicates movement coherence ($I \rightarrow \infty$), such as a twitch; low mutual information indicates noise or other random movement ($I \rightarrow 0$). If zero mutual information between two variables is found, it means the variables are independent [80].

Overall, MI is an effective way of distinguishing between the small scale coherent motions of fasciculations and the underlying noise of the image. However, it has been reported that this method is unable to distinguish between fasciculations and other physiological motion such as blood vessels as these too display coherent motion [9]. In order to successfully detect fasciculations without also detecting other motion such as blood vessel pulsations, alternative methods will be required.

3.2 Optical Flow Analysis

The KLT analysis used in studies for the identification of fasciculations in ultrasound images [9] are based on the Lucas Kanade method of optical flow [76]. Further methods for this application were also investigated to find an appropriate alternative technique for comparison. The search for new methods was conducted for the purpose of this thesis by investigating

an additional method of optical flow; Horn-Schunck optical flow (see Appendix 9.1).

Horn Schunck

The Horn-Schunck method of optical flow, like the Lucas-Kanade method, is a method to calculate movement within image sequences, providing constraints in relation to brightness patterns. Where Lucas-Kanade optical flow is considered a local method of optical flow calculation, due to the calculation of motions within local neighbourhoods. Horn-Schunck provides a much more global approach [81]. Only one independent measurement (u or v) is available from the image sequence at a point, while the flow velocity has two components, meaning, a second constraint is needed. In this case, this is known as the smoothness constraint, which can be represented by:

$$\left(\frac{\delta u}{\delta x}\right)^2 + \left(\frac{\delta u}{\delta y}\right)^2, \left(\frac{\delta v}{\delta x}\right)^2 + \left(\frac{\delta v}{\delta y}\right)^2 \quad (3.10)$$

The additional constraint or brightness constraint (see Section 3.1) can be expressed by minimising the square magnitudes of the gradient of the optical flow velocity.

$$\int \int (I_x u + I_y v + I_t)^2 + c(u_x^2 + u_y^2 + v_x^2 + v_y^2) \quad (3.11)$$

where c is the regularization constant, where larger values will lead to smoother flow. Once both constraints have been formulated, it is required that the sum of the errors are minimised through the equation:

$$e_{BC} = I_x u + I_y v + I_t \quad (3.12)$$

for the brightness constraint error and

$$e_{SC}^2 = \left(\frac{\delta u}{\delta x}\right)^2 + \left(\frac{\delta u}{\delta y}\right)^2 + \left(\frac{\delta v}{\delta x}\right)^2 + \left(\frac{\delta v}{\delta y}\right)^2 \quad (3.13)$$

for the smoothness constraint error. Therefore the combined error to be minimised can be written as

$$= e_{BC} + c e_{SC} \quad (3.14)$$

$$e = \int \int (I_x u + I_y v + I_t)^2 + c(u_x^2 + u_y^2 + v_x^2 + v_y^2) \quad (3.15)$$

The minimisation process requires suitable values for the optical flow velocity, u and v , to be found. By applying a laplacian mask and taking an average of the four neighbours and subtracting from the central one and

repeating the process until it converges, the minimization will be accomplished. The discrete version of smoothness error for each pixel may be written:

$$\begin{aligned}(I_x u + I_y v + I_t) I_x + c(u - u_a v) &= 0 \\ (I_x u + I_y v + I_t) I_y + c(v - v_a v) &= 0\end{aligned}\tag{3.16}$$

Solve using an iterative scheme starting with $k = 0$:

$$\begin{aligned}u^k &= u_{av} - I_x \left(\frac{I_x u_{av} + I_y v + I_t}{c + I_x^2 + I_y^2} \right) \\ v^k &= v_{av} - I_y \left(\frac{I_x u_{av} + I_y v + I_t}{c + I_x^2 + I_y^2} \right)\end{aligned}\tag{3.17}$$

where u^k and v^k are the velocity estimates for pixel (x,y) and u_{av} and v_{av} are the neighbourhood averages.

The Horn Schunck method provides a global optical flow method where the field is constrained by the local average as well as the optical flow constraints. It not only requires consistency between intensities in image sequences but also requires that changes be small providing smoothness within the flow field.

The Horn-Schunck optical flow method offers a different solution to the calculation of optical flow in contrast to the Lucas-Kanade method. Motion is calculated based on a more global analysis compared to the local neighbourhood based analysis of the Lucas-Kanade. However, it still does not offer the highly discriminatory motion analysis that would be required

to solve a number of the limitations stated in [9] (such as the inclusion of blood vessel pulsations) and be successfully applied to further muscles which may raise further issues such as breathing motion in trunk muscles and voluntary activation. In order to circumvent such issues, a more adaptive and discriminatory technique is required.

3.3 Foreground Detection Analysis

Gaussian Mixture Models

Mixture models are probabilistic models that represent subpopulations within overall populations. Foreground detection is a technique which allows foreground objects to be extracted from an image [82]. This method of image analysis is frequently used for applications such as the detection of people from CCTV images for the purposes of security and cars in traffic monitoring. It is based on the assumption that the background will be more frequently visible than any foreground events and that it has modes with narrow variance. For example image regions with a person or car moving across it will show large variations in pixel intensity in comparison to that of a wall or a road. In order to accurately detect objects of interest, especially in noisy or busy scenes, the application of a Gaussian Mixture Model (GMM) analysis requires a number of stages. Initially the model is built based on the data contained within a set of training frames, this is then used to assign pixels in subsequent frames to a specific distribution. Outliers are classified as foreground, with all others being assigned to the

background. A blob analysis can then be used to threshold the minimum size of groups of pixels or "objects", to remove smaller scale objects that may not be of interest.

The basis of the GMM is the assumption that every pixels intensity value in the image may be modeled using K Gaussian distributions (GMM) and each object that comes into view of a pixel is represented by a set of states. [83]. The probability that a pixel has a value of X_t at time t is given by:

$$p(X_t) = \sum_{j=1}^K w_{j,t} \eta(X_t; \mu_{j,t}, \Sigma_{j,t}), \quad (3.18)$$

where w_k is the weight parameter of the j^{th} Gaussian component $\eta(X; \mu_j, \Sigma_j)$ is the Gaussian distribution of the j^{th} component.

The Gaussian mixture model is defined as:

$$\eta(X_t, \mu, \Sigma) = \frac{1}{(2\pi)^{n/2} |\Sigma_k|^{1/2}} e^{-1/2(X_t - \mu_t)^T \Sigma_t^{-1} (X_t - \mu_t)}. \quad (3.19)$$

There is a mixture model for every pixel in the image and every new pixel value is compared against the existing K Gaussian distributions until a match is found. If none of the distributions match the pixel value, the least probable distribution is replaced with a distribution with the current

value as its mean, an initially high variance and low prior weight. The first B distributions are selected as background when:

$$B = \underset{j=1}{\operatorname{argmin}} \left(\sum_{j=1}^b \omega_k > T \right), \quad (3.20)$$

where the threshold T is the minimum amount of the image that should be accounted for by the background. This threshold is set as any pixel that is more than 2.5 standard deviations from the B distributions [83].

When a Gaussian component is matched models are updated in accordance with the equations:

$$\hat{w}_k^{N+1} = (1 - \alpha)\hat{w}_k^N + \alpha\hat{p}(\omega_k|x_{N+1}), \quad (3.21)$$

where α is the learning rate² and $1/\alpha$ is the time constant which determines the speed with which the parameters change.

The values for μ and σ distributions, when unmatched remain the same, but are updated when matched by:

$$\hat{\mu}_k^{N+1} = (1 - \alpha)\hat{\mu}_k^N + \alpha\hat{p}(\omega_k|x_{N+1}), \quad (3.22)$$

$$\hat{\Sigma}_k^{N+1} = (1 - \alpha)\hat{\Sigma}_k^N + \rho(x_{N+1} - \hat{\mu}_k^{N+1})(x_{N+1} - \hat{\mu}_k^{N+1})^T, \quad (3.23)$$

where

$$\rho = \alpha\eta(x_N + 1, \hat{\mu}_k^N, \hat{\Sigma}_k^N), \quad (3.24)$$

$$\hat{p}(\omega_k|x_{N+1}) = \begin{cases} 1; & \text{if } \omega_k \text{ is the first match Gaussian component.} \\ 0; & \text{otherwise.} \end{cases}, \quad (3.25)$$

Foreground objects are determined through analysis of the density distribution of foreground pixels using connected components [84]. Areas of foreground pixels of size above a given threshold are classed as foreground objects with all other, more sparsely distributed foreground pixels disregarded. This can be parameterised for the specific application of the GMM.

Due to the GMM analysis' robustness to noise and the ability to train it based on previous examples (i.e. frames), it is predicted it will be a successful technique for the detection of involuntary motion within ultrasound images. These motions tend to be random and sporadic, which are likely to appear as foreground objects due to the high variance in contrast to the image in general. Also with the GMMs ability to ignore small repetitive motions within the background scene [83], it is predicted that other physiological motion such as blood vessels will also be ignored.

3.4 Summary

The KLT algorithm for motion tracking when applied to ultrasound images has been used successfully in many different studies relation to skeletal

muscle. However, for the task of identifying small scale involuntary muscle activation, it is clear that this method has a number of limitations. For this reason, a new method (GMM) will be assessed for its suitability in the detection of fasciculations due to its ability to detect abnormalities within a scene. The following chapters will assess the GMMs suitability through comparisons with the KLT method as well determining its accuracy when compared to EMG. It is predicted that the GMM will offer improved accuracy in comparison to the KLT due to its robustness to noise, adaptability and non-reliance on heterogeneity of the image (i.e. corner features).

Chapter 4

Ultrasound Image-based Motion Analysis Techniques for the Detection of Muscle Fasciculations: Comparison of Computational Analyses with Manual Identifications

4.1 Introduction

This chapter introduces an alternative technique for the detection of fasciculations; the GMM approach (see 3.3), with the aim being to determine whether a more adaptive technique can outperform the only other technique found in the literature, using operator ID's as a truth signal. The

GMM offers a more adaptive technique which is robust to noise and able to ignore small scale repetitive motion. These features of the GMM are particularly pertinent to ultrasound image analysis due to the high levels of noise and presence of other physiological movements present in the image. Although the KLT/ MI combination can disregard the incoherent motion due to noise. However, other coherent motion such as voluntary activation and blood vessels will still appear in the signal (as reported in [9]). It is predicted that, for the aforementioned reasons the GMM will provide for a more suitable analysis technique.

In skeletal muscles, fasciculations are spontaneous, intermittent, involuntary contractions of muscle fibres [85]. Although fasciculations can occur in healthy individuals, their frequency, morphology and presence across multiple muscles throughout the body can be an indicator of neuromuscular disorders such as Motor Neurone Disease (MND) [16].

Standard clinical diagnostic techniques for the detection of fasciculations involve the insertion of needle electrodes into the muscles to detect the electrophysiological potentials associated with fasciculations (i.e. fasciculation potentials - see Section 2.1.2). However a number of studies have demonstrated the use of ultrasound imaging as a more sensitive, less invasive alternative [5], [86].

B mode ultrasound is a medical imaging modality with good spatial and temporal resolution. This allows for the collection of greyscale images of internal structures in close to real time, from the skins surface. Studies such as [65] and [6] have investigated the viability of ultrasound for de-

termining the presence of fasciculations when compared to human operator identifications. [6] examined the echo intensity of 12 different muscle groups, whilst simultaneously screening for fasciculations. The combination of these two measures produced sensitivity and specificity values as high as 96% and 84%, respectively, when distinguishing MND and MND mimics.

Although operator identifications of fasciculations in ultrasound images deliver promising results, a number of drawbacks exist with this method. For example, the requirement of the assessment of large numbers of ultrasound image sequences by human operators can be time consuming and requires high levels of operator concentration. This may become problematic if ultrasound was to be introduced as a clinical diagnostic technique.

To address the issues of manual identifications, other studies such as [9], applied computational analyses (Kanade Lucas Tomasi (KLT) feature tracking with Mutual Information (MI)) to ultrasound images to provide an automated method for fasciculation detection. In contrast to previous studies, manual identifications were based on each fasciculation event, rather than classifying image sequences based on the presence or absence of fasciculations. These also yielded high levels of accuracy (ROC - area under the curve [87]), with results of 88-94% in healthy participants and 83-84

Although results from the automated analysis were high, variability was noted between muscles and between healthy and MND images, with accuracy decreasing by as much as 11 percentage points in MND affected participants. This may be due to a number of limitations associated with

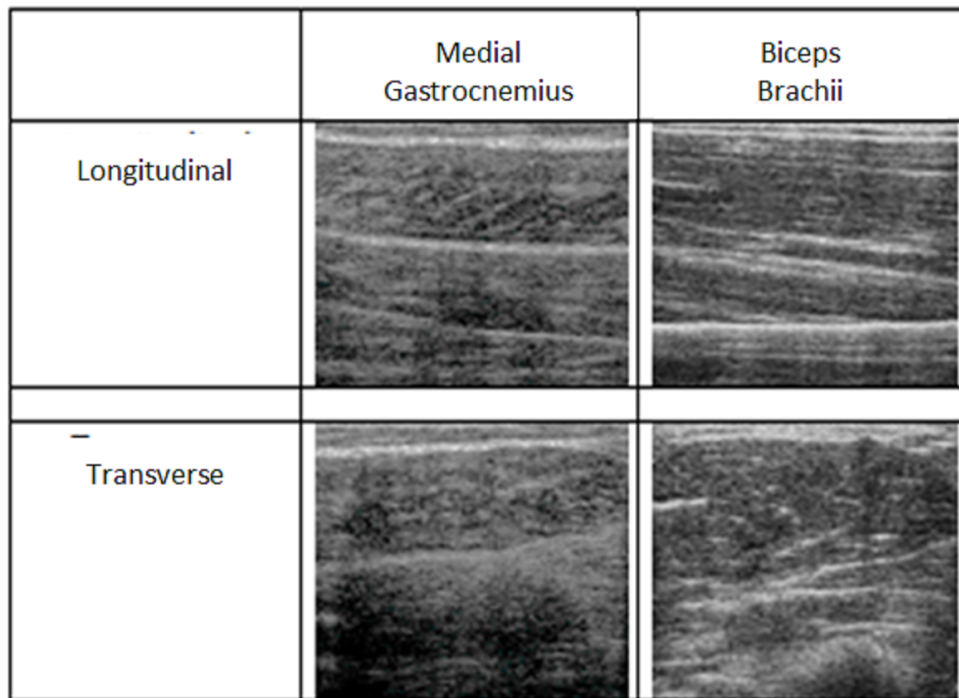


Figure 4.1: Examples of ultrasound images collected in each muscle (MG and BB) and each probe orientation (Longitudinal and Transverse), demonstrating the diversity of image content.

the KLT and MI. Firstly, the KLT analysis requires heterogeneous structure within the image to perform well (i.e clear definition between anatomical features of the muscle [78]). Such structure is evident in a longitudinal probe orientation (along the long axis of the muscle) but is not so defined in transverse orientations, meaning that probe orientation relative to the muscle could significantly affect algorithm performance. This problem can be circumvented by ensuring great care is taken during probe placement, however, this may be difficult to regulate if the approach were to be used more widely (e.g. in the clinic). A change in muscle structure is also experienced due to MND [88],[53], this may have been the cause of a reduction

in accuracy levels seen between healthy and MND muscle [9]. Other physiological movements (blood vessels) were also detected by the KLT and not disregarded, as the calculation of MI of the displacement values peaks during coherent local movement, which a blood vessel pulsation appears as within an ultrasound scan. In order to overcome issues highlighted in previous studies and implement a more selective process for image motion, an adaptive algorithm is required.

Hypothesis: The GMM will offer improved accuracy when compared to a human operator identification truth signal due to its robustness to noise and more adaptive nature. This will yield an alternative method to the KLT, less prone to false positives due to other physiological motion within the ultrasound image sequences.

4.2 Methods

Participants and Data Collection

The dataset used within this chapter was all previously collected as part of the Harding et al. (2016) study [9] and was a separate dataset to that used in Chapters 5, 6 and 7. An outline of the original data collection protocol is noted below.

US sequences were collected from 20 healthy participants (10 female, 10 male, 33 ± 13 years, 172 ± 8.6 cm, 73 ± 21.8 kg), recruited from the general population; and five MND affected participants (two female,

time since diagnosis: 3–18 months, 61.7 ± 15.7 years, 170.67 ± 6.03 cm, 75.33 ± 14.74 kg), recruited through the Motor Neuron Disease Care and Research Centre at the Royal Preston Hospital. All participants provided informed consent, and the study was approved by Ethics committees at Manchester Metropolitan University and Preston Royal Hospital. Ultrasound image sequences were collected (75 fps) from two muscles: the biceps brachii (BB) in the upper arm and the medial gastrocnemius (MG) in the lower leg. During data collection from the BB, participants were in a seated position with their left arm supported in a relaxed position on a bench, which was approximately shoulder height. The linear probe (7 MHz, 59 mm field of view, LogicScan 128, Telemed Ltd., Lithuania) was coated in acoustic gel and placed parallel to the long axis of the muscle (longitudinally). When studying MG, participants lay prone on a treatment couch, with their legs fully extended. The US probe was placed centrally in the muscle belly region of the MG. It was requested that participants remained as still as possible during data collection. Two trials of duration 40s were collected in each of the two muscles.

Operator Identifications

This chapter reproduces the methods used in [9], with the addition of the alternative GMM analysis for comparison.[9] compared a KLT/ MI analysis of ultrasound images with human operator ID's compiled by two separate operators and then combined using the union and intersection of the ID's.

Muscle twitches were defined as localized displacement of tissue [89].

The manual ID truth signal consisted of the frame number at which each twitch was identified as starting. Each sequence was viewed on a frame-by-frame basis using video editing software (VirtualDub 1.10.4). Operators viewed ultrasound sequences on a frame by frame basis and once tissue displacement was visible, recorded the frame number, which were to be compared with the computational analyses.

For the purpose of this study, only one (the operator with the greatest levels of accuracy) of the two operators ID's were used . In [9], out of the two operators, operator A consistently delivered higher accuracy levels when compared to the KLT analysis, therefore it is their identifications that will be carried through as the truth signal for this study. However, operator B's accuracy values were always within 2 percentage points of operator A and the intersection values being within 3 percentage points of both operators. This indicates that although A gave greater agreement with the KLT, B was generally consistent with A.

Extensive calibration of the KLT and GMM techniques was carried out to determine the optimal parameters for each muscle (see Appendix 9.1). For this purpose, data from a subset of five, randomly selected, healthy participants (not necessarily the same 5 used in [9], 3 female, 2 male) were used for the purposes of calibration. These participants were then removed from data set. The KLT analysis was parameterised based on the MI bin sizes relating to speed and direction of motion (as in [9]) and the GMM, which had a far more extensive parameterisation stage was calibrated based on the number of Gaussians, background area, learning rate and blob size. This was done for each individual muscle (see Appendix

9.1) - Table 1 and 2.

Application of Computational Analyses

KLT and GMM algorithms were implemented in Matlab 2013, using the computer vision toolbox. The KLT analysis (as in [9]), was initialised by reading in the image frame and overlaying an 80 x 100 Lucas Kanade feature grid to track on a frame by frame basis. The resulting displacement values (magnitude and direction of displacement of each feature) were then used to calculate the MI of the resulting values to distinguish coherent from random movement. A windowing factor of 5 was also applied to improve the signal to noise ratio of the KLT signal, as described in the original paper. This compared every n th frame to frame $n+5$.

The GMM analysis was also applied to the same data set for comparison. The GMM works on the assumption that the background will be more frequently visible than any foreground events and that pixel intensities will have low variance (As described in Section 3.3). A model of the background is built based on the predetermined number of training frames. This model reflects the mixture of Gaussian distributions that are based on each pixels intensity value. Pixels that fall within a given threshold (2.5 standard deviations) are classified as background and pixels that do not match with the background are classified as foreground pixels. Foreground objects, or groups of foreground pixels large enough to be above a set threshold are then used to highlight areas of interest in the image. Five hundred training frames were selected from the start of each image sequence to form the

model to which the remaining 2300 frames were compared.

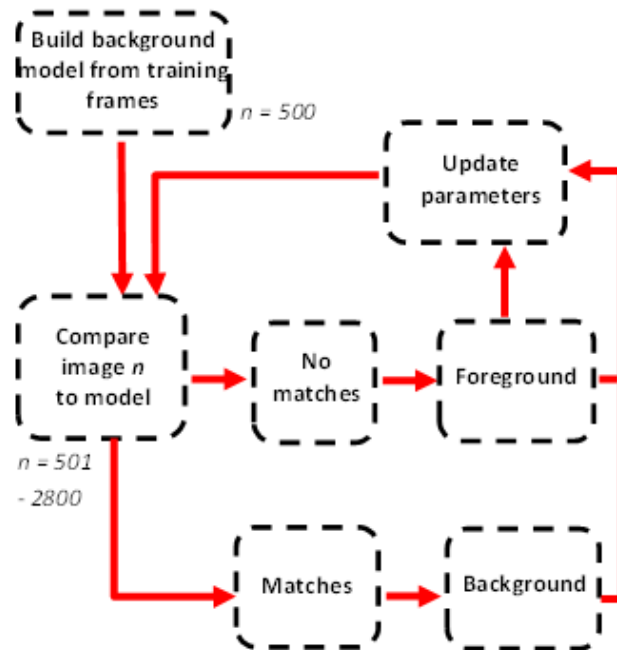


Figure 4.2: Flowchart showing major steps in the GMM Analysis.

Statistical Analysis

Once both the motion analysis signals and the logical ID's had been obtained, statistical analyses in the form of Receiver Operator Characteristics (ROC's) were performed [87]. ROCs produce a curve which allows for the assessment of accuracy between a signal and a binary classifier, at different thresholds, by comparing the sensitivity (number of true positives) and $1 - \text{specificity}$ (number of true negatives). The area under the curve (AUC) is used to quantify accuracy for comparison, where AUC give the

accuracy of a technique as a percentage. Individual ROC curves showing the performance of each technique across muscle types and probe orientation and combined curves, showing differences in accuracy between all data in the healthy control group and all data in the MND affected group were produced.

4.3 Results

ROC Curves indicating the agreement between the two image analysis approaches and operator identifications are shown in Figure . Accuracy levels varied dependent on the conditions and the method of analysis used.

Both the GMM and the KLT produced good percentage agreements throughout all conditions, with all results over 82%, with the accuracy reaching almost 94% when applying the GMM to healthy muscle.

Results for the GMM showed accuracy of 93.64% (Healthy) and 88.16% (MND) in the BB and 93.85% (Healthy) and 88.68% (MND) in the MG. In contrast, the KLT achieved accuracy of 91.01% (Healthy) and 82.37% (MND) in BB and 88.53% (Healthy) and 84.17% (MND) in BB (See Table 4.1). A reduction in accuracy for the MND affected muscle was noted across all trials, with differences of between 4.36 percentage points in the MG (KLT) and 8.64 percentage points in BB (KLT). The GMM delivered results within 1 percentage point between muscle groups, indicating a robustness to changes in the structural differences present in images of different muscles. A change in muscle caused changes in accuracy of

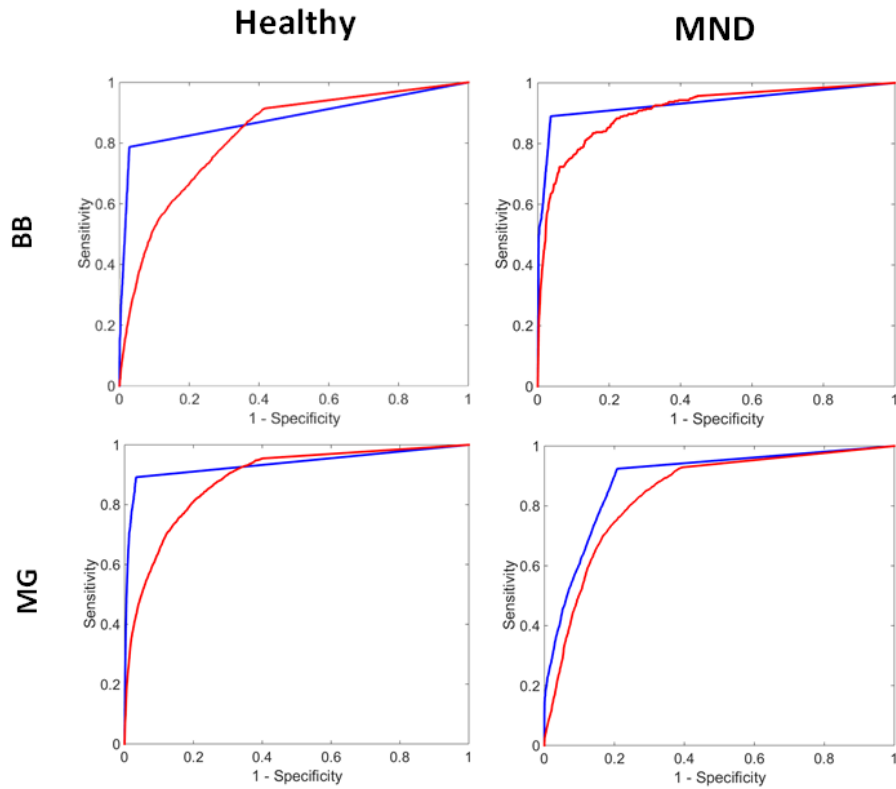


Figure 4.3: ROC curves of GMM (Blue) and KLT (Red) analysis approaches in BB (Top) and MG (Bottom) in healthy (Left) and patient (Right) populations when compared with the manual identification truth signal.

between 1.80 and 2.48 percentage points between the BB and MG results.

4.4 Discussion

This chapter investigated how a GMM approach would perform in comparison to a previously tested KLT/MI analysis in the identification of fascic-

	MG		BB	
	LONG	CROSS	LONG	CROSS
GMM	93.85	93.64	88.68	88.16
KLT	88.53	91.01	84.17	82.37

Table 4.1: Agreement results for healthy participants (In Percent%) in MG and BB for healthy and MND affected participants.

ulations in ultrasound images when using operator identifications as truth signals. To our knowledge this is the first time a foreground detection approach has been applied to analyse ultrasound image sequences.

KLT Performance

However, the KLT results achieved fell short of those reported in [9], which reported levels of accuracy of a similar level to the GMM in healthy data (94% in the BB and 93% in the MG). This implementation only achieved accuracy levels of 91% in BB and 89% in MG. However, the MND affected results were comparable, with this study reporting accuracy levels of 82% in the BB and 84% in the MG and [9] reporting accuracy levels of 83% in the BB and 84% in the MG (see 4.3 and 4.1).

The differences in the healthy results (KLT) is likely due to the randomisation of participants during the parametersation stage. All participants included in the parameterisation were selected randomly and independent of the initial parameterisation conducted in [9]. As this implementation was constructed independently of the original implementation and as

it is unknown the exact participants used for calibration of the technique, differences in results were highly likely. Measures for speed and direction of motion deemed optimal varied between studies. In [9] as 8 and π for magnitude and direction of motion in the BB and 2 and $\pi/2$ for MG. In contrast, this study found optimal parameters of 1 and $\pi/8$ for magnitude and direction in BB and 1 and $\pi/4$ for MG.

GMM Performance

Results showed consistently higher accuracy obtained using the GMM analysis approach in comparison to the previously reported KLT/MI approach, with results sitting between 88 and 94%. Overall, the GMM was more robust to changes in muscle type and the existence of pathology, however, both analysis methods showed reductions in accuracy between healthy and MND affected participants.

The higher results achieved by the GMM may be explained by its more selective approach to motion detection. Although the KLT/MI analysis attempts to provide a more selective approach by minimising motion with low coherence, such as noise, it cannot discount other physiologically based movements in the image such as blood vessel pulsation.

Limitations

Lower values of accuracy for MND affected data for both analyses techniques is likely attributed to the drastic changes that the muscle experiences during MND and how these are exhibited within the images. These changes, such as increased echogenicity and image homogeneity may affect the performance of tracking techniques such as the KLT, which heavily relies on the presence of "trackable" features. Further from this, although the GMM did outperform the KLT, it underperformed in relation to the results obtained from healthy data. Although this method does not rely on corner features for tracking as the KLT does, it is also known to struggle in images of low contrast [90]. In addition to the limitations of the image analysis, there are also a number of issues with the current truth signal. Firstly, it has no clinical significance in relation to fasciculation detection/ diagnosis and ID's cannot be confirmed to be fasciculations over other motions within the muscle. In addition to this, as they are subjective assessments made by human operators, their quality as a truth signal may be dependent on variables such as skill level, fatigue, presence of distractions etc. In order to provide further assessment of computational analyses of ultrasound images for the detection of fasciculations, additional truth signals should be considered.

4.5 Conclusion

Overall, the GMM analysis provided the highest levels of accuracy when compared to operator identifications as a truth signal. The KLT underperformed in comparison to the GMM, however, previously reported values for the KLT were comparable with the accuracy levels achieved with the GMM.

Further work should be carried out to investigate additional truth signals to further test the viability of computational analysis for fasciculation detection as although operator identifications can provide a proof of concept, it would be difficult to apply this method to large scale analysis due to the time commitment required for operator analysis of each video. In addition to this ID's have no physiological basis and are simply another measure of what is occurring in the ultrasound images. To add further credence to the computational analyses, comparisons should be made to myoelectric data as the standard clinical test. This would allow for a greater level of certainty that positive identifications made using computational analysis were fasciculations and not any other types of motion.

Chapter 5

Ultrasound Image-based Motion Analysis Techniques for the Detection of Muscle Fasciculations: Comparison with Intramuscular Electromyography

5.1 Introduction

This chapter introduces an alternative truth signal for comparison with the two previously used techniques; the GMM and KLT/ MI approaches (see Chapter4), with the aim being to determine which technique offers greater accuracy in comparison to a clinically relevant truth signal, which has not

previously been tested. A secondary aim of which technique shows more consistent accuracy across different muscles and probe orientations will also be explored.

Muscle fasciculations are one of a number of indicators of denervation of muscle tissue and the possible presence of neuromuscular diseases such as MND. The reliable, objective detection of fasciculations has long been sought after as a possible alternative to current diagnostic methods, which are currently based on clinical and electrophysiological assessments (see 2.1 and Figure 2.1). These assessments have long been criticised in terms of accuracy and certainty of diagnosis [91] and tend to be relatively invasive with the requirement of the insertion of needle electrodes into the muscle to record the electrical activity across the muscle membrane.

Hypothesis: The GMM will offer greater accuracy over the KLT when compared to a intramuscular EMG truth signal due to its robustness to noise and more adaptive nature.

Current Methods for the Detection of Fasciculations in Ultrasound Images

The idea that ultrasound images can allow for the visualisation of fasciculations as they appear in muscle tissue has existed since it was first tested in [44]. More recently, the use of ultrasound imaging for diagnosis has been investigated, with specific focus on MND. Initially using human operators to determine whether fasciculations were present or absent in

images sequences of various muscles [65], [6], [9] (see 2.3.3 and 4.1). This technique was found to be more sensitive than the current detection method of intramuscular EMG [5]. However, a number of problems exist with this method. Firstly this analysis method is very time consuming and would likely require large numbers of operators if it were to replace the current diagnosis methods. Large numbers of operators would introduce variations in image interpretations between operators (as it is a very subjective approach) and would also require any costs associated with the training of operators for the task.

A computational analysis was introduced [9] in an attempt to avoid the potential problems that would be encountered with human operator identifications and to provide an automated approach as an alternative to the time consuming, subjective human operator analysis. An automated analysis would provide a fast, objective method for the identification of fasciculations in ultrasound imaging. [9] was able to apply a combination of KLT/MI algorithms (see Section 3.1) to produce high agreement (between 83% and 94%) with operator ID's, however a number of potential limitations were highlighted such as the inclusion of motion due to blood vessels and other physiological motion within the MI signal and the decrease in accuracy between healthy and MND affected participant data. This was also confirmed in Chapter 4.

The GMM for the Detection of Fasciculations in Ultrasound Images

GMM analysis of ultrasound images offers a more adaptive method for fasciculation detection than the KLT and remains an automated, objective

technique in contrast to manual ID's. It is used to classify the image into foreground and background pixel, it operates on the assumption that the pixel intensities of the background of the image will vary significantly less between frames (see Section 3.3). In Chapter 4 the GMM was shown to outperform the Matlab implementation of the KLT (see 4.1) and was comparable to KLT results reported in [9]. However, as the GMM and KLT were compared to operators ID's which is not an infallible truth signal and has no clinical basis To improve the assessment of the accuracy levels of the GMM and KLT techniques for fasciculation detection an additional, more clinically relevant truth signal is required. For this purpose, intramuscular EMG is suggested.

Introduction of Intramuscular EMG as a Truth Signal

EMG is a method used to record the electrophysiological activity occurring within the muscle (see Section 2.1.2). Intramuscular EMG, which requires the insertion of a needle electrode into the muscle tissue is the current gold standard technique used in the diagnosis of certain neuromuscular disease, such as MND. It is proposed that EMG would offer a more objective truth signal for comparison with the GMM and KLT and would provide a level of certainty that all events indicated by the automated analyses are definitely fasciculations, which operator ID's cannot.

This chapter will again assess the accuracy of the GMM and KLT analyses, but using simultaneously collected EMG as a novel truth signal for comparison. The aim is to further validate the automated analyses tech-

niques for the detection of fasciculations, whilst also determining if either technique shows superiority over the other. It is predicted that as in chapter 4 the more adaptive GMM analysis will outperform the KLT and show more robustness for changes in image content (i.e. that may occur due to pathology and in different muscle types etc.)

5.2 Methods

Participants

Twenty patients, who had previously been diagnosed with MND (59 ± 14 years, 174.8 ± 9.2 cm, 86.8 ± 13.2 kg, 1078 ± 1148 days since diagnosis) were recruited through Royal Preston Hospital. Twenty self-declared healthy controls, who were free from any neurological disorders (54 ± 20 years, 168.8 ± 11.4 cm, 79.0 ± 18.1 kg), were also recruited from staff and students at Manchester Metropolitan University and the general population for comparison. The study was approved by both the Local Ethics Committee in Faculty of Science and Engineering at Manchester Metropolitan University and the National Research Ethics Service Committee; written consent was obtained from all patients and healthy controls prior to their inclusion in the study in accordance with the WORLD Medical Association Declaration of Helsinki (2008). In any cases where patients were not physically able to write on the consent form (due to disease symptoms), verbal consent was given for a witness (independent of the research team) to sign on their behalf.

Experimental Protocol

Ultrasound and myoelectric data were collected from the MG, a muscle with oblique (pennate) fascicle alignment relative to the long axis of the muscle and BB a muscle with fascicles arranged in parallel. The limbs to be tested were rested on supports placed under the ankle and the knee during assessment of MG and under the forearm for BB assessment. This provided access to the muscles, while ensuring the limb and patient in general, remained relaxed. To minimise infection risk, the ultrasound probe was inserted into a sterile glove prior to the start of the data collection and sterile ultrasound transmission gel was used as the intermediary between skin and probe.

Ultrasound image sequences (approx. 82 fps) were collected using a linear probe (8 MHz frequency, 59 mm long, LogicScan 128, Telemed Ltd, Lithuania). The probe was manually held in position, alongside a concentric needle electrode (Teca 37mm length, 0.46mm diameter), which had been inserted into the muscle by an experienced clinician (Dr. N. Combes). Two 35 second trials were collected this duration of data collection, the trial duration of 35 seconds was chosen so that it was in line with the literature [9] and were largely dictated by the length of time both researchers and participants could remain still and comfortable for. It has been reported that between 90 seconds and five minutes to collect the amount of EMG data required to detect [92], which is why multiple trials were recorded. In addition to this, the needle electrode was placed prior to the placement of the probe, with fasciculations and/ or other electro-

physiological activity generally being observed prior to ultrasound image acquisition. The ultrasound probe was/ positioned in either longitudinal or transverse orientations relative to the long axis of each muscle. During the trials participants were asked to remain as still and relaxed as possible. Ultrasound and myoelectric data collection was initialized simultaneously using the rising edge trigger output from the ultrasound device. Myoelectric signals were collected at 48 kHz using the Matlab 2013 data acquisition toolbox and a USB data acquisition device (X Series-USB 6341, National Instruments, USA). Myoelectric data were amplified (x1000) using a Dantec Keypoint Classic system or a Grass Amplifier (x 1000) for MND affected and healthy participants, respectively (Figure5.1).

Myoelectric Signal Processing

Prior to comparison between the myoelectric and ultrasound derived data, a number of pre-processing steps were completed. All myoelectric signals were bandpass filtered (4th order Butterworth, 30-500 Hz cut-off), to remove any non-physiological noise. Voluntary activation, defined as the repeated, regular firing of individual motor units, was evident in some recordings. These were identified using a freely available Matlab add on software (EMGLab 1.03) and removed from the original signal using template matching, leave the sporadic, involuntary fasciculation potentials [93].The template matching technique removes action potentials of the same shape within a certain time frame, meaning that voluntary activation, showing repetitive activation of the same motor units (which display the same shape

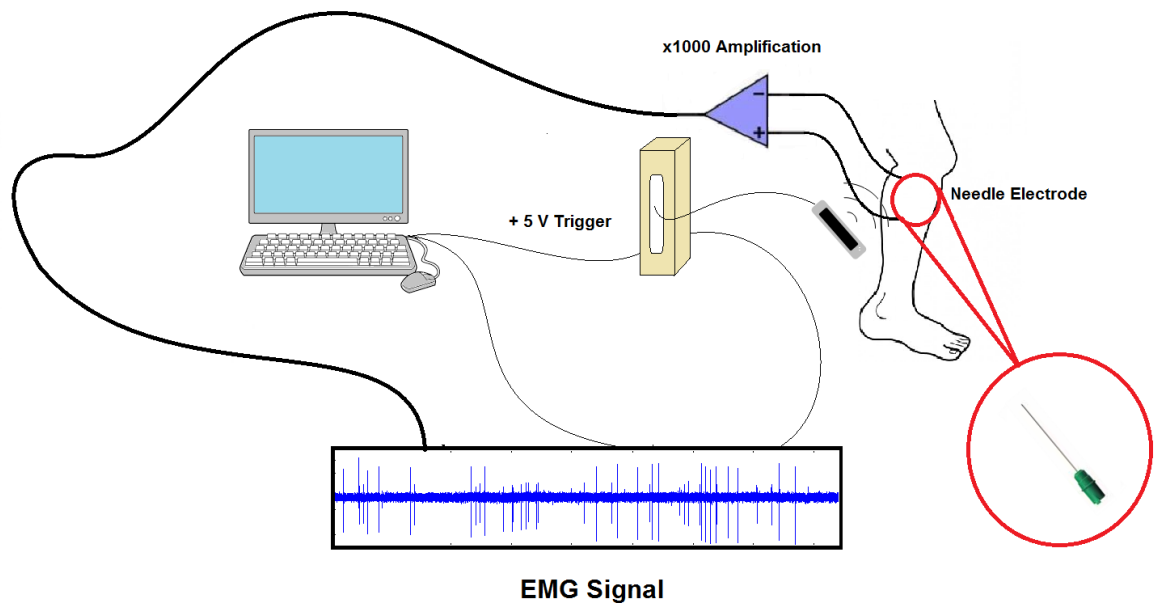


Figure 5.1: Overview of Experimental Set-up

action potential) can be removed leaving sporadic fasciculation potentials. These results were also confirmed through visual inspection of the final signals.

Although the literature has many methods for the segmentation of voluntary activity within an EMG trace, there is very little that addresses the identification of periods of sporadic, involuntary activity. For the purpose of this study, Periods of involuntary activity were identified using thresholding methods:

$$n(\text{mean}(\text{abs}(x))), \quad (5.1)$$

The optimal threshold was calculated using multiples (n) of the absolute mean of the signal (x), which were compared to the original signal using a receiver operator characteristic (ROC) (see Section 4.2) to maintain an accurate representation of the original signal but in binary form (1 being activation, 0 being quiet periods) (Figure 5.2). To identify an appropriate threshold for the collected data set, thresholds were applied to approximately one third of the healthy participant group ($n = 7$), who were randomly selected and not included in the final analysis. The number of parameterisation participants were increased from 5 to 7 from the previous chapter, due to the increased standard deviation of the age of participants from ± 13 years to ± 20 years. As increased age can have a major impact on the image content, a larger number of participants to parameterise the technique was considered to be the best option to account for the increased spread of the data.

A logical signal was produced classifying all activity above the threshold as one and all below the threshold as zero. The value of X that produced the maximum accuracy levels between the logical signal and the myoelectric signals was used as the standard value across signals from all participants (Figure 5.3). This value allowed the maximum number of fasciculations to be included, while rejecting peaks at levels which are likely

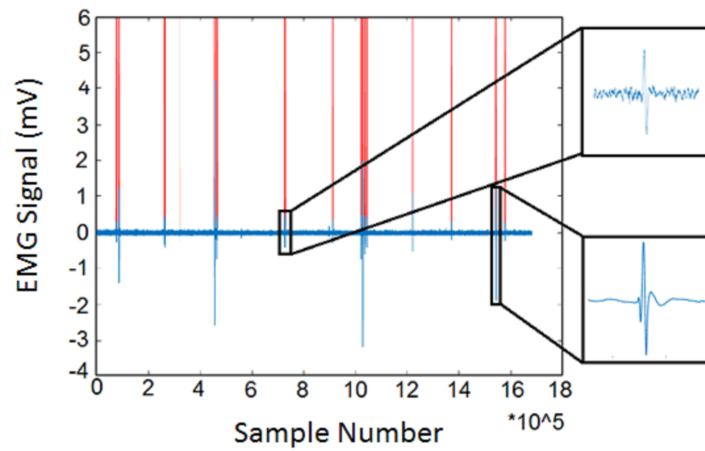


Figure 5.2: Example myoelectric signals showing fasciculation potentials (Top left). Red lines indicate position of fasciculation potentials identified using the describe threshold technique. Two identified potentials are shown in detail on the right.

to be noise (Figure 5.2).

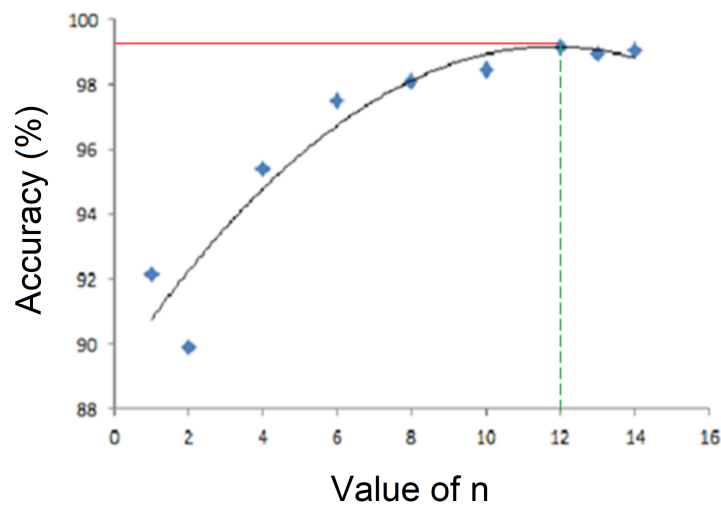


Figure 5.3: Plot of accuracy calculated by thresholding myoelectric signals by method given in Equation 5.2. Plateau point shown by red line and value of X taken forward to analysis stage shown by green dashed line.

Image Sequences and Motion Tracking

KLT and GMM analysis were parameterised and implemented as described in Chapter 4.2. Prior to analysis, images were manually cropped to the lower aponeuroses of the superficial muscle (i.e. gastrocnemius or biceps brachii) in order to remove any muscles deep to those containing the EMG needle. Due to the relatively large pick up area of the ultrasound, images tended to contain multiple muscles (e.g. biceps brachii and brachialis in the arm, gastrocnemius and soleus in the leg). As the myoelectric activity is not conducted through separate muscles, any fasciculations appearing in muscles deep to the ones containing the EMG needle, would appear as false positives, despite not necessarily being so.

Statistical Analysis

Myoelectric based fasciculation potentials and physical twitches represented in the ultrasound data occur over very different timescales (e.g. approximately 10 ms [4] for fasciculation potentials and 500 ms [44] for twitch contraction in MG). This would cause an underrepresentation of the signal accuracy without any additional processing of results. Therefore, to ensure fair comparison, the start and end of each twitch peak in the ultrasound derived signals were determined by locating the points at which the peaks fell below the noise level and compared to the fasciculation potentials in the myoelectric signals. If a fasciculation potential occurred within the time period between the start and end of the twitch, then the logical

myoelectric signal was adjusted so the whole twitch time frame was classified as a positive event. This was based on the methodology used in [9].

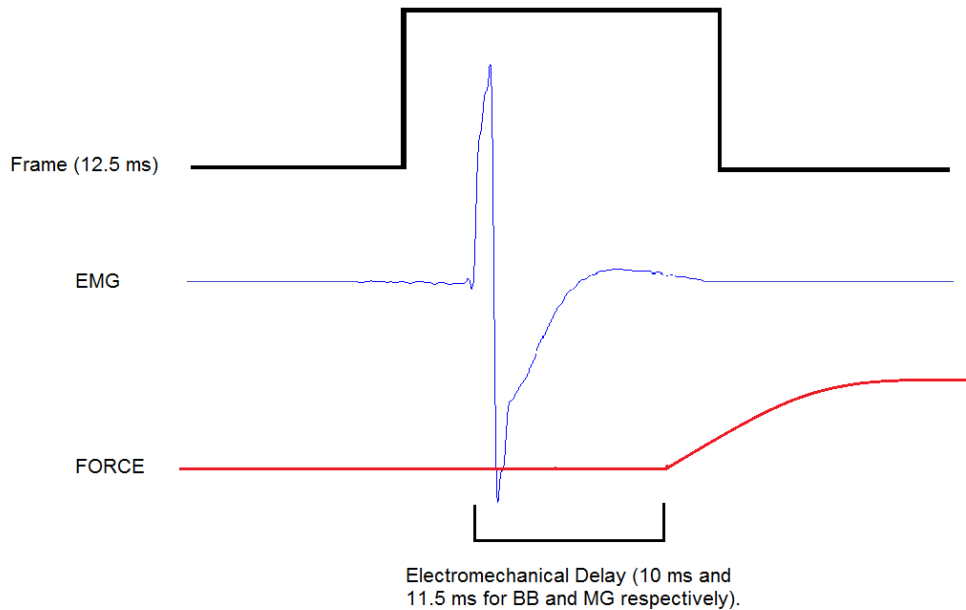


Figure 5.4: Figure showing comparison of EMG signal (blue), muscle force (red) and frame length (black).

The frame rate displayed on screen for the ultrasound was an average value, with the exact individual frame times being variable. The approximate frame rate given by the ultrasound was 80 fps, giving an average frame length of 12.5 ms. The GMM and KLT signals were interpolated based on the exact frame times output at the end of each data collection so that a direct comparison with the EMG signals could be carried out. In addition to this there was a 30 ms (approximately 2.4 frames) delay between the initiation of the trial and the collection of ultrasound data. In addition to the constant to the ultrasound frame collection delay, there are also

electromechanical delays between electrophysiological activity and force production. As the EMG signal and ultrasound images were sampled differently, comparisons were made by classing the entirety of the frame where fasciculations were present as active. The frame duration at 80 fps was higher than the electromechanical delay; approximately 10 ± 2.09 ms [94] and 11.5 ± 1.51 ms [49] in the BB and MG, respectively, even if a fasciculation were to occur at the end of a frame the total disparity between the two signals would be no more than 1 frame. This potential disparity along with a constant delay in the ultrasound frame collection was accounted for by offsetting the EMG activity signal by three frames.

Once both the motion analysis signals and the logical myoelectric signals had been obtained, statistical analyses in the form of ROC's were performed [87]. ROCs produce a curve which allows for the assessment of accuracy between a signal and a binary classifier, at different thresholds, by comparing the sensitivity (number of true positives) and $1 -$ specificity (number of true negatives). The area under the curve (AUC) is used to quantify accuracy for comparison. Individual ROC curves showing the performance of each technique across muscle types and probe orientation and combined curves, showing differences in accuracy between all data in the healthy control group and all data in the MND affected group were produced.

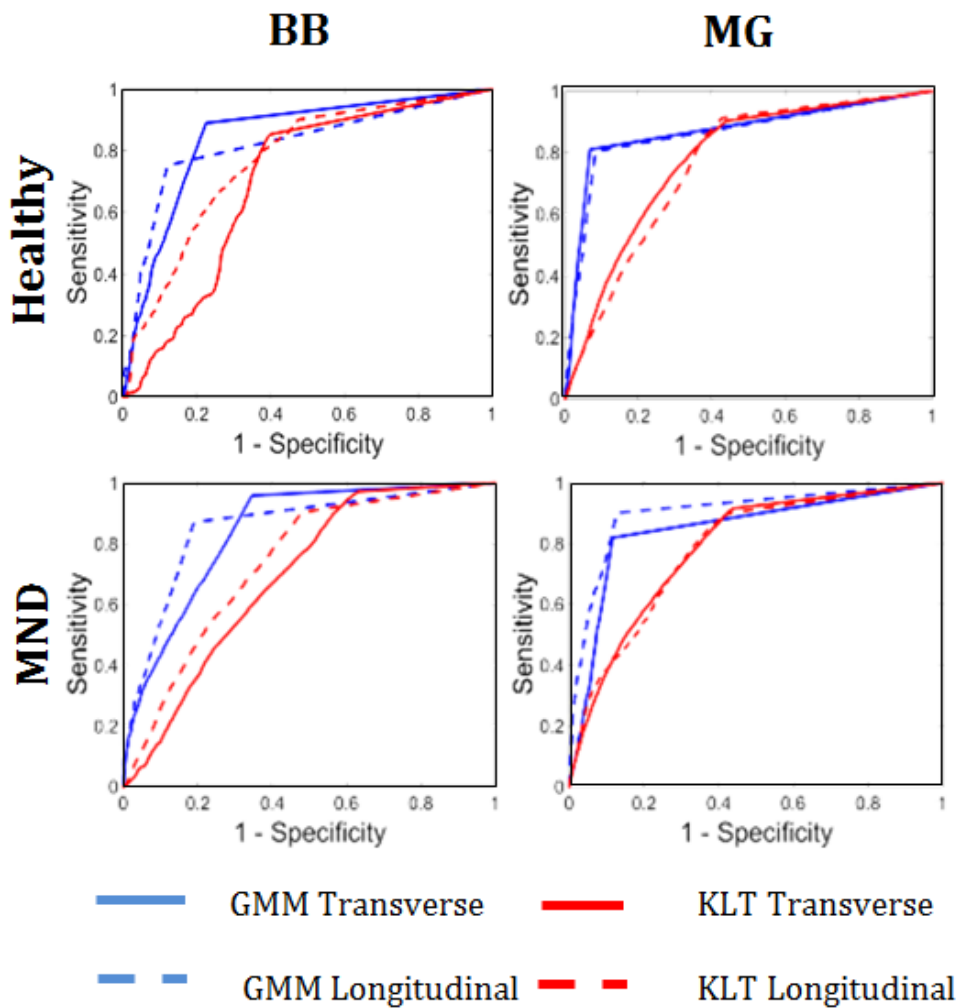


Figure 5.5: ROC curves of GMM (Blue) and KLT (Red) analysis approaches in BB (Left) and MG (Right) for different probe orientations (Transverse: Solid line, Longitudinal: Dashed line) in healthy (Top) and patient (Bottom) populations when compared with the myoelectric truth signal.

5.3 Results

Results from Healthy Data

ROC Curves indicating the agreement between the two image analysis approaches and the myoelectric data and the accuracy in different muscles

and probe orientations are shown in Figure 2.8. The levels of agreement varied greatly between conditions and the method of image analysis used.

The GMM produced good percentage agreements throughout all conditions, with most achieving results between 82 and 85%, with the exception of the healthy MG longitudinal condition, where accuracy reached 90.31%. The difference between probe orientation results in BB were approximately 2.14 percentage points (82.36% for longitudinal and 84.50% for transverse), but increased to nearly 5 percentage point difference in MG (90.31% for longitudinal and 84.91% for transverse).

The opposite was true for the KLT/MI, where the highest levels of agreement occurred in the analysis of the MG, with an accuracy of 78.42% and 78.80% for longitudinal and transverse probe orientation, respectively. This was 3.56 percentage points less than the lowest result from the GMM. The KLT/MI also had greater variation in results between probe orientation and muscle type. Although agreement remained reasonably constant between probe orientations in MG, decreases in accuracy of between 6.59 and 4.52 percentage points were noted in BB for unaffected and MND affected muscle. Agreement was also lower in BB when compared to MG overall, with highest agreement levels in MG reaching 78.19% in contrast to highest agreement levels in BB at 75.99%..

A small number of trials were not taken through to analysis due to file corruption of the raw data in either the EMG or ultrasound files. The total number of trials collected and the number then taken forward to analysis can be seen in Table 5.2.

	MG		BB	
	LONG	CROSS	LONG	CROSS
GMM	90.31	84.19	82.36	84.50
KLT	78.19	75.07	75.99	72.10

Table 5.1: Area under Curve of ROC Results for Healthy Participants

	Long		Trans	
	Num. of Trials Collected	Num. of Trials Analysed	Num. of Trials Collected	Num. of Trials Analysed
MG (n = 19)	38	34	38	36
BB (n = 19)	38	36	38	36

Table 5.2: Number of Trials Taken Forward to Analysis (Healthy Participants)

Results from Motor Neurone Disease Affected Data

The results from MND affected participants showed a similar pattern to the unaffected group. The GMM gave overall accuracy levels of between 84.05% and 86.21%. Between the MG and BB, changes in accuracy were between 0.41 and 7.94 percentage points and probe orientation caused variations in accuracy of between 0.84 percentage points in the MG and 3 percentage points in the BB.

In contrast the KLT/MI again gave results below 80%, with the best accuracy achieved in the MG transverse probe orientation (79.83%) and the lowest in the BB transverse probe orientation (70.79%). Changes in muscle yielded changes in accuracy between 9.04 and 0.96 percentage points and variations in probe orientations gave differences in accuracy of 3.72 and 4.36 percentage points for MG and BB, respectively.

	MG		BB	
	LONG	CROSS	LONG	CROSS
GMM	86.21	87.05	85.41	84.05
KLT	76.1	79.83	70.79	75.15

Table 5.3: Area under Curve of ROC Results for Motor Neurone Disease Affected Participants

	Long		Trans	
	Num. of Trials Collected	Num. of Trials Analysed	Num. of Trials Collected	Num. of Trials Analysed
MG (n = 19)	36	25	36	24
BB (n = 19)	36	18	36	18

Table 5.4: Number of Trials Taken Forward to Analysis (MND Affected Participants)

Fewer number of trials were suitable to be taken forward to analysis in the MND affected trials. This was due to a number of reasons such as file corruption as in the healthy data, but also due to excessive voluntary activation that could not be removed in EMGlab (possibly due to complexity of the action potentials) and other electrophysiological activation such as complex repetitive discharges. The total number of trials collected and the number taken forward to analysis can be seen in Table 5.4.

	BB		MG	
	LONG	TRANS	LONG	TRANS
Healthy	167	325	182	208
MND	263	402	254	208

Table 5.5: Number of fasciculations detected using GMM in healthy and MND affected participants from BB and MG muscles).

Fasciculation numbers obtained from the GMM (Table 5.5) showed generally higher numbers of fasciculations in MND affected participants

than in healthy participants with 1102 occurrences in MND affected participants and 882 in healthy participants in total. There was one exception, in the MG in transverse orientation where the numbers were the same (208). Greater numbers of fasciculations were generally detected in transverse orientation than in longitudinal (true for seven of the eight cases). Transverse orientation gave total fasciculation numbers of 1143, in comparison to longitudinal orientation which yielded 866. Similar numbers of fasciculations were detected in longitudinal orientation for the BB and MG muscles, with 430 detected in BB and 436 detected in MG. In comparison, much larger numbers of fasciculations were detected in transverse orientation in BB (727) than MG (416). Individual participant fasciculation numbers can be seen in Appendix 9.2

5.4 Discussion

This study evaluated: i) how a GMM approach would perform in comparison to the previously reported KLT/MI in identification of fasciculations in ultrasound images; and ii) how accurately each method performed when compared to a myoelectric signal based ground truth.

Consistently higher accuracy was obtained using the GMM approach in comparison to the previously reported KLT/MI approach. Overall, the GMM was more robust to changes in muscle and probe orientation, whilst maintaining good accuracy across both unaffected and MND affected groups.

The results may be explained by the GMMs more selective approach

to motion detection. Although the KLT/MI analysis attempts to provide a selective approach by minimising motion with low coherence (i.e. noise), it cannot discount other physiologically based movements in the image sequences such as blood vessel pulsation [9]. In contrast the GMM is able to classify regularly occurring motions such as blood vessel pulsation, as background and detect large, sporadic events such as fasciculations.

Although the GMM outperformed the KLT/MI here, the accuracy of both techniques fell short of that in previous work (83-94%) [9] (also see Chapter 4). Human operator identifications were used as the truth signal for comparison in the previous study, so both the KLT/MI and ground truth comparator were based on analyses of motion in the image. In contrast, myoelectric signals denote changes in muscle fibre membrane potential, a precursor of muscle fibre contraction, not a measure of the motion of the muscle tissue itself. In addition, the pick-up volume of the needle differs greatly from the ultrasound pick-up area meaning that fasciculations may appear in the ultrasound that may not appear in the myoelectric data and vice versa.

Disparities between levels of activation detected by the two modalities have frequently been reported, with larger levels of fasciculations being detected in ultrasound in comparison to EMG [65], [5]. It may be that the lower levels of agreement between the image based signals and myoelectric data, in comparison to the KLT/MI and manual identifications, are due to poorer detection of fasciculations by the truth signal rather than the performance of the image analysis approaches. Although previous studies have shown higher agreement levels when using manual ID's as

truth signals. This would not be a practical method to employ on a large scale due to the time and work required. A possible alternative truth signal may be surface EMG arrays which provide more information on spatial distributions of activations and cover a larger area of the muscle albeit the superficial layers. This is an aspect which should be considered in future work.

Limitations

To fully evaluate the capabilities of automated analysis of ultrasound images for the diagnosis and monitoring of neuromuscular disease, further work will need to apply the analysis across a wider range of muscles in order to demonstrate suitability for application to diseases such as MND, which requires evidence of fasciculations in muscles across multiple body regions [91]. In addition, assessment of spatial and temporal twitch information should be further explored to provide detailed characterisation of the twitch events which may be valuable for patient stratification and/or monitoring of disease progression. This information may be extracted from the GMM, using data such as foreground object locations, area of objects and peak durations.

5.5 Conclusion

The work presented here provides the first assessment of the accuracy of two image analysis algorithms to detect fasciculations, compared to

a myoelectric ground truth signal, and by extension their potential to be applied to the diagnosis of neuromuscular disease. Differences do exist between the performance of the algorithms when they are applied to different image content, with results indicating a more selective GMM based analysis should be used in order to discount the physiological movements (e.g. blood vessel pulsation, voluntary activation) and for greater tolerance of differences in collected images resulting from the presence of disease, muscle fascicle geometry and probe orientation. Further work is required to evaluate performance of the GMM across a wider range of muscles of different sizes, shapes and functions to further establish the viability of this method as a means of non-invasively detecting involuntary muscle activation in the clinic.

Chapter 6

Application of Foreground Detection Analysis to Additional Muscles

6.1 Introduction

This chapter explores the accuracy of the GMM, when compared to the EMG truth signal, across a wider range of muscles than has previously been assessed in the literature and in previous chapters of this thesis. This is an important area to explore due to the need to provide evidence of the presence of fasciculations in a number of regions to form any kind of diagnosis of MND. It would also be the first instance where a computational technique has been applied to such a wide range of muscles.

MND is characterised by the degeneration of both upper and lower motor neurones to varying degrees. Electrophysiological signs of MND, such as fasciculations and fibrillations are a major diagnostic indicator of the

disease. However, the location and extent of these symptoms can vary between patients.

Diagnostic criteria for MND are developing and changing as understanding of the disease increases. The most recent amendments (Awaji Shima Recommendations) [91] were introduced in 2012. The amended criteria require that there be evidence of lower motor neurone loss, reinnervation and the presence of fasciculation potentials or fibrillation potentials and positive sharp waves. These signs should be apparent in a minimum of two muscles in the cervical and lumbar – sacral region and a minimum of one muscle in the bulbar and thoracic region. It is therefore necessary for any diagnostic methods to be easily and successfully applicable to a wide range of muscles across all spinal regions.

Hypothesis: The GMM will offer good accuracy and generalise well to a wider range of muscles for the task of fasciculation identification when compared to an EMG truth signal. This is due to its robustness to noise and more adaptive nature, allowing it to ignore other underlying physiological motion within the image which is particularly pertinent to trunk muscles which contain clear breathing motion within the images.

Studies such as [65] have assessed ultrasound for diagnostic purposes throughout a wide range of muscles (biceps brachii, rectus femoris, tibialis anterior, rectus abdominis, extensors of the forearm and abductor pollicis brevis). They showed promising results with increased detection of fasciculations in comparison to EMG in all muscles with ultrasound detecting

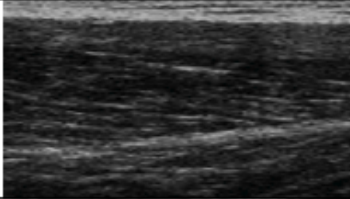
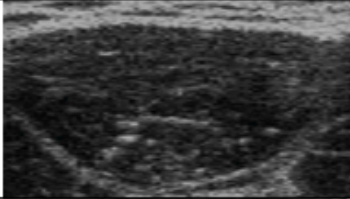
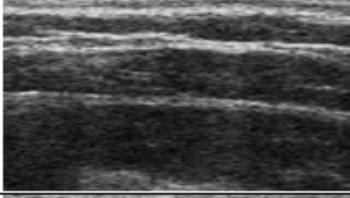
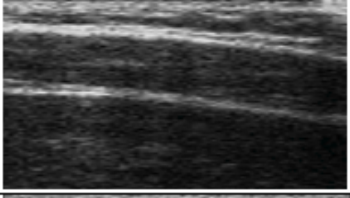
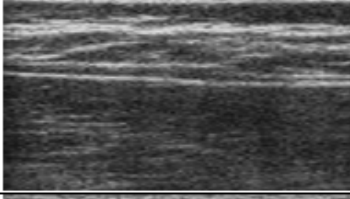
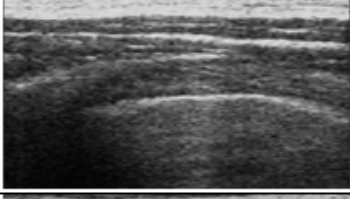
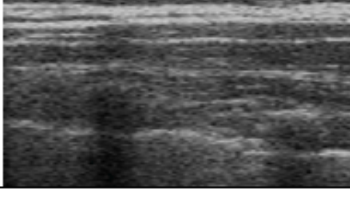
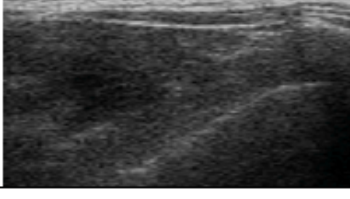
	Longitudinal	Transverse
Rectus Femoris		
Rectus Abdominis		
Trapezius		
Thoracic Paraspinals		

Figure 6.1: Examples of ultrasound images collected from muscles rectus femoris, rectus abdominis, trapezius and thoracic paraspinals and in both probe orientations (longitudinal and transverse).

fasciculations in 292 out of 391 instances in contrast to 182 out of 335 detected by EMG. However, the only analysis carried out was based on whether image sequences and EMG traces showed a presence of fasciculations or not and did not investigate frequency of occurrence, time duration of fasciculations or location of occurrence. The evidence does however show that fasciculations are visible in ultrasound image sequences and therefore suggests they should be detectable using computational approaches.

Previous applications of computational analysis for the purpose of fasciculation detection, such as [9] and Chapter 4/5, have been restricted to large muscles of the limbs (MG and BB). However, these muscles alone would not be sufficient to support a diagnosis. MG and BB have a number of characteristics that make them ideal for the application of computer vision techniques. They are limb muscles and therefore are not affected by any motion due to breathing as muscles in the trunk may be. They also have a relatively large surface area, with relatively simple architecture and high contrast between connective and muscle tissue, which make them relatively easy to image (See Figure 4.1 for examples of MG and BB and Figure 6.1 for examples of RF, RA, TRAP and TP).

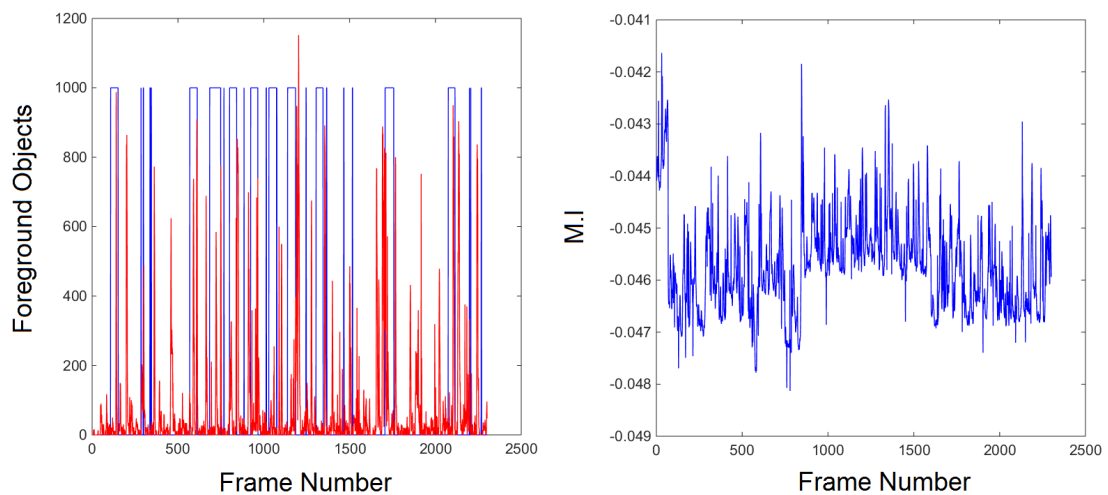


Figure 6.2: GMM signal (red) overlaid with EMG logical signal (blue) and KLT/MI signal (right)

Chapters 4 and 5 have shown that when comparing the KLT/MI and

GMM methods to both manual ID's and EMG, the GMM is either comparable or offers improved accuracy in contrast to the KLT. During preliminary work, the appropriateness of the KLT for the purpose of fasciculation detection in additional muscles in the trunk and limb was tested. This produced a signal that showed oscillations due to breathing with any potential fasciculation events sitting little higher than the noise level (Figure 6.2). This is likely due to breathing being the dominant motion within the image meaning that fasciculation detection would be extremely challenging using this approach. From this point onward due to the quality of the signal and the previous superior performance of the GMM methods, it was concluded that the GMM technique offered more benefits and therefore the KLT was not taken through for further analysis.

It is apparent from current criteria that govern diagnosis of MND, that any automated analysis should be robust to variations experienced in images of muscles with varying sizes, shapes and architecture (see Figure 6.1). This chapter will assess the performance of the improved analysis method (GMM) across additional muscles in order to determine its performance for fasciculation detection across a range of muscles that are assessed during MND diagnosis.

This chapter will again assess the accuracy of the GMM as in chapter 5. However, with the primary aim of assessing the capability of the GMM analysis across a wider range of muscles.

6.2 Methods

Participants and Experimental Protocol

For this study, data collected from the 20 patients, who had previously been diagnosed with MND (59 ± 14 years, 174.8 ± 9.2 cm, 86.8 ± 13.2 kg, 1078 ± 1148 days since diagnosis) was subject to GMM analysis for the purpose of fasciculation detection. Data from healthy participants was not assessed as not enough instances of fasciculations were contained within the data for comparison, with many containing no fasciculations at all. The dataset used was the same dataset used in Chapter 5 and was a novel dataset collected for the purpose of this thesis.

Simultaneous ultrasound images and EMG data were collected from four different muscles; rectus abdominis (RA), rectus femoris (RF), trapezius (TR) and the thoracic paraspinal (TP) muscles (Figure 6.1). Data were collected from participants while in the seated position with their legs supported except from the TP, when the participant was asked to lean forward to allow for access for the probe and EMG needle. The protocol for image data collection remained the same as described in Section 4.2, with images in both longitudinal and transverse orientation being collected for 35 seconds alongside EMG data.

Myoelectric Signal Processing

As in section 6.2, a number of pre-processing steps were completed. All myoelectric signals were bandpass filtered (4th order Butterworth, 30-500 Hz cut-off), with voluntary activation removed from the original signal us-

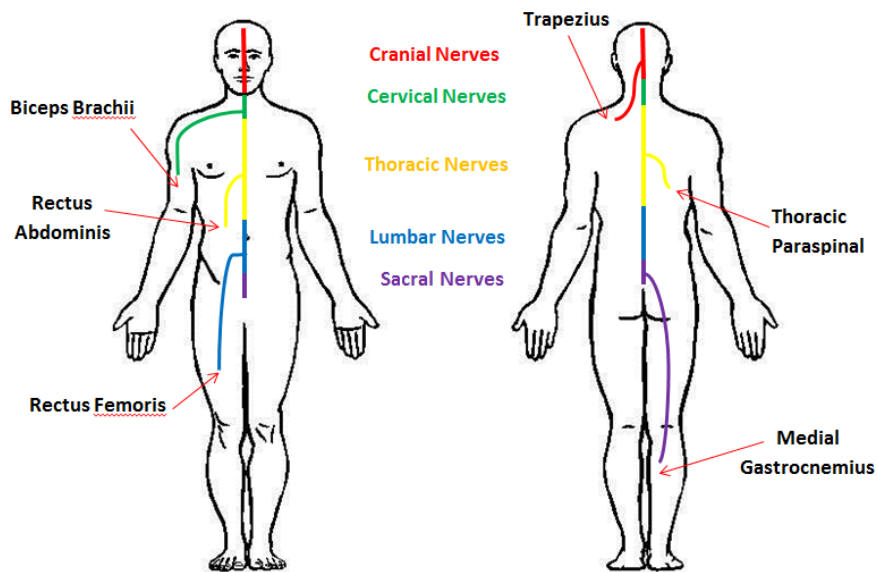


Figure 6.3: Overview of Muscles Assessed and their Innervation

ing template matching, leaving the involuntary fasciculation potentials [93]. As before, periods of involuntary activity were identified using thresholding methods, with the optimal threshold calculated using multiples of the absolute mean of the signal (Equation 5.2).

A logical signal was then produced, with all values above the threshold classified as 1 and all values below the threshold classified as 0. These threshold values for each muscle can be seen in Figure 6.4 .

The logical signal were then compared to the EMG signal using a ROC measures of accuracy. This technique was applied to approximately one third of participants in each muscle/ probe orientation group and parameterisation was carried out for each individual muscle (RA, RF, TP and TRAP). Participants were randomly selected and not included in the final analysis. These values of accuracy were recorded and plotted and the

plateau point of the curve was used to give the optimal value of n (Equation 5.2) for each individual muscle. These results can be seen in Figure 6.4.

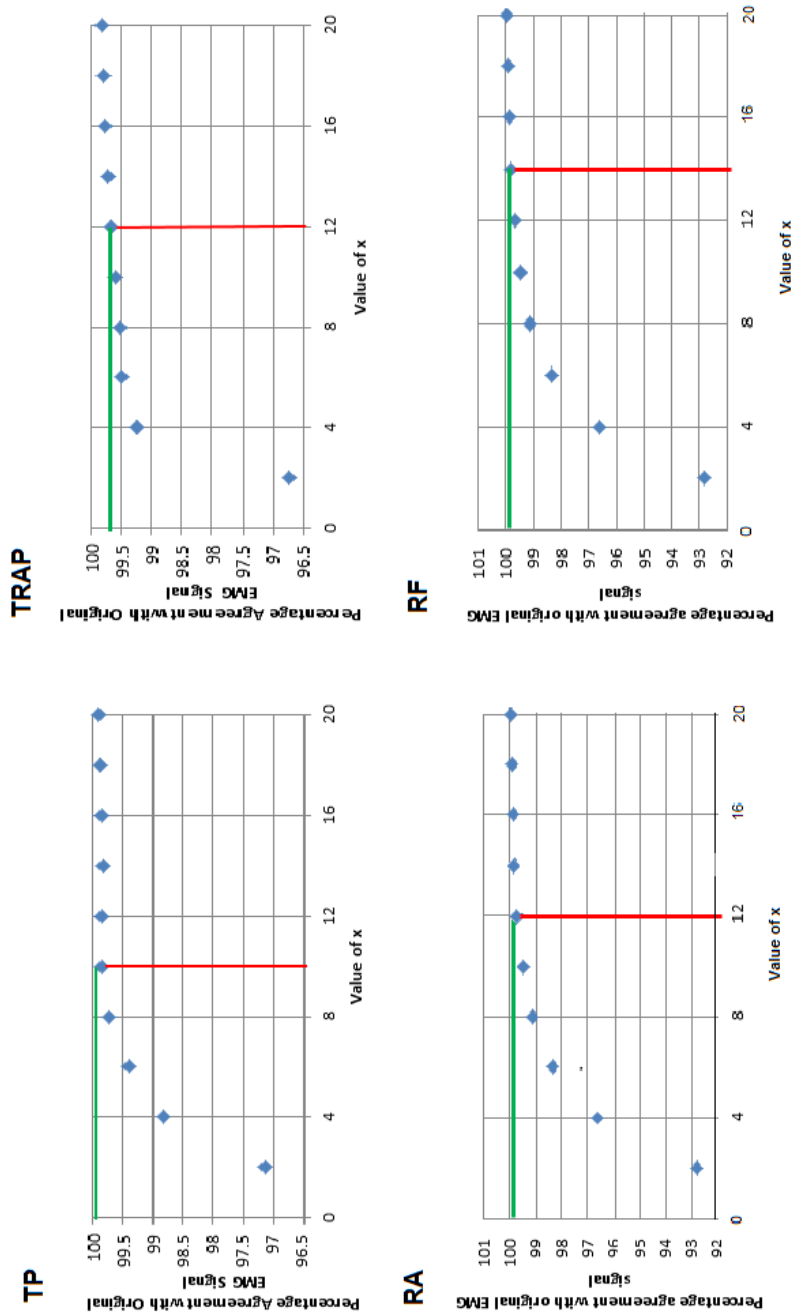


Figure 6.4: EMG signal Threshold Calculation for Fasciculation Identification in the Thoracic Paraspinals (top left), Trapezius (top right), Rectus Abdominis (bottom left) ad Rectus Femoris (bottom right) Muscle.

Image Analysis and Parameterisation

As healthy participants were not used in this study (due to the low level of fasciculation occurrence in the selected additional muscles), participants from the MND group were used for parameterisation, with all other parameterisation steps remaining the same as those carried out in Chapter 5. Prior to analysis, images were manually cropped to the lower aponeuroses of the superficial muscle in order to remove any muscles deep to those containing the EMG needle. Due to the relatively large pick up area of the ultrasound, images tended to contain multiple muscles. As the myoelectric activity is not conducted across individual muscles, any fasciculations appearing in muscles deep to the ones containing the EMG needle, would appear as false positives, despite not necessarily being so. Once parameterisation was completed the remaining two thirds of participant data was analysed using the GMM technique, with the number of foreground objects present in each frame being used to construct a one dimensional signal for comparison with the EMG.

Statistical Analysis

Once both the motion analysis (GMM) signals and the logical myoelectric (EMG) signals had been obtained, statistical analyses in the form of ROC's were performed [87]. ROCs produce a curve which allows for the assessment of accuracy between a signal and a binary classifier, at different thresholds and are the same method used for a measure of accuracy

in Chapter 4 and 5. The area under the curve (AUC) is used to quantify accuracy for comparison. Individual ROC curves showing the performance of each technique across muscle types and probe orientation and combined curves, showing differences in accuracy between all data in the healthy control group and all data in the MND affected group were produced.

6.3 Results

As in previous chapters, a number of trials were not taken through to analysis for an array of reasons. These were due to the presence of excessive voluntary activation that could not be removed using EMGlab and presence of excessive involuntary activations that were not the focus of the work presented here (i.e. complex repetitive discharges), which were particular problems in the TP and RA. A very small number of files were discarded due to file corruption. //

	Long		Trans	
	Num. of Trials Collected	Num. of Trials Analysed	Num. of Trials Collected	Num. of Trials Analysed
RF (n = 19)	36	29	36	30
TR (n = 19)	38	25	38	26
RA (n = 19)	24	18	24	24
TP (n = 19)	34	15	34	14

Table 6.1: Number of Trials Taken Forward to Analysis (MND Affected Participants)

In addition to this, a number of participants were ruled out for data collection in the RA due to the presence of a feeding peg and one participant

was ruled out of data collection from the TP due to another present medical condition. One participant was removed from data analysis in their entirety due to uncertainty of initial diagnosis. The total number of trials analysed can be seen in Table 6.1.

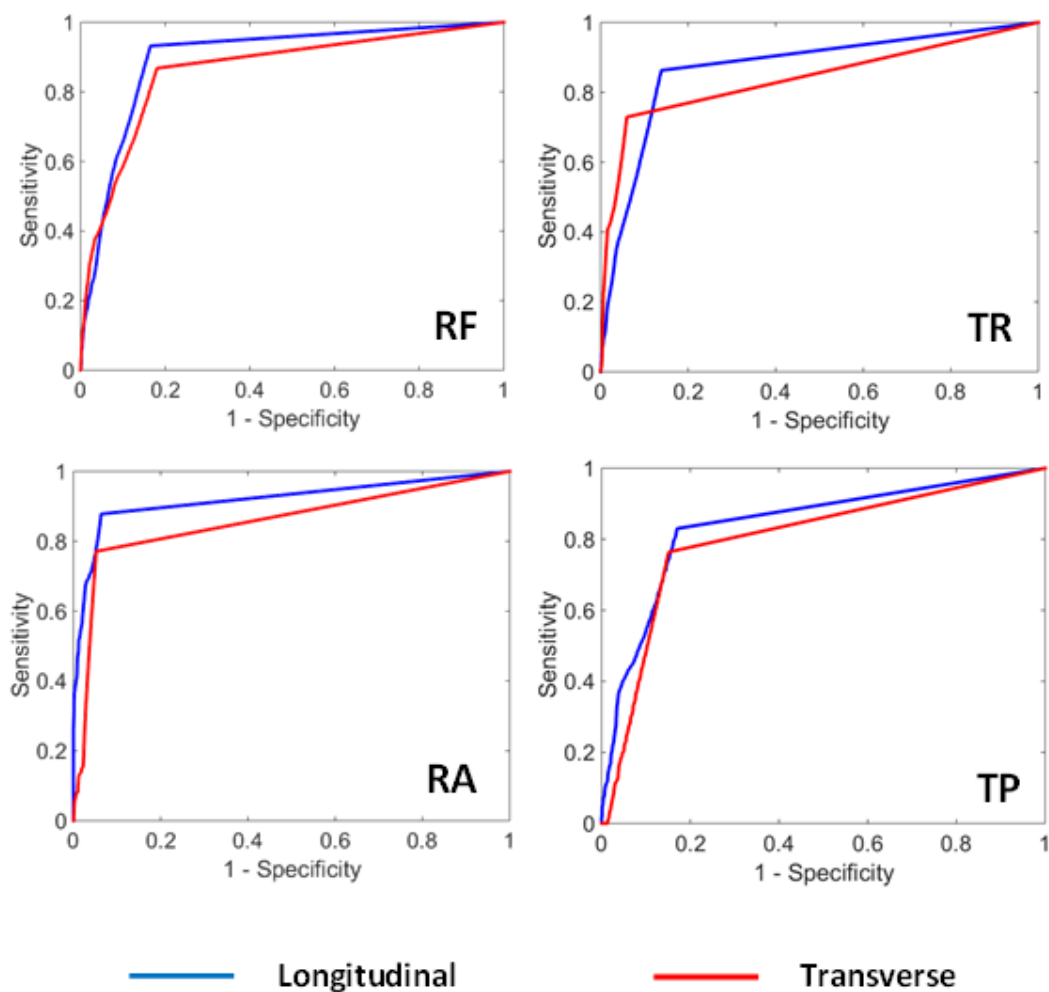


Figure 6.5: ROC curves of RF (top left), TR (top right), RA (bottom left), TP (bottom right) muscles in longitudinal (blue) and transverse (red) probe orientation for GMM analysis when compared with the myoelectric truth signal.

ROC Curves indicating the agreement between the two approaches and the myoelectric data and the accuracy in different muscles and probe orientations are shown in Figure 6.5. Results showed accuracy levels that were generally between 80 and 90%, with the exception of RA in longitudinal which gave 92.01% agreement. Reductions were apparent within all muscle groups when probe orientation was changed from longitudinal to transverse, with the exception of the thoracic paraspinals.

(%)	LONG	TRANS
RF	89.73	85.68
TR	86.57	84.45
RA	92.01	86.37
TP	80.17	84.16

Table 6.2: Results Table for MND Affected Participants in RF, TR, RA and TP.

The RF muscle yielded results of 89.73% in longitudinal probe orientation and 85.68% in transverse, a difference of 4.05 percentage points. In TR, results of 86.57% and 84.45% in longitudinal and transverse probe orientation respectively, a difference of 2.12 percentage points. Results in the RA were 92.01% in longitudinal and 86.37% in transverse, a difference of 5.64 percentage points and the TP results yielded results of 80.17% in longitudinal and 84.16% in transverse, a difference of 3.99 percentage points (see Table 6.2).

6.4 Discussion

The aim of this chapter was to assess the accuracy of the GMM, whilst comparing to the EMG as the truth signal across a number of muscles. These muscles have not previously been subject to any computational analysis according to the literature. The selected muscles exhibit different shapes, sizes and architectures (Figure 6.1) in contrast to muscles such as the MG and BB which have previously been subject to computational analyses. Robustness across a wide range of muscles would be required if this method were to be applied for the diagnosis of neuromuscular disease.

The GMM continued to provide highly accurate fasciculation detection, when compared to the EMG ground truth, with accuracy comparable to that found in the limb muscles (Chapter 5), with the majority of results between 80 and 90%. A reduction in accuracy was also found between longitudinal probe orientation and transverse. This is likely due to less visible structure in the transverse orientation compared to the longitudinal (Table 6.2). The GMM requires contrast within the image, which exists in longitudinal orientations as the white fascicles running through the image in contrast to the dark muscle tissue. In transverse, this is less apparent as the fascicles are viewed at a more perpendicular angle and so will contribute to a smaller area of the image and creating less of a contrast in the image. This is also likely why decreases in accuracy were seen between healthy and MND participant groups in Chapter 4 and 5. The findings also provide further evidence that the probe orientation is an im-

portant factor to consider when developing and assessing computational analysis approaches and should be considered in design of future experimental studies, whether manual or computational analysis is to be used.

Whilst a number of studies have compared whether fasciculations are present in ultrasound and EMG across a wide range of muscles [65], [6]. This is the first study which applies computational techniques for fasciculation detection to such a wide array of muscles, with the focus previously being the gastrocnemius and biceps brachii [9]. In addition to this there are no studies that compare difference between the accuracy of computational analyses or human operators between probe orientations as previous studies have tended to collect image data in either longitudinal or transverse. It further adds credence to the notion that GMM analysis of ultrasound images can act as a reliable alternative to EMG in the detection of fasciculations and is likely to be applicable to MND diagnosis due to its ability to retain high levels of accuracy across a number of different muscle types.

This chapter also demonstrates the GMM's ability to perform under circumstances which would cause non adaptive methods to fail, such as the presence of breathing patterns in a number of these muscles such as TP, RA and TR (See Figure 6.2). This is also emphasised in established MND due to additional muscle recruitment for breathing.

As stated in Section 5.4, due to the small pick up volume of the EMG needle electrode in comparison to the ultrasound imaging area, the two methods are showing the same data from two different perspectives. Further investigation should be carried out using different truth signal methods

such as surface EMG, in particular array based methods [95], which provide a wider detection area with more spatial information in comparison to intramuscular EMG, to further scrutinise of the GMM and its agreement with the electrophysiological activity of the muscle.

6.5 Conclusion

The analysis of a further four muscles shows no drastic change in accuracy levels when compared to results from the larger limb muscles, previously assessed Chapter 5. The GMM analysis retained high levels of agreement across TP, RA, TR and RF muscles and across both probe orientations. However, differences in accuracy were noted between longitudinal and transverse probe orientations indicating that characteristics of the image determined by probe orientation are an important factor in fasciculation identification.

As this and the previous chapter has provided good results across a wide range of muscles, further confirming its ability to be applied to MND diagnosis, future work should assess the ability of the GMM to assess twitch characteristics to provide a quantitative method through which presence of disease can be determined.

Chapter 7

Comparison of Fasciculation Characteristics in Motor Neurone Disease Affected Participants and Healthy Controls

7.1 Introduction

This chapter aims to determine whether spatial and temporal characteristics of fasciculations extracted from ultrasound images of muscle tissue can be used to differentiate between healthy and MND affected participants.

A positive diagnosis for MND can be a long, drawn out process with varying degrees of certainty attached to it depending on symptoms present

(Figure 2.2). It can also be characterised by the combined presence of a number of symptoms (see Figure 2.1) including muscle atrophy and involuntary muscle twitches such as fasciculations. However, patients generally will be subjected to a number of tests and procedures in order to build a larger picture of the symptoms they are presenting with as well as other possible disorders that can be ruled out. Although fasciculations can be observed in healthy muscles, certain characteristics of the electrophysiological activity in the muscle can indicate the presence of neuropathy. EMG is the gold standard technique used as part of the diagnosis for MND and the primary way which fasciculations are detected. Measures such as variability of duration, frequency of occurrence and discharge interval as well as phenomena such as complex fasciculations and jitter (see Section 2.1.2) can all add to the weight of an MND diagnosis.

Studies have shown that a number of measures of fasciculation potentials differ between those attributed to MND and benign fasciculations. For example in [20], number, time duration, number of turns and amplitude were all greater in MND patients in comparison to those with Benign Fasciculation Syndrome. Also, due to the patterns of denervation and reinnervation that occur during MND, fasciculation potentials display increased complexity in comparison to those occurring in healthy individuals [21].

Quantitative analysis of fasciculations have been carried out using ultrasound images of healthy muscle, with [44] reporting duration in muscles such as Gastrocnemius, Biceps and Triceps Brachii, Tibialis Anterior and Paraspinals, for which a average time duration of 500 ms was recorded.

However, it has not currently been investigated whether the twitches captured in ultrasound images can be determined to be from a healthy participant or participant with neuromuscular disease in any quantitative way other than the overall occurrence during each trial, such as in [65] and [6].

In order to allow for ultrasound to be considered as a valid technique to aid diagnosis, as is the case for EMG, it is necessary to determine whether individual fasciculations in healthy and MND affected participants can be distinguished from the image sequences. The aim for this chapter is to quantify any significant differences between twitch time duration and morphology as they appear in ultrasound images when assessed using a GMM analysis.

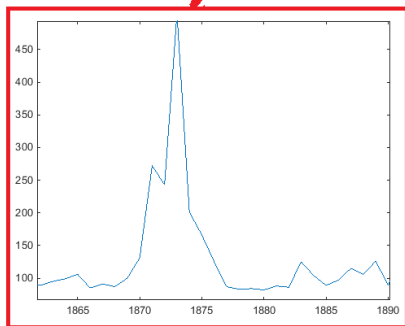
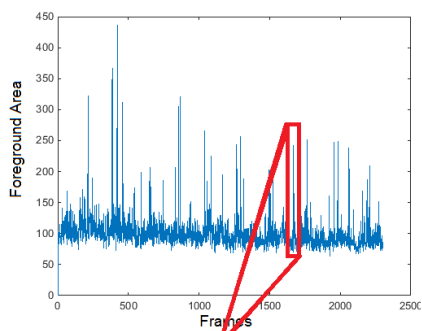
Hypothesis: Spatial and temporal characteristics of fasciculations extracted from ultrasound images can be used to differentiate between healthy and MND affected participant groups.

7.2 Methods

For this study, data collected from 20 MND affected (59 ± 14 years, 174.8 ± 9.2 cm, 86.8 ± 13.2 kg, 1078 ± 1148 days since diagnosis) and 20 healthy participants (54 ± 20 years, 168.8 ± 11.4 cm, 79.0 ± 18.1 kg) as described in Chapter 4 was analysed. MG and BB data were selected, with images collected in both longitudinal and transverse probe orientation. This study was restricted to MG and BB as it was a comparative study be-

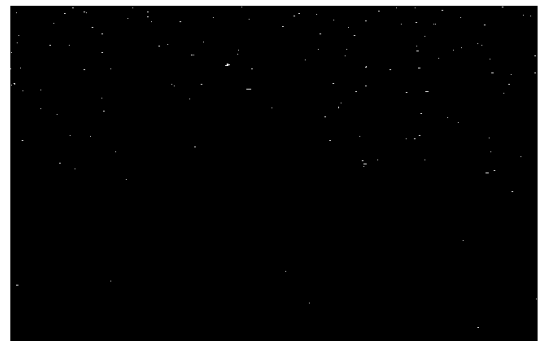
tween fasciculations in healthy and MND affected participants; additional muscles did not provide enough healthy fasciculations to allow for effective comparison.

A. One dimensional signal calculated based on the total area of image that is foreground pixels.

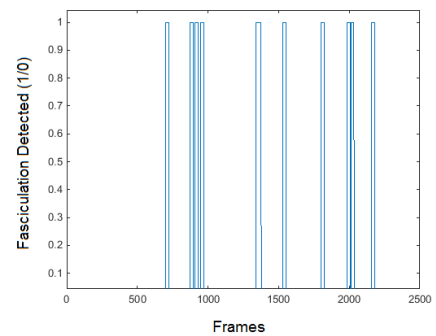


D. Individual twitches are segmented from the area signal.

B.



Foreground pixels are detected using the GMM analysis.



C. Fasciculation detection signal from chapter 5 used to segment area signal

Figure 7.1: Example of the process through which individual twitches are extracted from image for further analysis using the one dimensional foreground area signal (Example taken from MG in longitudinal orientation from a MND participant).

A GMM analysis was performed on images as described in Chapter 5 at optimal parameters for each muscle and probe orientation (further de-

tails in Appendix 2), however, for the purpose of this chapter, clusters of foreground pixels were not rejected based on blob size and all were taken into account. This was done in order to maintain the maximum amount of information from the image. Twitches were segmented from the signal using the output GMM signal from Chapter 5, as this was cleaner and better suited GMM signal for twitch identification purposes, but left little detail in how the signal developed through time. Output values for each frame were the total area of foreground pixels, the Euler number of the binary mask and the foreground object centroid locations. The total area of foreground pixels, which was represented as a one dimensional signal, demonstrates how the amount of the image classed as foreground varies through time (see Figure 7.1). The Euler number is calculated from a binary image (foreground/ background pixels) and is the number of objects minus the number of holes (see Figure 7.2), this will give an idea of the how concentrated or diffuse the foreground pixels were spread throughout the image. The centroid locations will also give information on the spatial distribution of foreground pixels during a fasciculation and how the locations of objects change throughout the duration of twitch.

Analysis of Temporal Twitch Characteristics

Start and end points of each twitch were determined by calculating the location in the foreground area signal either side of the twitch where $dy/dx = 0$. Due to the movement of twitches through the muscle tissue, twitches present as a double peak in the GMM signal, due to the distinct contractile,

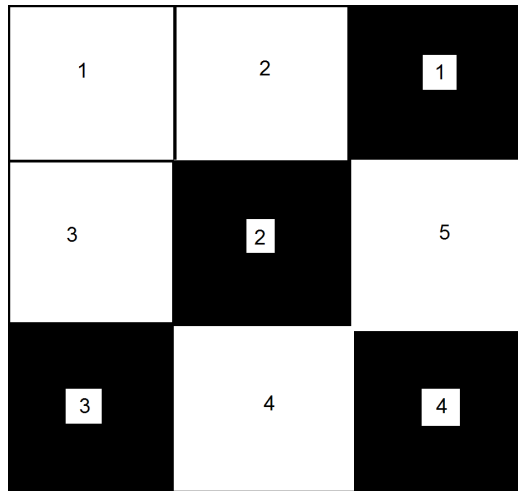


Figure 7.2: Example of how the Euler number of a binary image is calculated; number of foreground objects (white) minus the number of holes (black) ($E_{num} = Obj_f - Obj_b$).

plateau and relaxation phases of the fasciculation. Therefore to obtain an accurate measure of the twitch time duration the first minima point after the twitch peak was ignored and the end point was counted as the next frame where $dy/dx = 0$.

The difference between the start and end points was then calculated to determine the twitch duration measures shown in Figure 7.3. Four timing measures were calculated; total twitch duration, contraction phase duration, relaxation phase duration and inter peak duration and presented using boxplots. The total twitch duration represented the period of time that motion was present in the image and was classed as a foreground object. Twitches also generally displayed a double peak morphology, which was split into what was considered to be the contraction and relaxation phase of the twitch due to observations from images that showed a phase of

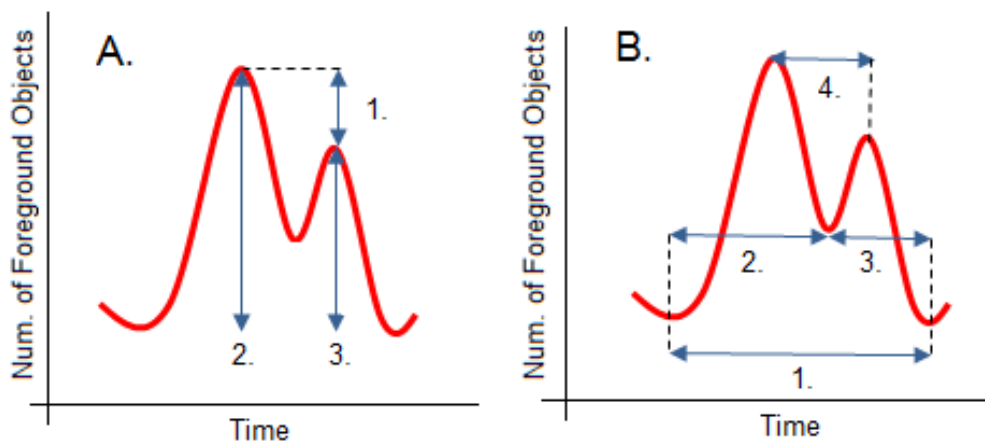


Figure 7.3: A. Example of peak analysis measures: 1. Peak to peak difference. 2. Maximum peak height. 3. Minimum peak height. B. Example of twitch timing analysis measures: 1. Total twitch time duration. 2. Contraction phase duration. 3. Relaxation phase duration. 4. Inter peak duration.

initial motion a period of tension and then another period of motion in the opposite direction. These timing measures were calculated from the twitch start point to the minima and from the minima to the twitch end point for the contraction and relaxation phase respectively. Finally, the peak to peak time was calculated as the time between the two local maxima points (i.e. peak contraction phase, peak relaxation phase).

7.2.1 Foreground Area Analysis

During the GMM analysis, data on the area of foreground pixels for each frame was recorded. To ensure fair comparison, the total area of each cropped image was also calculated and the foreground area signal was divided by the total image area. Four different measures were calculated;

Peak to peak distance, maximum peak height and minimum peak height (Figure 7.3), these values were measured for each individual twitch. As stated in the previous section, twitches generally displayed a double peak morphology, which was split into what was considered to be the contraction and relaxation phase. These measures were then visualised using boxplots so any variations during different twitch phases and across participant group, muscle and probe orientation could be noted.

7.2.2 Foreground Object Centroid Analysis

The (x,y) values for the centroids of each foreground object in each frame were used to determine how spread foreground objects were throughout the image. Nearest neighbour values for each centroid location were calculated and total distances were summed to give a value for the total distance between the foreground objects per frame. This value was divided by the total area of the cropped image (which was dependent on muscle size as it was presented in the image) to provide a fairer comparison between muscles which filled a larger proportion of the total image.

The Euler number of the binary mask of the image was also collected. This gave the number of objects in the image minus the number of holes in the object and will indicate how sparse or dense the distribution of the foreground objects are.

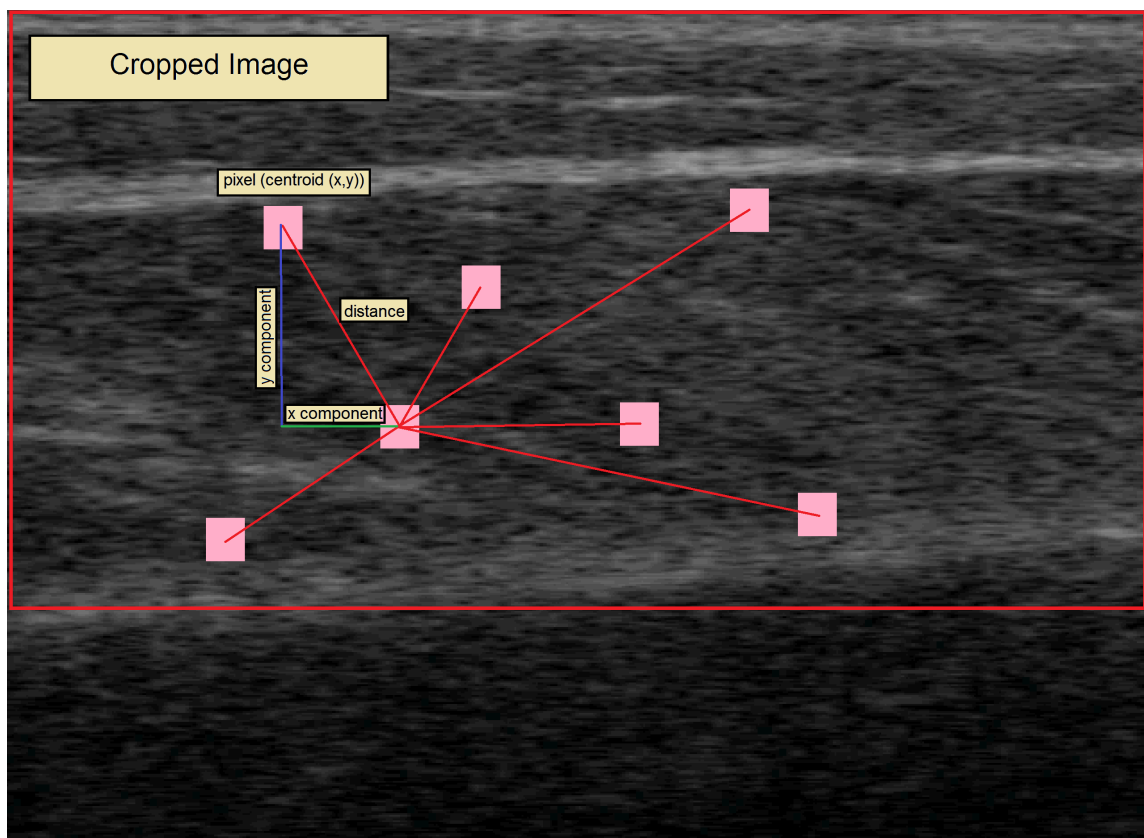


Figure 7.4: Example of the total distances (red) and the calculation of x (green) and y (blue) components using k nearest neighbours from foreground object centroids (pink)

7.2.3 Statistical Analysis

Statistical analysis was carried out to determine any significant differences in temporal or area twitch characteristics between the healthy and MND affected participants. The normality of the data was tested using an Anderson-Darling test to determine the type of significance test that would be used. Data as the twitch timing and peak height data appeared to have a log-normal distribution, data was transformed by taking the log of all values for the twitch timing data and the cube root transform of the twitch peak

data. This produced data that looked to be normally distributed. Although further tests to determine the distribution of the data rejected the null hypothesis that it was normally distributed, as the data distribution looked approximately normal according to histogram and qq-plots, it was decided that an ANOVA would be used to calculate p values for the differences between the healthy and MND affected participant groups as well as between the MG and BB muscle groups a mixed effects model was used due to the presence of both fixed (muscle, probe orientation and participant group) and random effects (participant). Due to the reduced number of tests when using an ANOVA, the critical level at which p values were deemed significant were set at $\alpha = 0.05/4$ or 0.0125, using a Bonferroni correction [96].

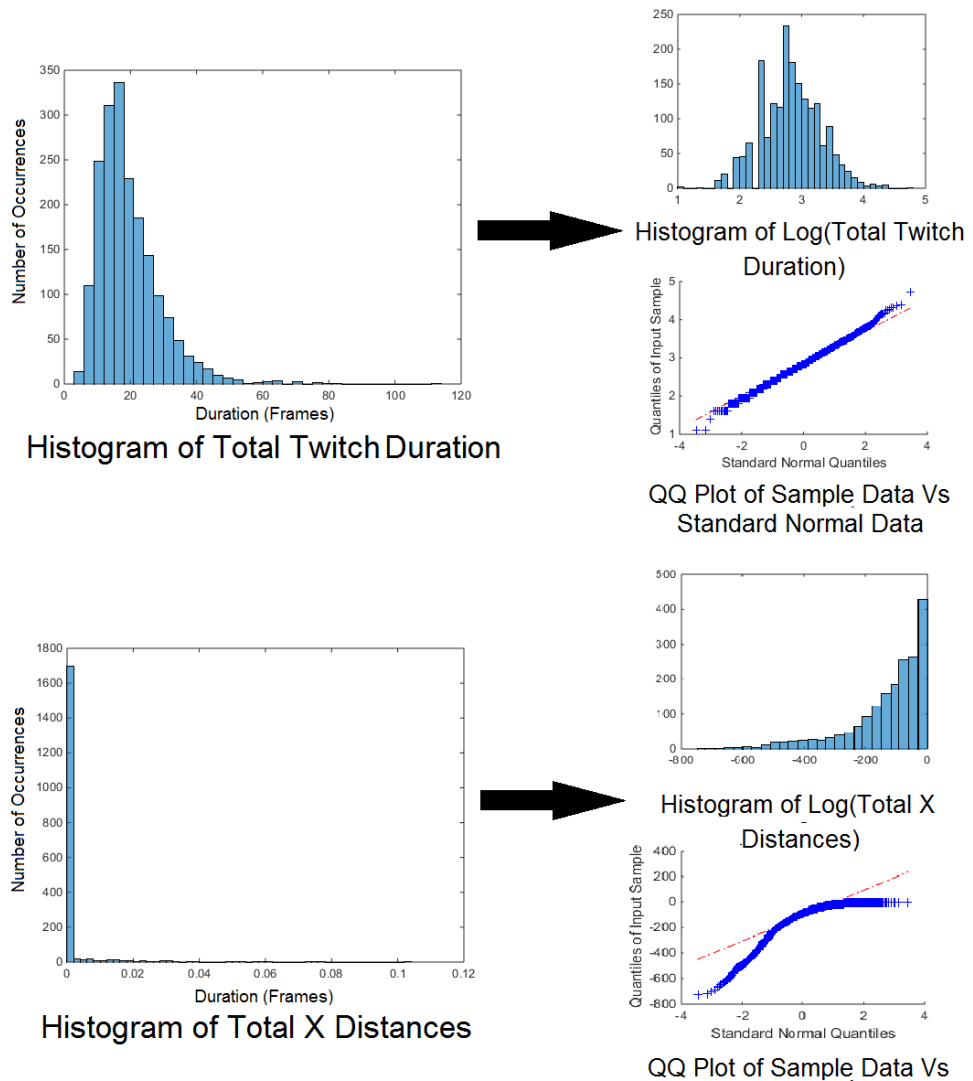


Figure 7.5: Two examples of data distributions successfully transformed (top) and which could not be successfully transformed (bottom)

The distance between foreground objects was determined to be not normally distributed and could not be successfully transformed, p values were calculated using the non-parametric Wilcoxon signed rank test. Examples of the distribution of the data can be seen in Figure 7.5 the critical level at which p values were deemed significant were set at $\alpha = 0.05/6$ or

0.0083.

7.3 Results

7.3.1 Twitch Phase Timings

Results showed variations in most measures between the healthy and MND affected participant groups. However, these variations did not appear to be consistent across all muscle groups and probe orientations. The distributions of results from each measure in for healthy and MND participants groups are shown as boxplots in Figure 7.6.

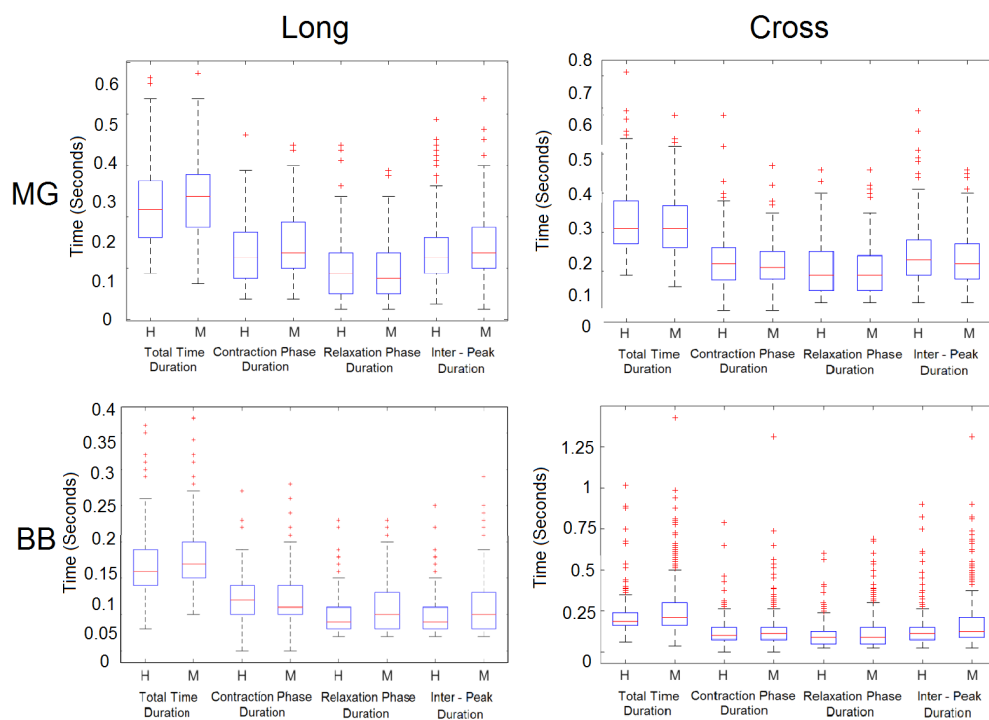


Figure 7.6: Boxplots showing comparisons of healthy (H) and MND (M) results for twitch time duration

MND								
	MG (frames/seconds)				BB (frames/seconds)			
	long		cross		long		cross	
	Mean	SD	Mean	SD	Mean	SD	Mean	SD
1	23.88/0.291	8.01/0.098	22.14/0.270	7.89/0.096	12.95/0.158	4.89/0.060	17.45/0.213	8.03/0.098
2	14.29/0.174	6.75/0.082	11.86/0.145	5.69/0.069	7.11/0.087	4.25/0.052	9.62/0.117	5.60/0.068
3	9.59/0.117	5.98/0.073	10.28/0.132	6.34/0.077	5.84/0.071	3.65/0.045	7.84/0.095	4.91/0.060
4	14.42/0.176	6.88/0.084	13.07/0.159	6.71/0.082	5.64/0.069	0.06/0.0007	10.38/0.127	0.03/0.0004

Healthy								
	MG (frames/seconds)				BB (frames/seconds)			
	long		cross		long		cross	
	Mean	SD	Mean	SD	Mean	SD	Mean	SD
1	22.49/0.274	7.68/0.094	23.30/0.284	8.82/0.108	11.98/0.146	4.58/0.056	17.42/0.212	9.08/0.111
2	12.75/0.155	6.03/0.074	12.51/0.153	6.99/0.085	7.29/0.089	3.18/0.039	9.69/0.118	6.28/0.077
3	9.74/0.119	6.09/0.074	10.79/0.132	6.55/0.080	4.69/0.057	2.90/0.035	7.73/0.094	5.60/0.068
4	13.99/0.171	6.80/0.083	14.29/0.174	8.35/0.102	4.97/0.061	3.14/0.038	10.97/0.134	9.14/0.111

Table 7.1: Table showing mean and standard deviation values for twitch phase durations (shown in frames/ seconds) in healthy and MND affected participants (1. total twitch time, 2. contraction phase time, 3. relaxation phase time, 4. peak to peak time).

In the MG muscle for longitudinal probe orientation, there was a greater spread in the total twitch duration for the MND participant group, with standard deviation of 0.094 in comparison to 0.084 in the healthy participants. The MND affected data also displayed a slight skew towards twitches with a greater duration in comparison to healthy participants, with mean durations of 0.291 and 0.274 seconds for MND and healthy twitches respectively. The contraction phase was also longer in the MND group when compared to healthy participants (mean values of 0.174 seconds in contrast to 0.155 seconds), however the relaxation phase was similar between the two groups (0.117 for MND and 0.119 for healthy). The peak to peak difference also showed greater twitch durations in the MND affected participants in comparison to healthy, with mean twitch times of 0.176 seconds

in MND and 0.171 seconds in healthy participants.

In contrast to the longitudinal probe orientation, the transverse orientation yielded shorter durations across all four measures for the MND affected participant group, with mean values of 0.270, 0.145, 0.132 and 0.159 seconds for the total twitch time, contraction time, relaxation time and peak to peak time respectively. In comparison, the corresponding healthy values were 0.284, 0.153, 0.132 and 0.174 seconds. A full set of mean and standard deviation values for the twitch timings as well as timing results in number of frames can be found in Table 7.1.

Time Based Measure	P - Value			
	Intercept	Group	Muscle	Probe
Total Twitch Time	<0.0125	0.712	<0.0125	<0.0125
Contraction Phase Time	<0.0125	0.015	<0.0125	<0.0125
Relaxation Phase Time	<0.0125	<0.0125	<0.0125	<0.0125
Peak to Peak Time	<0.0125	0.679	<0.0125	<0.0125

Table 7.2: Results from ANOVA Calculations Showing P Values for Muscle, Probe Orientation and Participant Groups for Each of the Four Timing Measures.

The results from the BB in longitudinal probe orientation show similar distributions of twitch durations as the MG, generally with greater durations being seen in the MND affected participant group. In the MND group the mean values were 0.158 seconds for the total twitch duration, 0.087 seconds for the contraction phase, 0.071 seconds for the relaxation phase

and 0.069 for the peak to peak time. The healthy participant group showed mean values of 0.146, 0.089, 0.057 and 0.061 seconds across the same measures. However, the differences were less pronounced in the contraction phase timings than in MG. Also, differences existed between the groups for the relaxation phase in the BB (but were not noted in the MG).

The transverse trials showed the largest differences between all other trials, with a large number of outliers. Large differences in the distributions between the total time and the peak to peak timings could be seen between the MND affected and healthy participant groups, with the MND being of longer duration. However, the mean values of these two measures did not differ greatly (0.212 in healthy and 0.213 in MND for total twitch duration and 0.134 in healthy and 0.127 in MND for peak to peak time). This may be due to the large number of outliers in the data. For the contraction and relaxation phase timings the differences in the distributions were smaller, but MND twitches still tended to be of longer duration.

Although the focus of this chapter was the differences between the healthy and MND affected participant groups, it was anticipated that interactions between muscle group, probe orientation and participant group would have some effect on overall results. Therefore, a linear mixed effects model combined with an ANOVA was used for analysis of the results. This allowed for the determination of levels of significance for each of the groupings. P values calculated for each of the four measures between the healthy and MND affected groups are shown in Table 7.2. For each of the four twitch timing measures, the participant grouping (healthy/ MND) was

significant for the timing of the relaxation phase of the twitch. This was also the case for the muscle type grouping and probe orientation.

7.3.2 Characteristics of Twitch Amplitude

Boxplots were again used to show the differences between MND affected and healthy participant groups for four measures based on the change in the number of foreground objects as a proportion of the total image size throughout the duration of a twitch. These again showed variations in most measures between the healthy and MND affected participant groups, which were not generally consistent between variations in muscle and probe orientation. The three measures used (shown in Figure 7.1) were; the difference between peaks, the maximum peak value and the minimum peak value.

For the MG trials in longitudinal probe orientation, peak height difference and the maximum peak height were greater in the healthy participants than in the MND affected group, with mean values of 0.082 and 0.069 in healthy participants and 0.069 and 0.055 in MND affected participants. However, the minimum peak value was greater in the MND affected participants than in healthy participants, with mean values of 0.022 and 0.019 for minimum peak height in healthy and MND participants respectively. The same patterns were apparent in the MG in transverse probe orientation with greater peak difference and maximum peak values in the

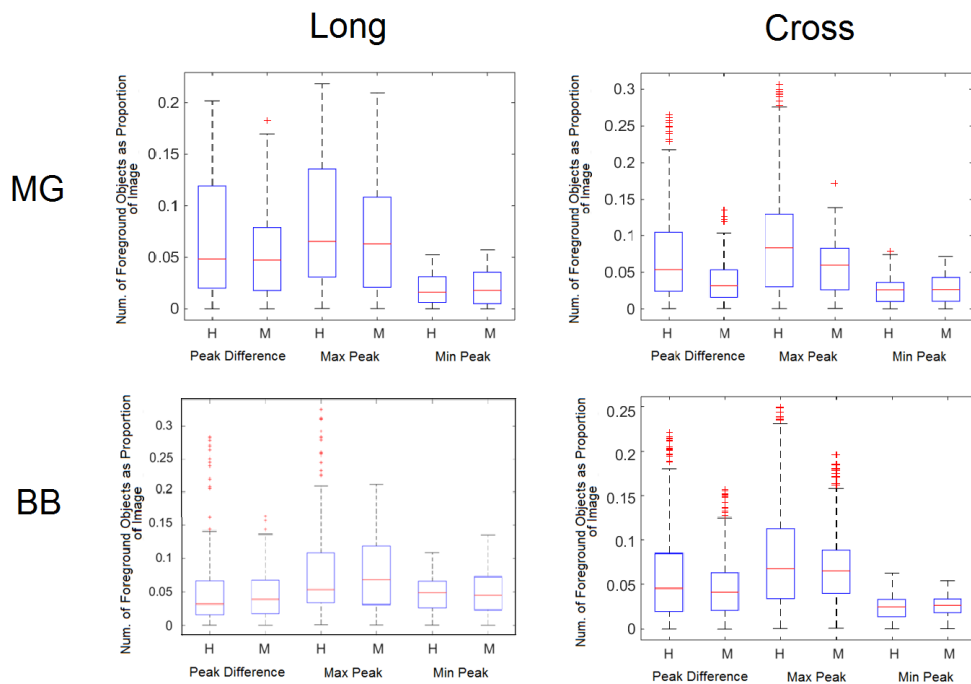


Figure 7.7: Boxplots to show comparisons of healthy (H) and MND (M) results for total area of foreground pixels

healthy group (mean values of 0.088 and 0.072 in healthy and 0.056 and 0.036 in MND) and greater minimum peak.

The BB showed more differences between the longitudinal and cross sectional probe orientation groups than in the MG. The longitudinal probe orientation seemed to give comparable peak difference. However, the mean values showed differences (with the peak difference giving values of 0.001 in healthy participants and 0.0009 in MND affected participants). The maximum and minimum peak height are greater in the MND affected group, with mean values of 0.071 and 0.044 in healthy and 0.055 and 0.033 in MND participants. In cross sectional probe orientation, the peak difference and the maximum peak value are greater in the healthy partic-

MND								
	MG				BB			
	long		cross		long		cross	
	Mean	SD	Mean	SD	Mean	SD	Mean	SD
1	0.069	0.052	0.056	0.037	0.075	0.072	0.065	0.042
2	0.022	0.017	0.028	0.020	0.044	0.033	0.025	0.031
3	0.055	0.044	0.036	0.027	0.047	0.055	0.044	0.035

Healthy								
	MG				BB			
	long		cross		long		cross	
	Mean	SD	Mean	SD	Mean	SD	Mean	SD
1	0.082	0.062	0.088	0.076	0.071	0.055	0.077	0.060
2	0.019	0.015	0.024	0.018	0.044	0.033	0.024	0.014
3	0.069	0.057	0.072	0.065	0.043	0.043	0.060	0.053

Table 7.3: Table showing mean and standard deviation values for twitch peak heights in healthy and MND affected participants (1. maximum peak height, 2. minimum peak height, 3. peak height difference) Values are reported as total foreground area as a proportion of the total area (in pixels) of the cropped image.

ipant group, with mean values of 0.077 and 0.024 for healthy participants and 0.065 and 0.025 for MND affected participants. The mean minimum peak values were less in the MND participants (0.044) in comparison to the healthy participants (0.053) , however, the healthy values had greater spread, with a standard deviation of 0.053 compared to 0.035 and a higher upper whisker value. The full set of results can be seen in Table 7.3.

Shape Based Measure	P - Value			
	Intercept	Group	Muscle	Probe
Peak Difference	<0.0125	0.712	<0.0125	<0.0125
Max Peak Height	<0.0125	<0.0125	0.573	0.039
Min Peak Height	<0.0125	<0.0125	<0.0125	<0.0125

Table 7.4: Results from ANOVA Calculations Showing P Values for Muscle, Probe Orientation and Participant Groups for Each of the Three Peak Amplitude Measures.

P values calculated for each of the four measures between the healthy and MND affected groups are shown in Table 7.4. The value used to determine significant results was found through the method described in 7.3.1 and gave a p value of 0.0125 or less. Significant values for the participant group were seen for the relaxation phase peak height and the contraction phase peak height, but was not significant for the peak difference measure which yielded a p value of 0.712. Significant p-values were found for peak difference and relaxation phase peak height, but not contraction phase peak height which gave a p-value of 0.039. This was also seen for the muscle type, which gave p-values of less than 0.0125 for the peak difference and relaxation phase peak height and a p-value of 0.573 for the contraction phase peak height.

7.3.3 Distance between Foreground Object Centroids

Results for the total distances between object centroids are shown in Figure 7.8, split into the x and y components. These boxplots show large differences between the x and y distances for both groups in the BB, which weren't as pronounced in the MG. The total distance between the x components of centroids was greater in the healthy twitches in BB in comparison to the MND twitches. The y components were less consistent, showing a greater distance in the healthy twitches when images were collected in transverse orientation. However, in longitudinal orientation y distance values were comparable.

Results from MG showed greater distances (x component) in the healthy group in longitudinal orientation (4.0×10^{-4} and 1.0×10^{-4} for healthy and MND respectively), however the healthy data had much greater spread (3.0×10^{-4} compared to 1.0×10^{-4}). The same true in transverse orientation, with the total distance between the x component of centroids being greater in healthy participants (2.0×10^{-4} compared with 1.0×10^{-4} in MND). For total y distances vary few differences can be seen between the different muscle, probe orientation and participant groups. All trials bar one gave mean values of $5.0 \times 10^{-4} \pm 1.0 * 10^{-4}$, with the BB CROSS trial in the MND affected participants giving a mean value of $4.0 \times 10^{-4} \pm 1.0 \times 10^{-4}$. As in 7.3.1. All full set of mean and standard deviation values for total x and y distances and Euler number can be viewed in Table 7.5.

Using the corrected α value of 0.0083 or less. The p values for the total distances between object centroids reported in Table 6.2 show significant

differences ($p = 0.005$ or less) between the healthy and MND affected participant groups in all but the MG CROSS trial for the total x component distances, where $p = 0.07$.

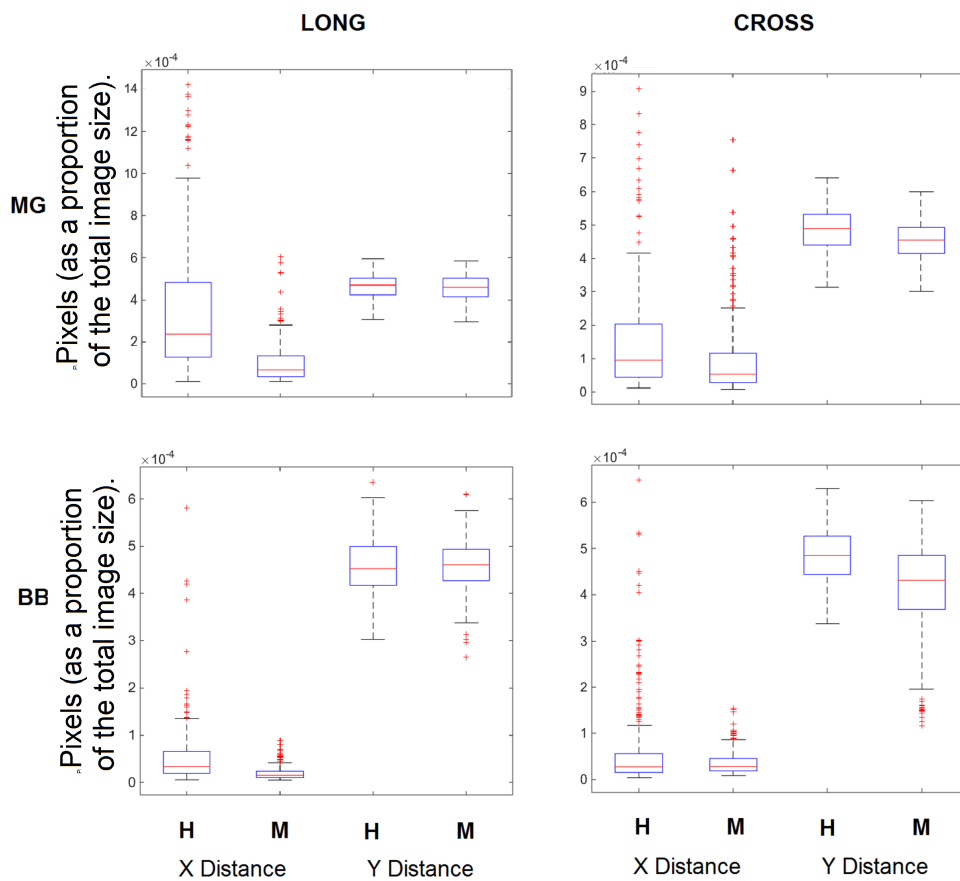


Figure 7.8: Boxplots showing total x and y distances between object centroids for healthy and MND affected participant groups in MG and BB.

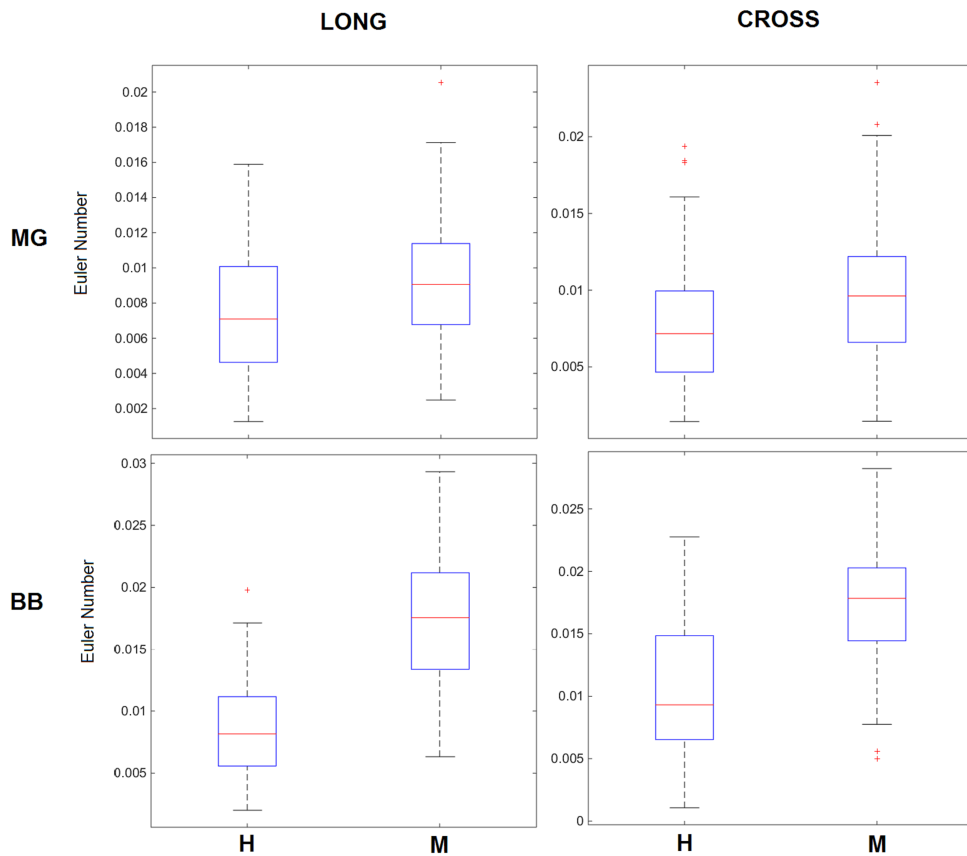


Figure 7.9: Boxplots showing mean Euler number of image for twitches from healthy and MND affected participant groups in MG and BB.

Mean Euler number values, shown in Table 6.2 showed highly significant results across both muscles and probe orientations, with the MND affected participant group showing greater Euler number values for all four trials (between 3.7×10^{-3} and 10.5×10^{-3} for healthy compared to between 9.2×10^{-3} and 17.3×10^{-3} for MND). These values were also generally higher in BB than in MG and generally higher in transverse compared to longitudinal with the exception on BB MND where mean values were 17.4×10^{-3} for LONG and 17.3×10^{-3} for CROSS (For all mean and stan-

dard deviation values see Table 7.5. These differences all gave p values of less than the corrected significance level of 0.0083. Distances between foreground objects in the y direction were less conclusive, with the level of significance only reached in the MG CROSS trial. However, the distances between foreground objects in the x direction all gave p values that were less than 0.04.

Healthy	Total X Distances		Total Y Distances		Euler Number	
	Mean	Standard Deviation	Mean	Standard Deviation	Mean	Standard Deviation
MG LONG	4.0×10^{-4}	3.0×10^{-4}	5.0×10^{-4}	1.0×10^{-4}	3.7×10^{-3}	2.0×10^{-3}
MG CROSS	2.0×10^{-4}	2.0×10^{-4}	5.0×10^{-4}	5.0×10^{-4}	7.6×10^{-3}	3.8×10^{-3}
BB LONG	1.0×10^{-4}	1.0×10^{-4}	5.0×10^{-4}	1.0×10^{-4}	8.7×10^{-3}	3.8×10^{-3}
BB CROSS	1.0×10^{-4}	1.0×10^{-4}	5.0×10^{-4}	1.0×10^{-4}	10.5×10^{-3}	5.4×10^{-3}

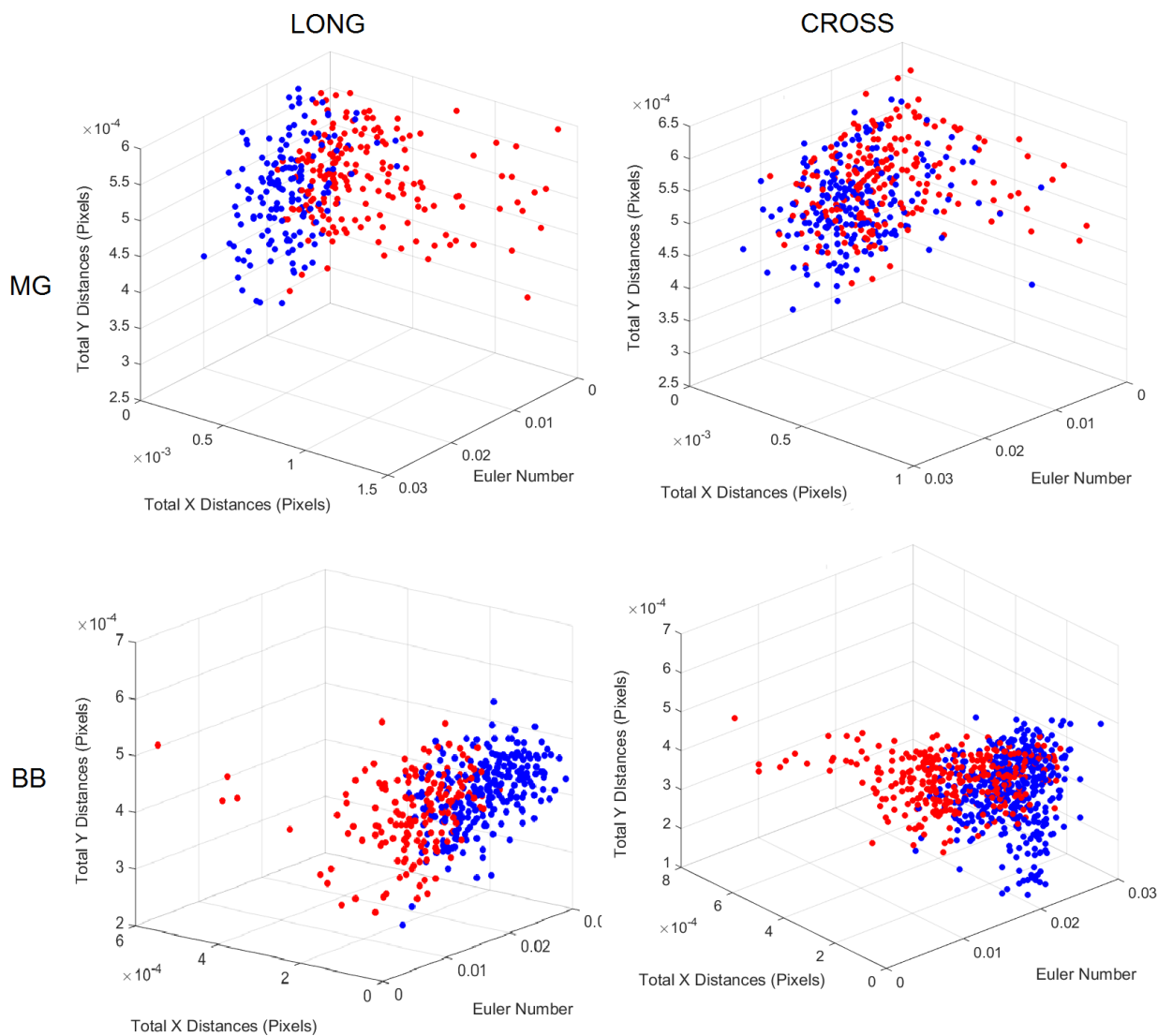
MND	Total X Distances		Total Y Distances		Euler Number	
	Mean	Standard Deviation	Mean	Standard Deviation	Mean	Standard Deviation
MG LONG	1.0×10^{-4}	1.0×10^{-4}	5.0×10^{-4}	1.0×10^{-4}	9.2×10^{-3}	3.5×10^{-3}
MG CROSS	1.0×10^{-4}	1.0×10^{-4}	5.0×10^{-4}	1.0×10^{-4}	9.7×10^{-3}	4.0×10^{-3}
BB LONG	2.0×10^{-5}	1.4×10^{-5}	5.0×10^{-4}	1.0×10^{-4}	17.4×10^{-4}	5.0×10^{-3}
BB CROSS	3.6×10^{-5}	2.4×10^{-5}	4.0×10^{-4}	1.0×10^{-4}	17.3×10^{-3}	4×10^{-3}

Table 7.5: Table Showing the Mean and Standard Deviation Values for Total X and Y Distances and Euler Number in Healthy (Top) and MND Affected (Bottom) Participant Groups.

	Total X Distances	Total Y Distances	Euler Number
MG LONG	< 0.0083	0.241	< 0.0083
MG CROSS	< 0.0083	< 0.0083	< 0.0083
BB LONG	< 0.0083	0.546	< 0.0083
BB CROSS	< 0.0083	0.977	< 0.0083

Table 7.6: Significance (P values) of total x and y distances between object centroids and object area differences between healthy and MND affected participant groups.)

The differences between the two participant groups were visualised using 3D scatter plots, shown in Figure 7.10 it can be seen that although there is overlap between the two groups, in three of the four trials (MG LONG, BB LONG and BB CROSS) the majority of twitches cluster into two distinct groupings. However, this is not the case in the MG CROSS trials where the overlap of the two groups is absolute.



1 pixel is approximately 0.07 x 0.09 mm²

Figure 7.10: 3D scatter plot showing total distances between object centroids (x and y components) and Euler number in MG and BB with MND participants in red and healthy participants in blue.

7.4 Discussion

This chapter aimed to provide a more in depth, quantitative analysis of muscle twitches as they occur in ultrasound images and consider two main questions; are there differences between spatial and timing data related to twitches when detected using the GMM and do these differ between muscle and probe orientation?

Results were split in to three groups; time durations of the different twitch phases, the variations in number of foreground objects during different twitch phases and the distances between object centroids. The twitch timing duration measures showed similar patterns in the longitudinal and cross sectional probe orientations of the BB. However, between the two probe orientations in the MG the longitudinal generally showed larger time durations in the MND affected group while the cross sectional orientation generally showed greater time durations in the healthy participant group. The possible reasons behind these differences between the MG and BB may be due to the structural differences and fibre orientation between the two muscles. With the BB being a parallel fibre orientation, when the probe is orientated longitudinally images are collected along the length of the fibres and perpendicular to the fibres in cross sectional orientation. However, the MG is a pennate muscle meaning that when the probe is placed either in longitudinal or cross sectional orientation the fibres will run through the imaging window at an oblique angle, which may explain the similarities in results in the BB and differences in the MG. Significant differences were seen between the participant groups in one timing

measure, which was the relaxation phase time. Although the contraction phase did not reach a level of significance equal to alpha its p value was less than 0.05, which could reach the alpha value with greater a number of fasciculations. This is an expected outcome as it is likely due to the differing tissue properties of healthy and MND affected muscle that muscle contraction and relaxation occur over different time scales.

The variations in number of foreground objects over time for MG showed greater values for peak difference and maximum peak values in the healthy participants, with the minimum peak value being greater in the MND group. Minimum peak values showed the inverse, with healthy participants having lower numbers of foreground objects during the secondary peak phase.

In the BB muscle, results were less consistent. In longitudinal probe orientation, similar peak difference and maximum peak values were seen between the two groups, with the MND group, generally having larger minimum peak values. In the cross sectional probe orientation, as in the MG, the peak difference and the maximum peak values were larger in the healthy participants. However, the Minimum peak values were larger in the healthy participants. In three out of the four muscle/ probe orientation combinations, lower peak difference and maximum peak values seemed to indicate the presence of MND.

In BB, the occurrence of fasciulations was infrequent in healthy participants. This may be one reason why BB results were less consistent than the results from the MG. This theory could be tested by collecting larger amounts of data from healthy participants so that the number of twitches

compared between the two groups was more even. Acceptable levels of significance were achieved in two out of the four measures; maximum peak height and minimum peak height.

The distance between foreground object centroids showed differences that were clear in the BB x components (Figure 7.8), with the total distances being greater in the healthy participants. The y components in BB CROSS showed again greater total distances in the healthy participants, however, results were similar in BB LONG. Overall, p values calculate for the differences between the healthy and MND affected participant groups showed that all results in BB were significant. This was not the case in MG and results were generally more varied. This is possibly due to the different fibre architecture of the two muscles. The parallel architecture of the BB means that a longitudinal probe orientation gives a view directly parallel to the muscle fibres and a transverse orientation gives a view perpendicular to the muscle fibres. Due to the pennate architecture of the MG, the view of the muscle collected in longitudinal and transverse probe orientations will always be oblique to the muscle fibres. It is also possible that this difference in architecture causes the fasciculation to move in a different manner between the MG and the BB, causing the spread of the foreground objects to be different between the two muscles and probe orientations.

The Euler number values showed conclusive differences between the healthy and MND affected participant groups and were significantly greater in the MND twitches in comparison to healthy twitches. As the Euler num-

ber is based on the number of foreground objects minus the number of holes in the objects, this indicates that the healthy twitches show a smaller total number of foreground objects or that such objects are more sparsely clustered and contain a large number of holes. This may be due to the reinnervation of denervated fibers to other motor units to create larger motor units.

By plotting the x and y component total distances against the Euler number, the individual twitch values were seen to separate, with reasonable distinction into two groups. However for one trial (MG CROSS) this was not the case. The reason for this is not clear, however, in addition to no clear groupings being apparent in the 3d plot, the MG CROSS also showed the highest p values for total distances between the x and y components of the centroids. It is possible that the probe orientation is just not suitable for an analysis of this type and this should be kept in mind in any future studies. It is also possible that due to awkward positioning required for probe access in MG CROSS that the problems may also be due to inferior image quality in comparison to other trials. Again this should be considered should any future work take place.

7.5 Conclusion

The more in depth analysis of individual twitches yielded possible methods with which to differentiate between healthy, involuntary activation and pathological, involuntary activation caused by MND. Although there were

indications of differences between the two participant groups, these were not necessarily consistent across the muscle and probe orientations, although differences were generally significant. Overall, the timing measures and spatial analysis yielded more consistent significant differences between the participant groups. To determine the feasibility of these measures as diagnostic markers, a larger scale study across a wider range of muscles would be required. As the majority of muscles in healthy participants will not twitch frequently enough to provide the data required, motor unit stimulation may also be an additional way to determine spatial and temporal characteristics in twitches. In addition to this, probe placement should be optimised on a per muscle basis to find the maximal differences between the participant groups.

Chapter 8

Discussion and Conclusions

The work presented here has answered a number of questions around the viability of the use of ultrasound imaging for the detection and analysis of involuntary muscle twitches, which may be applicable to MND diagnosis and monitoring. Firstly, the GMM analysis offers comparable accuracy to the KLT technique in relation to operator ID's and better accuracy in comparison to intramuscular EMG. It has also demonstrated the GMMs ability to perform across a number of muscles of different shapes, sizes and architecture which is necessary if a technique is to be considered as a potential tool for MND diagnosis. It has also provided a mixed number of positive results in relation to discriminating between individual twitches in the healthy and MND affected groups using spatial and temporal twitch characteristics. This has provided a solid basis for future work and offered potential methodological improvements that may enable future studies to accurately differentiate between healthy and pathological twitches.

Review and Suggestions for the GMM and Computational Analysis

The aims and objectives laid out for this thesis in Chapter 1.0.1 were focused on exploring the potential of computational analysis of ultrasound images for the detection and characterisation of fasciculations in healthy and MND affected participant groups. The objectives identified to achieve this aim were; the development of an additional analysis technique, the comparison of the new technique to the KLT, the application of techniques to previously untested muscles and comparison of spatial and temporal characteristics of twitches from the healthy and MND affected groups. The objectives stated above and in the introduction have been successfully carried out. Chapters 4 and 5 found high agreement between the KLT/GMM analyses and the manual ID truth signal, confirming the GMM as a valid fasciculation detection technique. The comparison with the EMG truth signal showed the GMM to be the superior technique as it offered improved accuracy compared to the KLT across both muscles and probe orientations. This highlighted the best current technique for the potential application of MND diagnosis, although as the GMM bases its identifications on the pixel intensity outliers rather than the actual motion between frames a possible alternative may be a technique that is a combination of both the GMM and the KLT, using the GMM to reduce noise and the optical flow method to calculate motion to determine directions and velocities of motion.

A further objective; extending the analysis to a wider array of muscles, highlighted a weakness in the KLT. In muscles where breathing patterns

were apparent, such as the TP and RA, the dominant component of the output signal was due to the inhalation and exhalation of the participant, with any underlying fasciculations lost. However, the GMM was able to adapt to the repetitive motion of breathing and detected the underlying fasciculations with good degrees of accuracy. This further supported the GMM as the optimal computational technique identified to date.

The final objective of this thesis was the characterization of twitches as either healthy or pathological based on their spatial and/ or temporal profile. Although a number of trials were shown to have significant differences between the healthy and MND affected participants this was not consistent across all trials. The most promising results were shown in the timing measures of twitch peaks and spatial analysis taken from the distribution of foreground objects across the image (Section 7.3.1 and 7.3.3). Twitch timing measures (total twitch duration, contraction phase duration, relaxation phase duration and peak to peak duration) in longitudinal orientation as well as the Euler number and x distances in the spatial analysis consistently and significantly higher in the MND group compared to the healthy group (Figure 7.9). However, the timing analysis results for transverse probe orientation showed less consistent differences, although differences between the participant groups were shown to be significant.

The 3d plots of the x and y components of the total distances between object centroids and the Euler number showed two clusters for healthy and MND affected participant groups for all but the MG CROSS trials (Figure 7.10). Although the image and centroid analysis showed promising results with relatively consistent differences between the healthy and MND

data, the peak amplitudes were not consistent between all trials (Section 7.3.1 and Section 7.3.2) and results were not always significant, meaning that particular markers for MND in relation to peak height could not be established with any great certainty. To further improve the computational analysis, one possible option would be to segment images during analysis in order to separate the superficial and deep muscles. Currently, images are cropped to include only the superficial muscles such as the BB and the MG, with muscles such as the Soleus and the Brachialis not included. A segmentation method such as active shape models (that have previously been used on ultrasound images of skeletal muscle [97], [9]) would mean that a much larger amount of data could be analysed with no additional data collection time required as analysis could be localised to specific muscles. This methodology would also allow for assessments to be made as to whether any differences, in relation to presence and characteristics of fasciculations, exist between superficial and deep muscles throughout the course of the disease.

Computational Analysis for Diagnosis and Clinical Trials

The characterisation of healthy and MND fasciculations was largely successful, with significant differences between groups found for a number of spacial and temporal measures. However, these results were only collected in the BB and MG muscles, which for the purpose of MND diagnosis would not be sufficient (due to the required presence of fasciculations in a number of locations). If this technique were to be presented as a potential

complimentary or alternative method to EMG, the methodology presented in Chapter 6 would, at the very least, need to be extended to the RF, RA, TP and TRAPS and additional muscles of different size, shape and architecture. These muscles could not be carried forward to analysis in Chapter 7 due to fasciculations being all but absent in healthy participants. This could potentially be remedied by conducting further studies into stimulated twitches, potentially using similar methodology to that used in [66] where twitches were stimulated from the skins surface and applying this across a wider range of muscles to ensure a large enough number of instances to enable a full scale analysis and comparison between groups. This may also improve the statistical power of results collected from the MG and BB, where fasciculations were captured in healthy participants, but in some cases not in the numbers collected from MND affected participants. A larger number of healthy fasciculations may decrease the p values that did not reach the predefined alpha value to a level of significance.

This work further supports the positive contributions ultrasound imaging could make for improved detection of involuntary activations in contrast to the current gold standard technique of EMG. The GMM has been shown to provide good agreement with two different truth signals and is robust to different muscles and probe orientations. It also offers a more objective alternative to the methods that currently exist within the literature [6], [65] which are generally based on ultrasound image assessment by clinicians or other expert operators. Such studies generally focus on distinguishing between MND patients and other neurogenic or myogenic disorders,

which has not been the focus of this thesis. The work presented here has focused on objective detection and determination of differences between involuntary activations within healthy and MND participant groups, but has stopped short of attempting to classify patients as MND affected based on such data. In order to answer this question conclusively, a larger scale data collection, potentially in the form of a clinical trial is needed (of either MND or other similar pathologies), possibly when patients initially present with particular symptoms at clinic. From these data, an attempt to classify patients as MND affected or MND unaffected could be made based on number and characteristics of involuntary muscle events, with sensitivity and specificity values of this technique being calculated, bringing it in line and enabling a direct comparison with the subjective analyses existing within the literature [65], [6], [5] and enabling an assessment in terms of what it may add to EMG protocols. Due to the relative rarity of MND, this could potentially require large numbers of participants in order to ensure enough cases of MND will be encountered.

Additional Future Work

In addition to previous suggestions for further work, it may also be of benefit to combine the ultrasound with surface EMG (sEMG) arrays to map the activation patterns of the myoelectric signals with the mechanical displacement displayed in the ultrasound images [95]. The intramuscular EMG that has been used for comparison with the ultrasound images in this thesis has a very small pick up volume, therefore it can indicate if a twitch has

occurred within the muscle, but gives no indication where it has originated or how it has been conducted through the tissue. A sEMG array for more localisation of activations which would allow for positions of activations to be compared to locations of twitches in the ultrasound, in contrast to simply comparing activation in the images and EMG based on the time with which they occur.

8.0.1 Limitations

This body of work has introduced an additional computational analysis method as well as showing significant differences between twitches identified in healthy and MND affected participants. However, the number of participants was relatively small ($n = 40$). Also the majority of MND affected participants were usually at least 3 months post diagnosis (for some this was years), with MND and its symptoms being well established. Therefore, the differences found between participant groups can not be assumed to exist during the early stages and this would require further investigation. Also, muscles such as the RA and TP had fewer successful trials in comparison to the other muscles due to issues with access. Mobility issues in some participants meant that they were unable to support themselves away from the couch, which meant there was not enough space for probe access. This could also not be remedied by repositioning participants as many could not be placed in the prone position due to breathing difficulties. In the RA participants were excluded from data collection in that particular

muscle if a feeding peg was present. This was due to increased infection risks that may be introduced by the needle electrode and probe.

Finally, lower accuracy levels still exist for the majority of results in the images taken from MND affected participants compared to healthy participants, which is likely due to the low contrast of the images from participants with MND due to changes in the muscle tissue properties. Accuracy levels were still above 80% in all cases, however, further investigation in how to improve the GMM in lower contrast images should also be considered to make a fairer comparison between the healthy and MND affected populations.

8.0.2 Conclusion

This thesis has contributed to validating an objective, computational analysis of ultrasound images as a non invasive means of the detection and characterisation of involuntary muscle activations. Through the testing of computer vision techniques for different probe orientations and a number of muscles, this method, which has not previously been used for this application has been found superior to the current analysis technique.

A number of different key contributions were made in this thesis, these include:

1. Finding comparable results between the GMM and KLT when using operator identifications as a truth signal.
2. Showing superior results from the GMM in contrast to the KLT, when

using the intramuscular EMG as truth signals.

3. Showing good levels of agreement with the EMG truth signal, across a wider range of muscles when using the GMM analysis.
4. Finding significant differences between the spatial and temporal characteristics of fasciculations, as they appear in ultrasound images.

Further work should initially be focused on clarifying spatial and temporal twitch markers through a much larger healthy participant dataset and the collection of images of stimulated twitches from healthy and MND affected participants. A larger data set may give greater statistical power to those trials that had not achieved significant p values, with a stimulated twitch study allowing for a comparative data collection across a wider range of muscles, which has not been possible here due to low numbers or absence of fasciculation in the healthy participant group. Once this has been achieved, a large scale clinical study collecting data at the pre-diagnosis stage with the aim of separating the MND data from all other data through the computational analysis. In addition to this, a comparison of the computational methods and surface EMG arrays would allow for electrophysiological data to be collected from a area similar to that viewed by the ultrasound potentially acting as an improved truth signal in contrast to the intramuscular EMG. This further work should enable a full conclusion to be made on whether computational analysis of ultrasound images

is a valid method for MND diagnosis.

Bibliography

- [1] Motor neurone disease. <http://www.nhs.uk/conditions/Motor-neurone-disease/Pages/Introduction.aspx>. Accessed: 31-12-2016, Reviewed: 29-05-2015.
- [2] Tests for motor neurone disease. <http://www.mndassociation.org/what-is-mnd/diagnostic-process/>. Accessed: 31-12-2016.
- [3] GM. Ginsberg and B Lev. Cost-benefit analysis of riluzole for the treatment of amyotrophic lateral sclerosis. *Pharmacoeconomics*, 12(5):578–584, 1997. doi: 10.2165/00019053-199712050-00008.
- [4] KR Mills. The basics of electromyography. *Journal of Neurology, Neurosurgery & Psychiatry*, 76(suppl 2):ii32–ii35, 2005. doi: 10.1136/jnnp.2005.069211.
- [5] S Misawa, Y Noto, K Shibuya, S Iose, Y Sekiguchi, S Nasu, and S Kuwabara. Ultrasonographic detection of fasciculations markedly increases diagnostic sensitivity of als. *Neurology*, 77(16):1532–1537, 2011. doi: 10.1212/WNL.0b013e318233b36a.

- [6] IM Arts, S Overeem, S Pillen, BU Kleine, WA Boekestein, MJ Zwarts, and et al. Muscle ultrasonography: A diagnostic tool for amyotrophic lateral sclerosis. *Clinical Neurophysiology*, 123(8):1662–1667, 2012. doi: 10.1016/j.clinph.2011.11.262.
- [7] A Esteva, B Kuprel, RA Novoa, J Ko, SM Swetter, HM Blau, and S Thrun. Dermatologist-level classification of skin cancer with deep neural networks. *Nature*, 542(7639):115–118, 2017. doi: 10.1038/nature21056.
- [8] Afsaneh J. Computer-aided detection/diagnosis of breast cancer in mammography and ultrasound: a review.
- [9] PJ Harding, ID Loram, N Combes, and EF Hodson-Tole. Ultrasound-based detection of fasciculations in healthy and diseased muscles. *IEEE Transactions on Biomedical Engineering*, 63(3):512–518, 2016. doi: 10.1109/TBME.2015.2465168.
- [10] J Rosenfeld and M Swash. What’s in a name? lumping or splitting als, pls, pma, and the other motor neuron diseases. *Neurology*, 66(5):624–625, 2006. doi: 0.1212/01.wnl.0000205597.62054.db.
- [11] Epidemiology of sporadic als. <http://www.nhs.uk/conditions/Motor-neurone-disease/Pages/Introduction.aspx>. Accessed: 11-03-2017.
- [12] Primary lateral sclerosis. <http://emedicine.medscape.com/article/1171782-overview>. Accessed: 11-03-2017, Reviewed: 30-12-2017.

- [13] Progressive bulbar palsy. <http://www.msmanuals.com/en-gb/professional/neurologic-disorders/peripheral-nervous-system-and-motor-unit-disorders/overview-of-peripheral-nervous-system-disorders>. Accessed: 11-03-2017, Reviewed: 30-10-2016.
- [14] Progressive muscular atrophy in the als spectrum. <http://www.medscape.com/viewarticle/720267>. Accessed: 11-03-2017.
- [15] Amyotrophic lateral sclerosis differential diagnoses. <http://emedicine.medscape.com/article/1170097-differential>. Accessed: 31-12-2016, Reviewed: 23-03-2016.
- [16] BJ Traynor, MB Codd, B Corr, C Forde, E Frost, and OM Hardiman. Clinical features of amyotrophic lateral sclerosis according to the el escorial and airlie house diagnostic criteria: A population-based study. *Archives of neurology*, 57(8):1171–1176, 2000. doi: 10.1001/archneur.57.8.1171.
- [17] M de Carvalho, R Dengler, A Eisen, JD England, R Kaji, and J et al Kimura. Electrodiagnostic criteria for diagnosis of als. *Clinical neurophysiology*, 119(3):497–503, 2008. doi: 10.1016/j.clinph.2007.09.143.
- [18] CD Reimers, U Ziemann, A Scheel, and P Rieckmann. Fasciculations: clinical, electromyographic, and ultrasonographic assessment. *Journal of neurology*, 243(8):579–584, 1996. doi: 10.1007/BF00900945.

- [19] J Desai and MI Swash. Fasciculations: what do we know of their significance? *Journal of the neurological sciences*, 152:s43–s48, 1997. doi: 10.1016/S0022-510X(97)00243-8.
- [20] KR Mills. Characteristics of fasciculations in amyotrophic lateral sclerosis and the benign fasciculation syndrome. *Brain*, 133(11):3458–3469, 2010. doi: 10.1093/brain/awq290.
- [21] Ni Hirota, A Eisen, and M Weber. Complex fasciculations and their origin in amyotrophic lateral sclerosis and kennedy’s disease. *Muscle & nerve*, 23(12):1872–1875, 2000. doi: 10.1002/1097-4598(200012)23:12.
- [22] B Chen and P Zhou. Detection of fasciculation potentials in amyotrophic lateral sclerosis using surface emg. In *Frontier and Future Development of Information Technology in Medicine and Education*, pages 2437–2442. 2014. doi: 10.1007/978-94-007-7618-0302.
- [23] B Katirji, HJ Kaminski, and RL Ruff. *Neuromuscular disorders in clinical practice*. Springer Science & Business Media, 2013.
- [24] MJ Aminoff. *Aminoff’s electrodiagnosis in clinical neurology*. Elsevier Health Sciences, 2012.
- [25] S West. *Rheumatology secrets*. Elsevier Health Sciences, 2014.
- [26] GH Kraft. Issues & opinions: Are fibrillation potentials and positive sharp waves the same? no. *Muscle & nerve*, 19(2):216–220, 1996. doi: 10.1002/(SICI)1097-4598(199602)19:2.

- [27] S Paganoni, EA Macklin, A Lee, A Murphy, J Chang, A Zipf, M Cudkowicz, and N Atassi. Diagnostic timelines and delays in diagnosing amyotrophic lateral sclerosis (als). *Amyotrophic Lateral Sclerosis and Frontotemporal Degeneration*, 15(5-6):453–456, 2014. doi: 10.3109/21678421.2014.903974.
- [28] D. Purves. *Neuroscience*. ISBN 9780878936953.
- [29] MW Barnett and PM Larkman. The action potential. *Practical Neurology*, 7(3):192–197, 2007. doi: PMID: 17515599.
- [30] SM Sine. End-plate acetylcholine receptor: Structure, mechanism, pharmacology, and disease. *Physiological Reviews*, 92(3):1189–1234, 2012. doi: 10.1152/physrev.00015.2011.
- [31] HS Cohen. *Neuroscience for Rehabilitation*. Lippincott Williams & Wilkins, 1999. ISBN 9780397554652.
- [32] JM. Shefner. Motor unit number estimation in human neurological diseases and animal models. *Clinical Neurophysiology*, 112(6):955 – 964, 2001. doi: [http://dx.doi.org/10.1016/S1388-2457\(01\)00520-X](http://dx.doi.org/10.1016/S1388-2457(01)00520-X).
- [33] J. Hegedus, C.T. Putman, and T. Gordon. Time course of preferential motor unit loss in the {SOD1G93A} mouse model of amyotrophic lateral sclerosis. *Neurobiology of Disease*, 28(2):154 – 164, 2007. doi: <http://dx.doi.org/10.1016/j.nbd.2007.07.003>.
- [34] J Hill. *Muscle: Fundamental Biology and Mechanisms of Disease*. Academic Press, 2012. ISBN 9780123815101.

- [35] V Zatsiorsky and B Prilutsky. *Biomechanics of Skeletal Muscles*. Human Kinetics. ISBN 9781450428842.
- [36] RL Lieber. *Skeletal Muscle Structure, Function, and Plasticity*. Skeletal muscle structure, function and plasticity: the physiological basis of rehabilitation. Lippincott Williams & Wilkins, 2002. ISBN 9780781730617.
- [37] RH Fitts. The cross-bridge cycle and skeletal muscle fatigue. *Journal of Applied Physiology*, 104(2):551–558, 2008. doi: 10.1152/jap-physiol.01200.2007.
- [38] DJ Aidley. *The Physiology of Excitable Cells*. Cambridge University Press, 1998. ISBN 9780521574211.
- [39] JC Eccles and CS Sherrington. Numbers and contraction-values of individual motor-units examined in some muscles of the limb. *Proceedings of the Royal Society of London. Series B, Containing Papers of a Biological Character*, 106(745):326–357, 1930. doi: 10.1098/rspb.1930.0032.
- [40] R. E. Burke, D. N. Levine, P. Tsairis, and F. E. Zajac. Physiological types and histochemical profiles in motor units of the cat gastrocnemius. *The Journal of Physiology*, 234(3):723–748, 1973. doi: 10.1113/jphysiol.1973.sp010369.
- [41] C Hammarberg and J-O Kellerth. Studies of some twitch and fatigue properties of different motor unit types in the ankle muscles of the

- adult cat. *Acta Physiologica Scandinavica*, 95(3):231–242, 1975. doi: 10.1111/j.1748-1716.1975.tb10047.x.
- [42] E Eisenberg and TL Hill. Muscle contraction and free energy transduction in biological systems. *Science*, 227(4690):999–1006, 1985. doi: 10.1126/science.3156404.
- [43] AJ Buller and DM Lewis. The rate of tension development in isometric tetanic contractions of mammalian fast and slow skeletal muscle. *The Journal of Physiology*, 176(3):337, 1965. doi: PMC1357200.
- [44] FO Walker, PD Donofrio, GJ Harpold, and WG Ferrell. Sonographic imaging of muscle contraction and fasciculations: a correlation with electromyography. *Muscle & nerve*, 13(1):33–39, 1990. doi: 10.1002/mus.880130108.
- [45] J Duchateau and K Hainaut. Nonlinear summation of contractions in striated muscle. i. twitch potentiation in human muscle. *Journal of Muscle Research & Cell Motility*, 7(1):11–17, 1986. doi: PMID: 3958155.
- [46] CT Leondes. *Medical Imaging Systems Technology: Volume 2: Modalities*. 2005. ISBN 9789814480161.
- [47] P Han, Y Chen, L Ao, G Xie, H Li, L Wang, and Y Zhou. Automatic thickness estimation for skeletal muscle in ultrasonography: Evaluation of two enhancement methods. *Biomedical Engineering Online*, 12(1):1, 2013. doi: 110.1186/1475-925X-12-6.

- [48] LK Kwah, RZ Pinto, J Diong, and RD Herbert. Reliability and validity of ultrasound measurements of muscle fascicle length and pennation in humans: A systematic review. *Journal of Applied Physiology*, 114(6):761–769, 2013. doi: 10.1152/jappphysiol.01430.2011.
- [49] A Nordez, T Gallot, S Catheline, A Guével, C Cornu, and F Hug. Electromechanical delay revisited using very high frame rate ultrasound. *Journal of Applied Physiology*, 106(6):1970–1975, 2009. doi: 10.1152/jappphysiol.00221.2009.
- [50] J. Darby, B. Li, N. Costen, I. Loram, and E. Hodson-Tole. Estimating skeletal muscle fascicle curvature from b-mode ultrasound image sequences. *IEEE Transactions on Biomedical Engineering*, 60(7):1935–1945, July 2013. doi: 10.1109/TBME.2013.2245328.
- [51] WW Gibbon. *Musculoskeletal Ultrasound: The Essentials*. Greenwich Medical Media. Greenwich Medical Media, 1996. ISBN 9781900151054.
- [52] B Ilnatsenka and AP Boezaart. Ultrasound: Basic understanding and learning the language. *International Journal of Shoulder Surgery*, 4(3):55, 2010. doi: 10.4103/0973-6042.76960.
- [53] NM Maurits, AE Bollen, A Windhausen, AE De Jager, and JH Van Der Hoeven. Muscle ultrasound analysis: Normal values and differentiation between myopathies and neuropathies. *Ultrasound in medicine & biology*, 29(2):215–225, 2003. doi: PMID: 12659909.

- [54] Ki Sogawa, H Nodera, N Takamatsu, A Mori, H Yamazaki, and Y Shimatani et al. Neurogenic and myogenic diseases: Quantitative texture analysis of muscle us data for differentiation. *Radiology*, 0(0):160826, 2016. doi: 10.1148/radiol.2016160826.
- [55] M Visser. Towards a definition of sarcopenia—results from epidemiologic studies. *JNHA-The Journal of Nutrition, Health and Aging*, 13(8):713–716, 2009. doi: PMID: 19657555.
- [56] BH Goodpaster, CL Carlson, M Visser, DE Kelley, A Scherzinger, TB Harris, and et al. Attenuation of skeletal muscle and strength in the elderly: The health abc study. *Journal of Applied Physiology*, 90(6):2157–2165, 2001. doi: PMID: 11356778.
- [57] FW Booth, SH Weeden, and BS Tseng. Effect of aging on human skeletal muscle and motor function. *Medicine and Science in Sports and Exercise*, 26(5):556–560, 1994.
- [58] J Lexell. Evidence for nervous system degeneration with advancing age. *The Journal of Nutrition*, 127(5):1011S–1013S, 1997. doi: PMID: 9164286.
- [59] JE Howard, KC McGill, and LJ Dorfman. Age effects on properties of motor unit action potentials: Ademg analysis. *Annals of Neurology*, 24(2):207–213, 1988. doi: 10.1002/ana.410240206.
- [60] A Grimm, B Heiling, U Schumacher, OW Witte, and H Axer. Ultrasound differentiation of axonal and demyelinating neuropathies. *Muscle & Nerve*, 50(6):976–983, 2014. doi: 10.1002/mus.24238.

- [61] S Pillen, IM Arts, and MJ Zwarts. Muscle ultrasound in neuromuscular disorders. *Muscle & Nerve*, 37(6):679–693, 2008. doi: 10.1002/mus.21015.
- [62] IMP Arts, S Overeem, S Pillen, HJ Schelhaas, and MJ Zwarts. Muscle changes in amyotrophic lateral sclerosis: a longitudinal ultrasonography study. *Clinical Neurophysiology*, 122(3):623–628, 2011. doi: 10.1016/j.clinph.2010.07.023.
- [63] S Pillen, M Nienhuis, JP van Dijk, IP Arts, N van Alfen, and MJ Zwarts. Muscles alive: Ultrasound detects fibrillations. *Clinical Neurophysiology*, 120(5):932–936, 2009. doi: 10.1016/j.clinph.2009.01.016.
- [64] N Van Alfen, M Nienhuis, MJ Zwarts, and S Pillen. Detection of fibrillations using muscle ultrasound: diagnostic accuracy and identification of pitfalls. *Muscle & nerve*, 43(2):178–182, 2011. doi: 10.1002/mus.21863.
- [65] A Grimm, T Prell, BF Décard, U Schumacher, OW Witte, H Axer, and J Grosskreutz. Muscle ultrasonography as an additional diagnostic tool for the diagnosis of amyotrophic lateral sclerosis. *Clinical Neurophysiology*, 126(4):820–827, 2015. doi: 10.1016/j.clinph.2014.06.052.
- [66] PJ Harding, EF Hodson-Tole, R Cunningham, I Loram, and N Costen. Automated detection of skeletal muscle twitches from b-mode ultrasound images: An application to motor neuron disease. In *Pattern*

- Recognition (ICPR), 2012 21st International Conference on*, pages 2630–2633. IEEE, 2012.
- [67] NM Tole and H Ostensen. *Basic Physics of Ultrasonographic Imaging*. Who/Diagnostic Imaging and Laboratory Technology Series. World Health Organization, 2005. ISBN 9789241592994.
- [68] PR Hoskins, K Martin, and A Thrush. *Diagnostic Ultrasound: Physics and Equipment*. Cambridge University Press, 2010. ISBN 9781139488907.
- [69] AF AbuRahma and J Bergan. *Noninvasive Vascular Diagnosis*. Springer London, 2013. ISBN 9781447138372.
- [70] J Avison. *The World of Physics*. Nelson, 2014. ISBN 9780174387336.
- [71] GD Ludwig. The velocity of sound through tissues and the acoustic impedance of tissues. *The Journal of the Acoustical Society of America*, 22(6):862–866, 1950. doi: 10.1121/1.1906706.
- [72] KB Wolf and G Krotzsch. Geometry and dynamics in refracting systems. *European Journal of Physics*, 16(1):14, 1995. doi: 10.1088/0143-0807/16/1/003.
- [73] GR Lockwood, DH Turnball, DA Christopher, and FS Foster. Beyond 30 mhz [applications of high-frequency ultrasound imaging]. *IEEE Engineering in Medicine and Biology Magazine*, 15(6):60–71, 1996. doi: 10.1088/0143-0807/16/1/003.

- [74] S Pillen and N van Alfen. Skeletal muscle ultrasound. *Neurological Research*, 33(10):1016–1024, 2011. doi: 10.1179/1743132811Y.0000000010.
- [75] QB Carroll. *Radiography in the Digital Age: Physics - Exposure - Radiation Biology (2nd Ed.)*. EBSCO ebook academic collection. Charles C. Thomas Publisher, Limited, 2014. ISBN 9780398080976.
- [76] BD Lucas, T Kanade, et al. An iterative image registration technique with an application to stereo vision. In *IJCAI*, volume 81, pages 674–679, 1981.
- [77] C Tomasi and T Kanade. *Detection and tracking of point features*. School of Computer Science, Carnegie Mellon Univ. Pittsburgh, 1991.
- [78] J Shi and C Tomasi. Good features to track. In *Computer Vision and Pattern Recognition, 1994. Proceedings CVPR'94., 1994 IEEE Computer Society Conference on*, pages 593–600. IEEE, 1994.
- [79] MD Binder, N Hirokawa, and U Windhorst, editors. *Aperture Problem*, pages 159–159. Springer Berlin Heidelberg, Berlin, Heidelberg, 2009. ISBN 978-3-540-29678-2.
- [80] C.E. Shannon. A mathematical theory of communication. *Bell Syst Tech. J.*, 27:379–423, 1948. doi: 10.1002/j.1538-7305.1948.tb0133.
- [81] BKP Horn and BG Schunck. Determining optical flow. *Artificial intelligence*, 17(1-3):185–203, 1981. doi: 10.1016/0004-3702(81)90024-2.

- [82] C Stauffer and WEL Grimson. Adaptive background mixture models for real-time tracking. In *Computer Vision and Pattern Recognition, 1999. IEEE Computer Society Conference on.*, volume 2. IEEE, 1999.
- [83] P KaewTraKulPong and R Bowden. An improved adaptive background mixture model for real-time tracking with shadow detection. In *Video-based surveillance systems*, pages 135–144. 2002. doi: 10.1007/978-1-4615-0913-411.
- [84] L He, Y Chao, K Suzuki, and K Wu. Fast connected-component labeling. *Pattern Recognition*, 42(9):1977–1987, 2009. doi: 10.1016/j.patcog.2008.10.013.
- [85] W Trojaborg and F Buchthal. Malignant and benign fasciculations. *Acta Neurologica Scandinavica*, 41(S13):251–254, 1965. doi: 10.1111/j.1600-0404.1965.tb01880.x.
- [86] S Pillen, A Verrips, N Van Alfen, IMP Arts, LTL Sie, and MJ Zwarts. Quantitative skeletal muscle ultrasound: diagnostic value in childhood neuromuscular disease. *Neuromuscular disorders*, 17(7):509–516, 2007. doi: 10.1016/j.nmd.2007.03.008.
- [87] JA Hanley and BJ McNeil. The meaning and use of the area under a receiver operating characteristic (roc) curve. *Radiology*, 143(1):29–36, 1982.
- [88] S Pillen, RO Tak, MJ Zwarts, MMY Lammens, KN Verrijp, and IMP et al Arts. Skeletal muscle ultrasound: correlation between fibrous

- tissue and echo intensity. *Ultrasound in medicine & biology*, 35(3): 443–446, 2009. doi: 10.1016/j.ultrasmedbio.2008.09.016.
- [89] A Grimm, U Teschner, C Porzelius, K Ludewig, J Zielske, and OW et al Witte. Muscle ultrasound for early assessment of critical illness neuromyopathy in severe sepsis. *Critical Care*, 17(5):1, 2013. doi: 10.1186/cc13050.
- [90] A Singh, P Jaikumar, SK Mitra, MV Joshi, and A Banerjee. Detection and tracking of objects in low contrast conditions. In *IEEE National Conference on Computer Vision, Pattern Recognition, Image Processing and Graphics (NCVPRIPG), Gandhinagar, India*, pages 98–103, 2008.
- [91] T Okita, H Nodera, Y Shibuta, A Nodera, K Asanuma, Y Shimatani, and et al. Can awaji als criteria provide earlier diagnosis than the revised el escorial criteria? *Journal of the Neurological Sciences*, 302(1):29–32, 2011. doi: 10.1016/j.jns.2010.12.007.
- [92] KR Mills. Detecting fasciculations in amyotrophic lateral sclerosis: duration of observation required. 82(5):549–551, 2011. doi: 10.1136/jnnp.2009.186833.
- [93] KC McGill, ZC Lateva, and HR Marateb. Emglab: An interactive emg decomposition program. *Journal of Neuroscience Methods*, 149(2): 121–133, 2005. doi: 10.1016/j.jneumeth.2005.05.015.
- [94] F Hug, T Gallot, S Catheline, and A Nordez. Electromechanical delay

- in biceps brachii assessed by ultrafast ultrasonography. *Muscle & nerve*, 43(3):441–443, 2011. doi: 10.1002/mus.21948.
- [95] A Botter, TMM Vieira, ID Loram, R Merletti, and EF Hodson-Tole. A novel system of electrodes transparent to ultrasound for simultaneous detection of myoelectric activity and b-mode ultrasound images of skeletal muscles. *Journal of Applied Physiology*, 115(8):1203–1214, 2013. doi: 10.1152/jappphysiol.00090.2013.
- [96] RA Armstrong. When to use the bonferroni correction. *Ophthalmic and Physiological Optics*, 34(5):502–508, 2014. doi: 10.1111/opo.12131.
- [97] J Darby, B Li, N Costen, I Loram, and E Hodson-Tole. Estimating skeletal muscle fascicle curvature from b-mode ultrasound image sequences. *IEEE Transactions on Biomedical Engineering*, 60(7):1935–1945, 2013. doi: 10.1109/TBME.2013.2245328.

Chapter 9

Appendicies

9.1 Appendix 1: Parameterisation Tables for GMM and KLT/MI from Chapter 4

- Subsequent tables show parameterisation results for GMM analysis, showing accuracy results for test data set when using variable values for number of Gaussians, learning rate and background ratio. Optimum values in red.

Table 1
Parameterisation Results for GMM Analysis (Biceps Brachii)

Background Ratio	No. of Gaussians	Learning Rate	Accuracy (%)
80	5	0.5	90.09
80	5	0.05	87.34
80	5	0.005	86.50
80	4	0.5	89.67
80	4	0.05	87.32
80	4	0.005	86.51
80	3	0.5	86.34
80	3	0.05	87.81
80	3	0.005	86.51
85	5	0.5	90.35
85	5	0.05	88.94
85	5	0.005	88.01
85	4	0.5	87.00
85	4	0.05	89.06
85	4	0.005	88.01
85	3	0.5	86.48
85	3	0.05	87.62
85	3	0.005	89.77
90	5	0.5	77.56
90	5	0.05	91.07
90	5	0.005	88.73
90	4	0.5	81.08
90	4	0.05	91.52
90	4	0.005	88.73
90	3	0.5	88.55
90	3	0.05	91.57
90	3	0.005	88.73

Table 2
Parameterisation Results for GMM Analysis (Medial Gastrocnemius)

Background Ratio	No. of Gaussians	Learning Rate	Accuracy (%)
80	5	0.5	88.6
80	5	0.05	84.2
80	5	0.005	83.45
80	4	0.5	86.08
80	4	0.05	84.39
80	4	0.005	83.45
80	3	0.5	83.07
80	3	0.05	84.76
80	3	0.005	83.45
<hr/>			
85	5	0.5	89.26
85	5	0.05	87.9
85	5	0.005	86.9
85	4	0.5	87.04
85	4	0.05	90.54
85	4	0.005	86.9
85	3	0.5	85.04
85	3	0.05	90.61
85	3	0.005	86.9
<hr/>			
90	5	0.5	92.04
90	5	0.05	92.72
90	5	0.005	93.16
90	4	0.5	88.47
90	4	0.05	92.73
90	4	0.005	92.3
90	3	0.5	82.52
90	3	0.05	92.95
90	3	0.005	92.3

2. Subsequent tables show parameterisation results for KLT/ MI analysis, showing accuracy results for test data set when using variable values for direction and speed of motion. Optimum values in red.

Table 3

Parameterisation Results for KLT/MI Analysis (Biceps Brachii – Transverse)

Direction of Motion \vec{m}	Speed of Motion m			
	1	2	4	8
Π	75.21	75.21	75.21	75.21
$\pi/2$	82.29	80.26	78.73	82.29
$\pi/4$	84.33	81.57	74.71	84.38
$\pi/8$	85.90	83.26	78.68	85.90

Table 4

Parameterisation Results for KLT/MI Analysis (Medial Gastrocnemius – Transverse)

Direction of Motion \vec{m}	Speed of Motion m			
	1	2	4	8
Π	78.61	78.61	76.11	80.85
$\pi/2$	82.92	81.97	85.86	85.08
$\pi/4$	88.65	87.55	86.45	83.59
$\pi/8$	88.25	88.21	81.22	71.17

9.2 Appendix 2: Parameterisation Tables for GMM and KLT/ MI from Chapter 5

- Subsequent tables show parameterisation results for GMM analysis, showing accuracy results for test data set when using variable values for number of Gaussians, learning rate and background ratio. Optimum values in red.

Table 1
Parameterisation Results for GMM Analysis (Biceps Brachii – Transverse)

Background Ratio	No. of Gaussians	Learning Rate	Accuracy (%)
80	5	0.5	82.12
80	5	0.05	69.55
80	5	0.005	81.25
80	4	0.5	80.01
80	4	0.05	69.69
80	4	0.005	81.25
80	3	0.5	83.14
80	3	0.05	69.91
80	3	0.005	81.25
85	5	0.5	81.26
85	5	0.05	74.25
85	5	0.005	79.89
85	4	0.5	81.34
85	4	0.05	74.37
85	4	0.005	79.89
85	3	0.5	82.06
85	3	0.05	76.32
85	3	0.005	79.89
90	5	0.5	80.56
90	5	0.05	62.6
90	5	0.005	77.66
90	4	0.5	80.15
90	4	0.05	62.65
90	4	0.005	77.66
90	3	0.5	80.54
90	3	0.05	62.94
90	3	0.005	77.66

Table 2
Parameterisation Results for GMM Analysis (Biceps Brachii – Longitudinal)

Background Ratio	No. of Gaussians	Learning Rate	Accuracy (%)
80	5	0.5	86.39
80	5	0.05	73.55
80	5	0.005	79.92
80	4	0.5	84.96
80	4	0.05	73.39
80	4	0.005	79.92
80	3	0.5	85.18
80	3	0.05	74.53
80	3	0.005	79.92
85	5	0.5	86.48
85	5	0.05	82.69
85	5	0.005	81.62
85	4	0.5	84.35
85	4	0.05	82.76
85	4	0.005	81.62
85	3	0.5	85.15
85	3	0.05	82.54
85	3	0.005	81.62
90	5	0.5	86.14
90	5	0.05	82.08
90	5	0.005	82.97
90	4	0.5	84.46
90	4	0.05	82.09
90	4	0.005	82.97
90	3	0.5	83.72
90	3	0.05	81.8
90	3	0.005	82.97

Table 3
Parameterisation Results for GMM Analysis (Medial Gastrocnemius – Transverse)

Background Ratio	No. of Gaussians	Learning Rate	Accuracy (%)
80	5	0.5	84.41
80	5	0.05	80.81
80	5	0.005	83.7
80	4	0.5	84.43
80	4	0.05	80.64
80	4	0.005	83.7
80	3	0.5	85.31
80	3	0.05	83.14

80	3	0.005	83.7
85	5	0.5	84.33
85	5	0.05	86.57
85	5	0.005	84.04
85	4	0.5	85.31
85	4	0.05	86.57
85	4	0.005	84.04
85	3	0.5	83.28
85	3	0.05	86.91
85	3	0.005	84.04
90	5	0.5	86.14
90	5	0.05	82.08
90	5	0.005	82.97
90	4	0.5	84.46
90	4	0.05	82.09
90	4	0.005	82.97
90	3	0.5	83.72
90	3	0.05	81.8
90	3	0.005	82.97

Table 4
Parameterisation Results for GMM Analysis (Medial Gastrocnemius – Longitudinal)

Background Ratio	No. of Gaussians	Learning Rate	Accuracy (%)
80	5	0.5	84.41
80	5	0.05	81.75
80	5	0.005	80.52
80	4	0.5	85.15
80	4	0.05	82.16
80	4	0.005	80.52
80	3	0.5	85.61
80	3	0.05	82.3
80	3	0.005	80.52
85	5	0.5	83.52
85	5	0.05	86.15
85	5	0.005	82.03
85	4	0.5	85.31
85	4	0.05	86.16
85	4	0.005	82.03
85	3	0.5	83.28
85	3	0.05	86.16
85	3	0.005	82.03
90	5	0.5	83.69
90	5	0.05	86.56

90	5	0.005	83.98
90	4	0.5	85.67
90	4	0.05	86.54
90	4	0.005	83.98
90	3	0.5	86.18
90	3	0.05	85.76
90	3	0.005	83.98

2. The subsequent table shows parameterisation results for GMM analysis, showing accuracy results for test data set when using variable values for minimum blob area. Optimum values in red.

Min blob area (as % of image)	MG TRANS	MG LONG	BB TRANS	BB LONG
1	53.27	64.94	50.2	52.56
5	72.69	74.68	46.61	61.73
8	82.85	84.45	65.38	74.29
10	85.95	87.81	74.55	79.54
15	88.6	89.94	83.26	85.31
20	89.13	89.57	82.8	86.34
25	89.12	86.24	71.99	83.95
30	88.82	85.48	49.07	83.38
35	88.57	82.51	49.56	78.17
40	88.63	82.66	49.81	75.08

3. Subsequent tables show parameterisation results for KLT/ MI analysis, showing accuracy results for test data set when using variable values for direction and speed of motion. Optimum values in red.

Table 5
Parameterisation Results for KLT/MI Analysis (Biceps Brachii – Transverse)

Direction of Motion \vec{m}	Speed of Motion m			
	1	2	4	8
Π	52.37	52.37	52.37	52.37
$\pi/2$	74.07	74.89	75.16	75.05
$\pi/4$	70.2	70.97	71.08	73.29
$\pi/8$	54.89	53.67	48.58	62.41

Table 6
Parameterisation Results for KLT/MI Analysis (Biceps Brachii – Longitudinal)

Direction of Motion \vec{m}	Speed of Motion m			
	1	2	4	8
π	59.29	59.29	52.37	52.37
$\pi/2$	74.07	74.89	75.16	75.05
$\pi/4$	70.20	70.97	71.08	73.29
$\pi/8$	54.89	53.67	48.58	62.41

Table 7
Parameterisation Results for KLT/MI Analysis (Medial Gastrocnemius– Transverse)

Direction of Motion \vec{m}	Speed of Motion m			
	1	2	4	8
π	52.80	59.29	53.35	53.35
$\pi/2$	65.47	65.53	68.75	68.75
$\pi/4$	64.93	68.73	71.04	75.95
$\pi/8$	54.10	61.78	65.65	65.65

Table 8
Parameterisation Results for KLT/MI Analysis (Medial Gastrocnemius– Longitudinal)

Direction of Motion \vec{m}	Speed of Motion m			
	1	2	4	8
π	65.58	65.58	65.68	65.68
$\pi/2$	70.99	70.88	70.81	71.12
$\pi/4$	71.57	72.19	72.78	74.49
$\pi/8$	67.13	68.16	71.68	74.99

Table 9

Parameterisation Results for GMM Analysis – Number of Training Frames

No of Training Frames	BB LONG	BB CROSS	MG LONG	MG CROSS
100	73.40	45.63	83.27	70.76
300	75.17	45.43	84.26	74.78
500	86.34	83.26	89.94	89.13
700	83.05	83.07	83.53	78.05

9.3 Appendix 3: Parameterisation and Supplementary Tables for GMM from Chapter 6

Table 1
Parameterisation Results for GMM Analysis (Trapezius - Longitudinal)

Background Ratio	No. of Gaussians	Learning Rate	Accuracy (%)
80	5	0.5	78.53
80	5	0.05	70.72
80	5	0.005	64.85
80	4	0.5	83.14
80	4	0.05	70.67
80	4	0.005	64.85
80	3	0.5	86.16
80	3	0.05	71.25
80	3	0.005	64.85
85	5	0.5	79.01
85	5	0.05	79.63
85	5	0.005	76.46
85	4	0.5	83.53
85	4	0.05	80.01
85	4	0.005	76.46
85	3	0.5	86.82
85	3	0.05	81.00
85	3	0.005	76.46
90	5	0.5	79.86
90	5	0.05	74.25
90	5	0.005	85.03
90	4	0.5	84.24
90	4	0.05	76.11
90	4	0.005	86.02
90	3	0.5	86.95
90	3	0.05	75.65
90	3	0.005	85.26

Table 2
Parameterisation Results for GMM Analysis (Trapezius - Transverse)

Background Ratio	No. of Gaussians	Learning Rate	Accuracy (%)
80	5	0.5	72.80
80	5	0.05	65.36
80	5	0.005	65.8
80	4	0.5	72.29
80	4	0.05	65.42
80	4	0.005	65.8
80	3	0.5	74.39
80	3	0.05	67.65
80	3	0.005	65.8

85	5	0.5	73.83
85	5	0.05	79.28
85	5	0.005	66.95
85	4	0.5	74.70
85	4	0.05	79.38
85	4	0.005	74.03
85	3	0.5	77.63
85	3	0.05	80.65
85	3	0.005	66.95
90	5	0.5	66.12
90	5	0.05	79.71
90	5	0.005	73.99
90	4	0.5	77.17
90	4	0.05	82.26
90	4	0.005	80.03
90	3	0.5	78.80
90	3	0.05	79.49
90	3	0.005	80.53

Table 3
Parameterisation Results for GMM Analysis (Rectus Femoris- Longitudinal)

Background Ratio	No. of Gaussians	Learning Rate	Accuracy (%)
80	5	0.5	79.39
80	5	0.05	71.03
80	5	0.005	74.80
80	4	0.5	78.39
80	4	0.05	71.16
80	4	0.005	74.80
80	3	0.5	79.88
80	3	0.05	72.72
80	3	0.005	74.80
85	5	0.5	79.06
85	5	0.05	78.23
85	5	0.005	78.86
85	4	0.5	78.89
85	4	0.05	78.09
85	4	0.005	78.86
85	3	0.5	80.10
85	3	0.05	78.59
85	3	0.005	78.86
90	5	0.5	79.45
90	5	0.05	76.45
90	5	0.005	80.71
90	4	0.5	79.70
90	4	0.05	78.14
90	4	0.005	80.71

90	3	0.5	78.85
90	3	0.05	71.59
90	3	0.005	80.71

Table 4
Parameterisation Results for GMM Analysis (Rectus Femoris- Trasverse)

Background Ratio	No. of Gaussians	Learning Rate	Accuracy (%)
80	5	0.5	77.66
80	5	0.05	67.30
80	5	0.005	70.28
80	4	0.5	77.10
80	4	0.05	67.35
80	4	0.005	70.28
80	3	0.5	79.84
80	3	0.05	67.71
80	3	0.005	70.28
85	5	0.5	78.87
85	5	0.05	75.76
85	5	0.005	75.77
85	4	0.5	78.33
85	4	0.05	76.28
85	4	0.005	75.77
85	3	0.5	76.62
85	3	0.05	76.28
85	3	0.005	75.77
90	5	0.5	78.92
90	5	0.05	76.05
90	5	0.005	79.64
90	4	0.5	80.30
90	4	0.05	78.39
90	4	0.005	79.64
90	3	0.5	80.71
90	3	0.05	76.27
90	3	0.005	79.64

Table 5
Parameterisation Results for GMM Analysis (Thoracic Paraspinals - Longitudinal)

Background Ratio	No. of Gaussians	Learning Rate	Accuracy (%)
80	5	0.5	58.36
80	5	0.05	65.22
80	5	0.005	73.16
80	4	0.5	49.8
80	4	0.05	68.69
80	4	0.005	73.14
80	3	0.5	53.57
80	3	0.05	73.3
80	3	0.005	72.4
85	5	0.5	59.11
85	5	0.05	77.79
85	5	0.005	75.18
85	4	0.5	55.25
85	4	0.05	76.63
85	4	0.005	73.23
85	3	0.5	59.27
85	3	0.05	74.51
85	3	0.005	72.92
90	5	0.5	59.4
90	5	0.05	63.09
90	5	0.005	80.46
90	4	0.5	61.34
90	4	0.05	74.42
90	4	0.005	83.28
90	3	0.5	58.19
90	3	0.05	78.16
90	3	0.005	84.19

Table 6
Parameterisation Results for GMM Analysis (Thoracic Paraspinals – Transverse)

Background Ratio	No. of Gaussians	Learning Rate	Accuracy (%)
80	5	0.5	63.21
80	5	0.05	61.61
80	5	0.005	56.17
80	4	0.5	60.2
80	4	0.05	62.32
80	4	0.005	56.07
80	3	0.5	62.76
80	3	0.05	65.27
80	3	0.005	60.13

85	5	0.5	64.68
85	5	0.05	68.15
85	5	0.005	67.94
85	4	0.5	59.87
85	4	0.05	67.23
85	4	0.005	67.56
85	3	0.5	63.79
85	3	0.05	68.12
85	3	0.005	59.48
90	5	0.5	66.08
90	5	0.05	75.36
90	5	0.005	76.49
90	4	0.5	78.2
90	4	0.05	62.29
90	4	0.005	76.83
90	3	0.5	63.31
90	3	0.05	74.85
90	3	0.005	77.49

Table 7
Parameterisation Results for GMM Analysis (Rectus Abdominus – Longitudinal)

Background Ratio	No. of Gaussians	Learning Rate	Accuracy (%)
80	5	0.5	81.85
80	5	0.05	69.25
80	5	0.005	82.26
80	4	0.5	84.4
80	4	0.05	88.01
80	4	0.005	82.26
80	3	0.5	86.57
80	3	0.05	66.1
80	3	0.005	82.26
85	5	0.5	81.85
85	5	0.05	84.47
85	5	0.005	71.84
85	4	0.5	82.9
85	4	0.05	81.98
85	4	0.005	71.84
85	3	0.5	85.73
85	3	0.05	82.5
85	3	0.005	71.84
90	5	0.5	82
90	5	0.05	85.23
90	5	0.005	82
90	4	0.5	83.3
90	4	0.05	84.17

90	4	0.005	82
90	3	0.5	81.06
90	3	0.05	84.49
90	3	0.005	82

Table 8
Parameterisation Results for GMM Analysis (Rectus Abdominus – Transverse)

Background Ratio	No. of Gaussians	Learning Rate	Accuracy (%)
80	5	0.5	72.92
80	5	0.05	67.08
80	5	0.005	62.62
80	4	0.5	75.02
80	4	0.05	66.47
80	4	0.005	62.62
80	3	0.5	79.01
80	3	0.05	66.68
80	3	0.005	62.62
85	5	0.5	72.25
85	5	0.05	81.59
85	5	0.005	71.89
85	4	0.5	75.57
85	4	0.05	82.11
85	4	0.005	71.89
85	3	0.5	81.21
85	3	0.05	82
85	3	0.005	71.89
90	5	0.5	73.01
90	5	0.05	89.01
90	5	0.005	82.26
90	4	0.5	84.4
90	4	0.05	88.13
90	4	0.005	82.26
90	3	0.5	85.97
90	3	0.05	87.51
90	3	0.005	82.26

Table 9
Parameterisation Results for GMM Analysis – Minimum Blob Area

Min Blob Area (as % of image)	TRAP LONG	TRAP CROSS	RF LONG	RF CROSS	TP LONG	TP CROSS	RA LONG	RA CROSS
1	56.95	61.49	52.61	51.88	37.15	54.19	51.47	59.36
5	75.87	74.27	73.17	66.20	59.71	68.62	54.32	71.61
8	86.80	81.29	78.55	76.37	79.01	79.00	79.30	80.51
10	86.95	82.26	80.71	80.71	84.19	77.49	85.23	89.01
15	85.79	57.28	75.08	81.68	81.48	68.91	81.97	86.87
20	84.68	53.96	69.23	70.33	70.5	60.58	83.98	83.79
25	80.15	49.63	67.47	60.04	49.74	56.76	83.45	84.21
30	76.54	49.81	64.87	53.93	49.87	58.38	84.13	68.73
35	73.43	49.94	62.30	54.09	50.00	54.67	80.45	49.87
40	66.00	49.94	61.90	54.28	50.00	50.00	81.40	50.00

Table 10
Parameterisation Results for GMM Analysis – Number of Training Frames

No. of Training Frames	TRAP LONG	TRAP CROSS	RF LONG	RF CROSS	TP LONG	TP CROSS	RA LONG	RA CROSS
100	84.65	79.47	80.36	78.92	81.34	80.14	73.30	71.65
300	84.85	76.35	80.95	79.09	84.90	79.81	77.02	73.58
500	86.95	82.26	80.71	81.68	84.19	79.00	85.23	89.01
700	84.90	81.97	78.32	80.70	82.21	78.81	77.51	75.23

Participant Number	BB		MG		Group
	LONG	CROSS	LONG	CROSS	
1	5	NO DATA	1.5	2.5	M
2	2	NO DATA	8	10.5	M
3	12	NO DATA	4	4.5	M
4	24	18	11	17	M
5	4	5	8	13.5	M
6	15	26	4.5	3	M
7	excluded	excluded	excluded	excluded	M
8	10	14	2.5	4	M
9	3	NO DATA	4	1	M
10	NO DATA	60	12.5	14.5	M
11	24	47.5	7.5	5.5	M
12	36	43.5	13.5	16.5	M
13	10.5	21	3	2.5	M
14	19.5	42	7	7	M
15	13.5	9	NO DATA	11	M
16	11	NO DATA	NO DATA	NO DATA	M
17	excluded	excluded	excluded	excluded	M
18	NO DATA	NO DATA	NO DATA	NO DATA	M
19	NO DATA	NO DATA	NO DATA	NO DATA	M
20	NO DATA	NO DATA	NO DATA	NO DATA	M
21	2.5	0.5	3	3	H
22	4.5	2.5	NO DATA	NO DATA	H
23	33.5	14	11.5	22	H
24	37.5	24.5	18.5	21	H
25	13	8	9	5.5	H
26	6.5	1.5	11	6.5	H
27	14	6	NO DATA	8.5	H
28	14.5	10	11.5	13.5	H
29	3.5	0	5	2.5	H
30	12.5	5.5	3.5	9	H
31	16.5	7.5	5.5	3	H
32	NO DATA	NO DATA	6.5	5.5	H
33	NO DATA	NO DATA	3	5	H

Table 9.1: Number of fasciculations detected using GMM in MND affected (M) and healthy (H) participants from BB and MG muscles (Excluding 7 healthy participants used in parameterisation).

9.4 Appendix 4: NHS Application for Ethical Approval

Application Number _____
Date Received _____

APPENDIX 2

APPLICATION FOR ETHICAL APPROVAL



Introduction

All university activity must be reviewed for ethical approval. In particular, all undergraduate, postgraduate and staff research work, projects and taught programmes must obtain approval from the Academic Ethics committee.

Application Procedure

The form should be completed legibly (preferably typed) and, so far as possible, in a way which would enable a layperson to understand the aims and methods of the research. Every relevant section should be completed. Applicants should also include a copy of any proposed advert, information sheet, consent form and, if relevant, any questionnaire being used. The Principal Investigator should sign the application form. Supporting documents, together with one copy of the full protocol should be sent to the Faculty/Campus Research Group Officer.

Your application will require external ethical approval by an NHS Research Ethics Committee if your research involves staff, patients or premises of the NHS (see guidance notes)

Work with children and vulnerable adults

You will be required to have an Enhanced CRB Disclosure, if your work involves children or vulnerable adults.

The Academic Ethics Committee will respond as soon as possible, and where appropriate, will operate a process of expedited review.

Applications that require approval by an NHS Research Ethics Committee or a Criminal Disclosure will take longer.

1. Details of Applicants	
1.1. Name of applicant (Principal Investigator): Dr Nicholas Combes	
Telephone Number:	
Email address: Nicholas.Combes@lthtr.nhs.uk	
Status: Consultant Neurophysiologist	Postgraduate Student (Taught or Research) Kate Bibbings (Postgraduate Research Student) Staff Dr Peter Harding (Research Associate)
Department/School/Other Unit: School of Healthcare Science	
Programme of study (if applicable): MPhil/PhD	

Application Number _____
Date Received _____

Name of supervisor/Line manager: Dr Emma Hodson Tole	
1.2. Co-Workers and their role in the project: (e.g. students, external collaborators, etc)	
Name:	Name:
Telephone Number:	Telephone Number:
Role:	Role:
Email Address:	Email Address:
2. Details of the Project	
Title: Motor Neurone Disease Diagnosis: The utility of standard frame rate b-mode ultrasound imaging.	
2.1. Description of the Project: (please outline the background and the purpose of the research project, 250 words max)	
<p>Current diagnostic techniques for motor neurone disease (MND) involve the insertion of needles into the affected muscles to record electrical activity that can be used to confirm the presence of fasciculations and fibrillations, which are an indicator of neuromuscular degeneration. These electrical impulses lead to localised muscle contractions, visible via b-mode ultrasound. Previous work has shown that ultrasound imaging provides an accurate means of identifying fasciculations, but previous work has only involved manual identification and classification of fasciculations and fibrillations. The project we propose will automate the process of identifying fasciculations and fibrillations in b-mode ultrasound recordings. Previous work has shown that the analysis algorithm we have created can identify stimulated muscle twitches with a greater than 90 percent accuracy. We intend to extend this work and test the algorithm extensively on data collected from MND patients.</p> <p>There are many advantages that ultrasound based diagnostic tests provide over traditional EMG recordings, even when disregarding the discomfort caused to the patient from intramuscular recording. Ultrasound may be used on a number of occasions without, in general, any discomfort, due to the low number of negative effects experienced from scanning. It is also very cheap and widely available, as well as not requiring specialist clinicians to operate the equipment. However, currently, the interpretation of ultrasound images, even by highly experienced individuals, is subjective in nature and takes time to complete. An automated method of detection, would remove subjectivity from the image analysis, decrease timescales and assist in the standardization of diagnosis.</p>	
2.2. Describe what type of study this is (e.g. qualitative or quantitative; also indicate how the data will be collected and analysed). Additional sheets may be attached.	
<p>This study is the provisional investigation into the use of standard frame rate, b-mode ultrasound for MND diagnosis. Data collected will be in the form of b-mode ultrasound (grayscale images of the body's internal structures) and intramuscular EMG (recordings of electrical activity taken from the muscle). Images obtained of patients muscles could not be used to identify the participant. In addition to this, the data will be removed from site and</p>	

Application Number _____
Date Received _____

<p>stored securely at Manchester Metropolitan University. The data will be analysed in a number of ways. Firstly, b-mode ultrasound footage will be manually viewed, and the presence of fasciculations and fibrillations (involuntary muscle activations) will be recorded. This gives a qualitative measure of the presence of fasciculations in that specific muscle, and also a quantitative measure of the exact time (video frame) at which each of these artefacts occurred. The EMG data will be analysed so as to extract the presence and timing of fasciculations and fibrillations, which can be used to confirm the accuracy of the manual identifications. Finally, the b-mode data will be analysed using our own algorithm, which identifies the presence of fasciculations and fibrillations automatically. These data will then be compared to ascertain the relative accuracy of each technique. The final method of analysis has not been confirmed, but our previous work made use of receiver operating characteristics and Cohen's Kappa statistic to measure the agreement between multiple identification systems. The only data collected which may allow patients to be identified is name, age, height and weight. This data will be stored securely, and the b-mode and EMG data associated with each participant will be stored separately from these data and with a random ID that does not allow the data to be linked back to identifiable participant data.</p>
<p>2.3. Are you going to use a questionnaire? YES (Please attach a copy) NO</p>
<p>2.4. Start Date / Duration of project: January 2014</p>
<p>2.5. Location of where the project and data collection will take place: Royal Preston Hospital</p>
<p>2.6. Nature/Source of funding: Motor Neurone Disease Association</p>
<p>2.7. Are there any regulatory requirements? YES (Provide details, e.g. from professional bodies) NO</p>
<p>3. Details of Participants</p>
<p>3.1. How many? 60</p>
<p>3.2. Age: 18 years plus</p>
<p>3.3. Sex: Male and Female</p>
<p>3.4. How will they be recruited? (Attach a copy of any proposed advertisement) Through Lancashire NHS Teaching Hospitals Specialist Motor Neurone Disease Nurses</p>
<p>3.5. Status of participants: (e.g. students, public, colleagues, children, hospital patients, prisoners, including young offenders, participants with mental illness or learning difficulties.) Hospital Patients</p>
<p>3.6. Inclusion and exclusion from the project: (indicate the criteria to be applied). Previously diagnosed with Motor Neurone Disease</p>

Application Number _____
Date Received _____

3.7. Payment to volunteers: (indicate any sums to be paid to volunteers). None
3.8. Study information: Have you provided a study information sheet for the participants? YES (Please attach a copy) NO
3.9. Consent: (A written consent form for the study participants MUST be provided in all cases, unless the research is a questionnaire.) Have you produced a written consent form for the participants to sign for your records? YES (Please attach a copy) NO
4. Risks and Hazards
4.1. Are there any risks to the researcher and/or participants? (Give details of the procedures and processes to be undertaken, e.g. if the researcher is a lone-worker.) 1. Risk from Sharps to researchers 2. Small risk of infection to the participant 3. Small risk of internal damage to the participant by misplaced EMG needle
4.2. State precautions to minimise the risks and possible adverse events: Dr Nicholas Combes, Consultant Neurophysiologist will be the only member of the research team to handle the EMG needles. He is fully trained and highly experienced in the diagnosis of MND and the placement of intramuscular EMG. 1. Researchers will be vaccinated against appropriate diseases and the coordination between the clinician (who will be placing the needle) and the researcher (who will be placing the ultrasound) will be practiced extensively in a safe environment before attempting a data collection with a patient. 2. The ultrasound probe will be placed in a sterile glove and sterile ultrasound gel and sterile needles will be used All consumables will be discarded after each patient examination or if the researcher or clinician considers any item to have become contaminated. 3. The PI of this project will be carrying out all invasive procedures, and has multiple years' experience within the Neurophysiological field. Additional to this, as one of the primary Neurophysiologists at Preston, he is highly likely to have been the diagnosing clinician that the patient originally saw.
4.3. What discomfort (physical or psychological) danger or interference with normal activities might be suffered by the researcher and/or participant(s)? State precautions which will be taken to minimise them: Intramuscular EMG will require the insertion of needles into the patient's muscles. This may cause a small amount of pain/ discomfort for the patient during the examination and in extreme cases bruising or muscle soreness may be experienced on subsequent

Application Number _____
 Date Received _____

days. To counteract this we will take the same steps as were taken during their initial diagnosis.
 Needles will be inserted by a consultant in Neurophysiology, who is fully trained in the practice of Intramuscular EMG.

5. Ethical Issues

5.1. Please describe any ethical issues raised and how you intend to address these:

1. A small risk of cell damage is possible when ultrasound is used. For this reason, only the required amount will be used in order to successfully yield results. There is an inbuilt safety feature present in the specific machines which we employ, that freezes all scanning after it has been active for over 10 minutes. We do not expect to be collecting more than 5 minutes of ultrasound footage from any single muscle.
2. Although all participants will have previously been diagnosed with MND, if any further disorders become apparent from the data collected during the study, the participants GP will be informed of these provisional findings.

6. Safeguards/Procedural Compliance

6.1. Confidentiality:

- 6.1.1. Indicate what steps will be taken to safeguard the confidentiality of participant records. If the data is to be computerised, it will be necessary to ensure compliance with the requirements of the Data Protection Act 1998.
- 6.1.2. If you are intending to make any kind of audio or visual recordings of the participants, please answer the following questions:
 - 6.1.2.1. How long will the recordings be retained and how will they be stored?
 - 6.1.2.2. How will they be destroyed at the end of the project?
 - 6.1.2.3. What further use, if any, do you intend to make of the recordings?

The nature of the image means that it would be very difficult to make any identification of the participant from their images. However, to safeguard the confidentiality of participants and their records, all recordings will be saved under names not relatable to the participant and kept on a password protected computer.

Recordings will be retained for a minimum of 3 years, but preferably indefinitely. The recordings will be stored on a password protected computer within a locked room, within Manchester Metropolitan University. Recordings will be stored on a RSA encrypted drive, which has a password distinct from that of the computer.

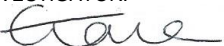
At the end of the project, all files will be overwritten on at least 5 occasions with randomly generated binary streams. The probability of being able to recover the data at this point by any means is effectively zero. The data storage drive will also be securely disposed of.

Recordings may be used to investigate previously undocumented techniques by which to diagnose MND. The recordings will never be used outside of persons directly related to this project (name people here? I.e. Pete?).

Application Number _____
Date Received _____

<p>6.2. The Human Tissue Act The Human Tissue Act came into force in November 2004, and requires appropriate consent for, and regulates the removal, storage and use of all human tissue.</p> <p>6.2.1. Does your project involve taking tissue samples, e.g., blood, urine, hair etc., from human subjects? YES NO</p> <p>6.2.2. Will this be discarded when the project is terminated? N/A YES NO</p> <p>If NO – Explain how the samples will be placed into a tissue bank under the Human Tissue Act regulations:</p>
<p>6.3. Insurance</p> <p>The University holds insurance policies in place to cover claims for negligence arising from the conduct of the University's normal business, which includes research carried out by staff and by undergraduate and postgraduate students as part of their course. This does not extend to clinical negligence.</p> <p>In addition, the University has provision to award indemnity and/or compensation in the event of claims for non-negligent harm. This is on the condition that the project is accepted by the insurers prior to the commencement of the research project and approval has been granted for the project from a suitable ethics committee.</p> <p>Research which is applicable to non-negligent harm cover involves humans and physical intervention which could give rise to a physical injury or illness which is outside the participant's day to day activities. This includes strenuous exercise, ingestion of substances, injection of substances, topical application of any substances, insertion of instruments, blood/tissue sampling of participants and scanning of participants.</p> <p>The following types of research are <u>not</u> covered automatically for non-negligent harm if they are classed as the activities above and they involve:</p> <ol style="list-style-type: none"> 1) Anything that assists with and /or alters the process of contraception, or investigating or participating in methods of contraception 2) Anything involving genetic engineering other than research in which the medical purpose is treating or diagnosing disease 3) Where the substance under investigation has been designed and /or manufactured by MMU 4) Pregnant women 5) Drug trials 6) Research involving children under sixteen years of age 7) Professional sports persons and or elite athletes. 8) Overseas research

Application Number _____
 Date Received _____

<p>Will the proposed project result in you undertaking any research that includes any of the 8 points above or would not be considered as normal University business? If so, please detail below: N/A</p>	
<p>6.4. Notification of Adverse Events (e.g., negative reaction, counsellor, etc): (Indicate precautions taken to avoid adverse reactions.)</p> <p>Please state the processes/procedures in place to respond to possible adverse reactions.</p> <p>In the case of clinical research, you will need to abide by specific guidance. This may include notification to GP and ethics committee. Please seek guidance for up to date advice, e.g., see the NRES website at http://www.nres.npsa.nhs.uk/</p>	
<p>SIGNATURE OF PRINCIPAL INVESTIGATOR: </p>	<p>Date 14/01/14</p>
<p>SIGNATURE OF FACULTY'S HEAD OF ETHICS:</p>	<p>Date:</p>

Checklist of attachments needed:

1. Participant consent form
2. Participant information sheet
3. Full protocol
4. Advertising details
5. Insurance notification forms
6. NHS Approval Letter (where appropriate)
7. Other evidence of ethical approval (e.g., another University Ethics Committee approval)

9.5 Appendix 5: NHS Participant Consent Form



Lancashire Teaching Hospitals
NHS Foundation Trust



Department of Neurophysiology
Royal Preston Hospital,
Sharoe Green Lane,
Fulwood,
PRESTON.
PR2 9HT

Tel: 01772 52255
Fax: 01772 528160

20 March 2017

Centre Number:
Study Number:
Patient Identification Number for this trial:

CONSENT FORM

Title of Project: Detecting muscle twitches with ultrasound imaging

Name of Researchers: Dr Nicholas Combes / Dr Emma Hodson-Tole / Ms. Kate Bibbings

Please initial box

1. I confirm that I have read and understand the information sheet dated.....
(version.....) for the above study. I have had the opportunity to consider the information,
ask questions and have had these answered satisfactorily.

2. I understand that my participation is voluntary and that I am free to withdraw at any time
without giving any reason, without my medical care or legal rights being affected.

3. I understand that relevant sections of my medical notes and data collected during the study,
may be looked at by individuals from Manchester Metropolitan University from regulatory
authorities or from the NHS Trust, where it is relevant to my taking part in this research.
I give permission for these individuals to have access to my records.

4. I agree to my GP being informed of my participation in the study.

5. I agree to take part in the above study.

Name of Patient

Date

Signature

Name of Person
taking consent

Date

Signature

When completed: 1 for participant; 1 for researcher site file; 1 (original) to be kept in medical notes.

File: Informed Consent MND A WP1
Version number: 1

Date: 18-11-2013

Page 1 of 1

9.6 Appendix 6: NHS Participant Information Sheet



Lancashire Teaching Hospitals
NHS Foundation Trust



Department of Neurophysiology
Royal Preston Hospital,
Sharoe Green Lane,
Fulwood,
Preston.
PR2 9HT

Tel: 01772 52255
Fax: 01772 528160

20 March 2017

PATIENT INFORMATION SHEET

Title of Project: Detecting muscle twitches with ultrasound imaging

You are being invited to participate in a research study done by Manchester Metropolitan University and their team at Lancashire teaching hospitals NHS trust. Please read the following information carefully before you decide whether to take part in the study or not.

WHAT IS THE PURPOSE OF THIS STUDY?

We are working on developing new methods of diagnosing degenerative diseases which affect skeletal muscles, an example of which is motor neurone disease. Currently, doctors usually diagnose conditions like motor neurone disease by using a technique called 'needle EMG'. The technique involves placing a needle in different muscles and recording the electrical activity which occurs when the muscle is activated. Different types of activation, or muscle twitches, occur between healthy and affected people. We wish to identify whether we can use ultrasound images of the muscles, recorded in the same way mothers are scanned during pregnancy, to identify the occurrence of different types of twitch and provide a painless, more sensitive diagnostic tool.

The first step in this process is to develop a computer program which is able to analyse a sequence of images and accurately identify when twitches occurred. The purpose of the study you are being invited to take part in is to collect needle EMG signals and image sequences which we can use to test the analysis program.

WHAT IS THE DIFFERENCE IN TREATMENT?

The research does not involve any treatment and will not affect any treatment you are currently receiving.

WHY HAVE I BEEN CHOSEN?

You have been chosen to take part in the study as you have been diagnosed as having motor neurone disease. It is important for us to test our computer software on images which have been recorded in people with the disease so we can establish its potential use in a clinic.

File: Participant Information Sheet MND WP1
Version number: 1

Date: 18-11-2013

Page 1 of 3

WHAT WILL HAPPEN IF I TAKE PART?

A member of the research team will arrange for you to visit the MND care and research centre at Preston Royal Hospital. During the visit we will record needle EMG and ultrasound images from six muscles:

- i) a muscle at the back of your lower leg [medial gastrocnemius]
- ii) a muscle in your thigh [rectus femoris]
- iii) a muscle in your upper arm [biceps]
- iv) a muscle on your shoulder [trapezius]
- v) a muscle on your back [thoracic paraspinal]
- vi) a muscle over your stomach region [rectus abdominis].

Recording the images involves placing a special probe, covered in a water based gel, over the top of the muscle of interest. The probe sends waves of ultrasound through the muscle which are bounced back and used to create an image which can be viewed and recorded on a computer. The images of your muscles' are in monochrome (black and white), and just show features within your muscle. Individual people cannot be identified from these images.

Recording EMG involves inserting a needle into the muscle, which will detect the electrical activity in the muscle which occurs when it contracts or twitches. This is the same technique you underwent as part of your diagnosis. The procedure will be completed by Dr. Nicholas Combes, who is a highly experienced Consultant Neurophysiologist at Preston Royal Hospital with extensive experience of making these recordings.

While we are collecting the EMG and the images you can sit on a chair or lie on a couch, depending on the muscle being scanned. You will not need to do anything else. We want to take recordings of the naturally occurring, involuntary twitches which occur in muscles when they are affected by motor neurone disease. We will take three recordings from each muscle, each lasting 30 – 40 seconds.

We will only need to visit once and in total it will take no more than 2 hours to collect all the ultrasound images and EMG required.

WHAT ARE THE POSSIBLE BENEFITS OF TAKING PART?

There will be no direct benefits to you for taking part in the study. We hope however that the work will contribute to the development of a new, non-invasive method of diagnosing some degenerative muscle diseases.

WHAT ARE THE POSSIBLE RISKS OF TAKING PART?

There are no risks associated with the ultrasound imaging. It is a minimally invasive technique which is commonly used to assess muscle tissue and unborn babies in pregnant women.

There are small risks associated with the needle EMG. It can cause a degree of pain and can lead to a small amount of bruising. There is also a very low risk of infection occurring at the site the needle was inserted.

WILL MY TAKING PART BE KEPT CONFIDENTIAL?

Yes. We will not need to record any of your personal information for this work. Details of your age, height, weight and period of time since your diagnosis will be noted but not linked to any information from which you could be identified. All the ultrasound videos and EMG recorded will be saved on a computer with a unique alphanumeric participant identifier, which will not be linked to any of your confidential records.

WHAT IF I CHANGE MY MIND ABOUT TAKING PART?

Your standard of care will not be affected if you change your mind. You are not obligated in any way to take part in this study it is entirely your choice. Once you have signed the consent form you are still free to withdraw at any time and without giving a reason and we will delete any data we had collected from you.

Contact details for further information

Dr Nicholas Combes
Consultant Neurophysiologist
Department of Neurophysiology
Royal Preston Hospital
Shaore Green Lane
Fulwood
PRESTON
PR2 9HT

Tel. 01772 522559

Dr. Emma Hodson-Tole
School of Healthcare Science
Manchester Metropolitan University
Oxford Road
Manchester, M1 5GD

Tel: 0161 247 5923
Email: e.tole@mmu.ac.uk

9.7 Appendix 7: MMU Application for Ethical Approval

Application Number SE141513
 Date Received 6/2/15
APPLICATION FOR ETHICAL APPROVAL

APPENDIX 2



Introduction

All university activity must be reviewed for ethical approval. In particular, all undergraduate, postgraduate and staff research work, projects and taught programmes must obtain approval from the Academic Ethics committee.

Application Procedure

The form should be completed legibly (preferably typed) and, so far as possible, in a way which would enable a layperson to understand the aims and methods of the research. Every relevant section should be completed. Applicants should also include a copy of any proposed advert, information sheet, consent form and, if relevant, any questionnaire being used. The Principal Investigator should sign the application form. Supporting documents, together with one copy of the full protocol should be sent to the Faculty/Campus Research Group Officer.

Your application will require external ethical approval by an NHS Research Ethics Committee if your research involves staff, patients or premises of the NHS (see guidance notes)

Work with children and vulnerable adults

You will be required to have an Enhanced CRB Disclosure, if your work involves children or vulnerable adults.

The Academic Ethics Committee will respond as soon as possible, and where appropriate, will operate a process of expedited review.

Applications that require approval by an NHS Research Ethics Committee or a Criminal Disclosure will take longer.

1. Details of Applicants	
1.1. Name of applicant (Principal Investigator): Miss Kate Bibbings	
Telephone Number: 0161 247 5924	
Email address: kate.bibbings@stu.mmu.ac.uk	
Status: Postgraduate Research Student	Postgraduate Student (Research)
Department/School/Other Unit: School of Healthcare Science	
Programme of study (if applicable): MPhil/PhD	
Name of supervisor/Line manager: Dr Emma Hodson Tole	
1.2. Co-Workers and their role in the project: (e.g. students, external collaborators, etc)	
Name: Dr Nicholas Combes	Name: Dr Pete Harding

Application Number _____
Date Received _____

Telephone Number:	Telephone Number: 0161 247 1126
Role: Clinical Consult	Role: Supervisor
Email Address: Nicholas.Combes@lthtr.nhs.uk	Email Address: p.harding@mmu.ac.uk

2. Details of the Project

Title: Combination of Intramuscular Electromyography and B-Mode Ultrasound for the Detection of Involuntary Muscle Twitches in Healthy Participants.

2.1. Description of the Project: (please outline the background and the purpose of the research project, 250 words max)

Current diagnostic techniques for motor neurone disease (MND) involve the insertion of needles into muscles to record electrical activity, used to confirm the presence of fasciculations and fibrillations, an indicator of neuromuscular degeneration. This activity leads to localised muscle contractions, visible via ultrasound. An analysis algorithm we have created can identify muscle twitches with greater than 90 percent accuracy. For this stage of the project, we intend to collect simultaneous intramuscular EMG, surface EMG and ultrasound data in healthy controls. This allows us to test our analysis algorithm in order to establish a profile of healthy muscle to compare to the data from MND affected individuals (ongoing work which has already received ethical approval). For the full MND data collection, six muscles will be assessed; Medial Gastrocnemius (MG), Biceps Brachii (BB), Rectus Femoris (RF), Trapezius (TRAP), Thoracic Paraspinals (TP) and Rectus Abdominis (RA). We intend to assess all aforementioned muscles using ultrasound and sEMG and a reduced number will be assessed using iEMG (MG (lower leg), RF (upper leg), BB (upper arm) and TRAP (on top of the shoulder)). The wide range of muscles that will be collected from provides as an extension of previous healthy studies, but will also be necessary at later stages of the project, as collecting data from muscles representative of the different segments of the body is an important requirement in the diagnosis of MND.

2.2. Describe what type of study this is (e.g. qualitative or quantitative; also indicate how the data will be collected and analysed). Additional sheets may be attached.

This study is the preliminary phase of an investigation into the use of standard frame rate, b-mode ultrasound for MND diagnosis and will be carried out on healthy controls. Data collected will be in the form of b-mode ultrasound (grayscale images of the body's internal structures) and surface and intramuscular EMG (recordings of electrical activity taken from the muscle). The images to be obtained cannot be used to identify the participant. The data will be analysed in a number of ways. Firstly, b-mode ultrasound footage will be manually viewed, and the presence of fasciculations (involuntary muscle activations) will be identified and recorded. This gives a qualitative measure of the presence of fasciculations in that specific muscle, and also a quantitative measure of the exact time (video frame) at which each of

Application Number _____
Date Received _____

<p>these events occurred. The EMG data will be analysed so as to extract the presence and timing of fasciculations, which can be used to confirm the accuracy of the manual identifications. Finally, the b-mode data will be analysed using our own algorithms, which identify the presence of fasciculations automatically. These data will then be compared to ascertain the relative accuracy of each technique and assess sensitivity to potential influencing factors such as the probe orientation and needle positioning. The final method of analysis has not been confirmed, but our previous work made use of receiver operating characteristics and Cohen's Kappa statistic to measure the agreement between multiple identification systems.</p>
<p>2.3. Are you going to use a questionnaire? YES (Please attach a copy) NO</p>
<p>2.4. Start Date / Duration of project: Jan 2015 – Sept 2015</p>
<p>2.5. Location of where the project and data collection will take place: Neurophysiology Laboratory T1.03 John Dalton, Manchester Metropolitan University</p>
<p>2.6. Nature/Source of funding: PhD studentship from the Motor Neurone Disease Association</p>
<p>2.7. Are there any regulatory requirements? YES (Provide details, e.g. from professional bodies) NO</p>
<p>3. Details of Participants</p>
<p>3.1. How many? 20</p>
<p>3.2. Age: 18 years plus</p>
<p>3.3. Sex: Male and Female</p>
<p>3.4. How will they be recruited? (Attach a copy of any proposed advertisement) Through the university, via word of mouth</p>
<p>3.5. Status of participants: (e.g. students, public, colleagues, children, hospital patients, prisoners, including young offenders, participants with mental illness or learning difficulties.) Students and colleagues</p>
<p>3.6. Inclusion and exclusion from the project: (indicate the criteria to be applied). Inclusion Participant must have good understanding of written and spoken English Participant must be aged between 18 and 90 years old Participant must be cognitively aware and able to consent to take part</p>

Application Number _____
Date Received _____

<p>Exclusion Participant with any medical/ neurological conditions impacting on fasciculations Underlying peripheral neuropathy Participants who do not have an understanding of the English language Participants unable to consent</p>
<p>3.7. Payment to volunteers: (indicate any sums to be paid to volunteers) None</p>
<p>3.8. Study information: Have you provided a study information sheet for the participants? YES (Please attach a copy) NO</p>
<p>3.9. Consent: (A written consent form for the study participants MUST be provided in all cases, unless the research is a questionnaire.) Have you produced a written consent form for the participants to sign for your records? YES (Please attach a copy) NO</p>
<p>4. Risks and Hazards</p>
<p>4.1. Are there any risks to the researcher and/or participants? (Give details of the procedures and processes to be undertaken, e.g. if the researcher is a lone-worker.)</p> <ol style="list-style-type: none"> 1. Small risk of pain and bruising to the participant due to EMG needle insertion. 2. Very low risk of infection to the participant 3. Small risk from injury to researcher, related to use of sharps
<p>4.2. State precautions to minimise the risks and possible adverse events:</p> <ol style="list-style-type: none"> 1. All needles and sterile equipment such as gel and gloves will be purchased from university approved suppliers and standard clinical practice for their use will be followed (i.e. Skin sterilization before needle insertion). 2. All consumables will be discarded in an appropriate manner after each examination, or if any of the researchers believes that any item has become contaminated. 3. The needle will only be inserted once the ultrasound probe has been placed and will be removed as soon as the data collection on the muscle is complete to minimize the time spent in the muscle. 4. Researchers will be vaccinated against appropriate diseases and coordination between the researcher placing the probe and the researcher placing the needle has been practiced extensively.

Application Number _____
 Date Received _____

4.3. What discomfort (physical or psychological) danger or interference with normal activities might be suffered by the researcher and/or participant(s)? State precautions which will be taken to minimise them:

Intramuscular EMG will require the insertion of needles into the participant's muscles. This may cause a small amount of pain/ discomfort for the participant during the examination and in some cases bruising or muscle soreness may be experienced on subsequent days. To minimise this, needles will be inserted for the minimum amount of time necessary for a data collection and will be placed to avoid visible blood vessels. In addition to this, needles will be replaced a maximum of two times per muscle and once inserted, needles will remain still, to minimise discomfort.

5. Ethical Issues

5.1. Please describe any ethical issues raised and how you intend to address these:

1. A small risk of cell damage is possible when ultrasound is used. For this reason, only the required amount will be used in order to successfully yield results. There is an inbuilt safety feature present in the specific machines which we employ, that freezes all scanning after it has been active for over 10 minutes. We do not expect to be collecting more than 5 minutes of ultrasound footage from any single muscle.

6. Safeguards/Procedural Compliance

6.1. Confidentiality:

- 6.1.1. Indicate what steps will be taken to safeguard the confidentiality of participant records. If the data is to be computerised, it will be necessary to ensure compliance with the requirements of the Data Protection Act 1998.
- 6.1.2. If you are intending to make any kind of audio or visual recordings of the participants, please answer the following questions:
 - 6.1.2.1. How long will the recordings be retained and how will they be stored?
 - 6.1.2.2. How will they be destroyed at the end of the project?
 - 6.1.2.3. What further use, if any, do you intend to make of the recordings?

The nature of the image (a grayscale image of a small area of muscle and other surrounding tissues) means that it will not be possible to make any identification of the participant from their images. However, to safeguard the confidentiality of participants and their records and in compliance with the Data Protection Act 1998, all recordings will be saved under a given alphanumeric code, not relatable to the participant and kept on a password

Application Number _____
 Date Received _____

protected computer.

Recordings will be retained for a minimum of 7 years. The recordings will be temporarily stored on a password protected laptop, within Manchester Metropolitan University. Recordings will be stored on a RSA encrypted drive, which has a password distinct from that of the computer. Backup will be stored physically separate to the primary data, and will be stored on an encrypted drive and stored in a locked cabinet in a secure office.

At the end of the retention period, all files will be overwritten on at least 5 occasions with randomly generated binary streams. The probability of being able to recover the data at this point by any means is effectively zero. The data storage drive will also be securely disposed of.

Any videos/ data collected may potentially be used in manuscripts, supplementary material and conference papers. However, no participants will be identifiable from the images.

6.2. The Human Tissue Act

The Human Tissue Act came into force in November 2004, and requires appropriate consent for, and regulates the removal, storage and use of all human tissue.

6.2.1. Does your project involve taking tissue samples, e.g., blood, urine, hair etc., from human subjects?

YES

NO

6.2.2. Will this be discarded when the project is terminated? **N/A**

YES

NO

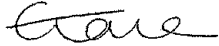

If NO – Explain how the samples will be placed into a tissue bank under the Human Tissue Act regulations:

6.3. Insurance

The University holds insurance policies in place to cover claims for negligence arising from the conduct of the University's normal business, which includes research carried out by staff and by undergraduate and postgraduate students as part of their course. This does not extend to clinical negligence.

In addition, the University has provision to award indemnity and/or compensation in the event of claims for non-negligent harm. This is on the condition that the project is accepted by the insurers prior to the commencement of the research project and approval has been granted for the project from a suitable ethics committee.

Application Number _____
 Date Received _____

<p>Research which is applicable to non-negligent harm cover involves humans and physical intervention which could give rise to a physical injury or illness which is outside the participant's day to day activities. This includes strenuous exercise, ingestion of substances, injection of substances, topical application of any substances, insertion of instruments, blood/tissue sampling of participants and scanning of participants.</p> <p>The following types of research are <u>not</u> covered automatically for non-negligent harm if they are classed as the activities above and they involve:</p> <ol style="list-style-type: none"> 1) Anything that assists with and /or alters the process of contraception, or investigating or participating in methods of contraception 2) Anything involving genetic engineering other than research in which the medical purpose is treating or diagnosing disease 3) Where the substance under investigation has been designed and /or manufactured by MMU 4) Pregnant women 5) Drug trials 6) Research involving children under sixteen years of age 7) Professional sports persons and or elite athletes. 8) Overseas research <p>Will the proposed project result in you undertaking any research that includes any of the 8 points above or would not be considered as normal University business? If so, please detail below: N/A</p>	
<p>6.4. Notification of Adverse Events (e.g., negative reaction, counsellor, etc): (Indicate precautions taken to avoid adverse reactions.)</p> <p>Please state the processes/procedures in place to respond to possible adverse reactions.</p> <p>Adverse reactions due to the procedure are unlikely. However, if any are experienced by the participants (e.g. infection around the site of needle insertion), the advice given will be to contact their GP as soon as possible.</p> <p>In the case of clinical research, you will need to abide by specific guidance. This may include notification to GP and ethics committee. Please seek guidance for up to date advice, e.g., see the NRES website at http://www.nres.npsa.nhs.uk/</p>	
SIGNATURE OF PRINCIPAL INVESTIGATOR: 	Date: 07/01/2015
SIGNATURE OF FACULTY'S HEAD OF ETHICS: 	Date: 18th February 2015

Application Number _____

Date Received _____

--	--

Checklist of attachments needed:

1. Participant consent form
2. Participant information sheet
3. Full protocol
4. Advertising details
5. Insurance notification forms
6. NHS Approval Letter (where appropriate)
7. Other evidence of ethical approval (e.g., another University Ethics Committee approval)

9.8 Appendix 8: MMU Participant Consent Form

Study Name:

Combination of Electromyography and B Mode Ultrasound for the Detection of Involuntary Muscle Twitches in Healthy Participants.

Name of Researchers: Kate Bibbings

Ethical Approval Number:

Patient Identification Number for this trial:

CONSENT FORM

Please initial box

1. I confirm that I have read and understand the information sheet dated for the above study. I have had the opportunity to consider the information, ask questions and have had these answered satisfactorily.
2. I understand that my participation is voluntary and that I am free to withdraw at any time without giving any reason, without legal rights being affected.
3. I understand that data collected during the study may be looked at by individuals from Manchester Metropolitan University from regulatory authorities or from the NHS. I give permission for these individuals to have access to these data.
4. I agree to take part in the above study.

Name of Participant Date Signature

Name of Person taking consent Date Signature

9.9 Appendix 9: MMU Participant Information Sheet

PATIENT INFORMATION SHEET

Title of Project: Detecting muscle twitches with ultrasound imaging

You are being invited to participate in a research study carried out at Manchester Metropolitan University. Please read the following information carefully before you decide whether to take part in the study or not.

WHAT IS THE PURPOSE OF THIS STUDY?

We are working on developing new methods of diagnosing degenerative diseases which affect skeletal muscles, an example of which is motor neurone disease. Methods have been previously developed at MMU that have provided a method that detect certain types of muscle twitches in ultrasound images. Currently, doctors usually diagnose conditions like motor neurone disease by using a technique called 'needle EMG'. The technique involves placing a needle in different muscles and recording the electrical activity which occurs when the muscle is activated. Different types of activation, or muscle twitches, occur between healthy and affected people. We wish to provide healthy control data including both ultrasound and EMG, in order to initially test ultrasound based methods of twitch detection that have been developed and also provide a comparison to the patients muscle at a later date.

WHAT WILL HAPPEN IF I TAKE PART?

During the data collection we will record needle EMG and ultrasound images from four muscles:

- i) a muscle at the back of your lower leg [medial gastrocnemius]
- ii) a muscle in your thigh [rectus femoris]
- iii) a muscle in your upper arm [biceps]
- iv) a muscle on your shoulder [trapezius]

Recording the images involves placing an ultrasound probe, covered in a water based gel, over the top of the muscle of interest. The probe sends waves of ultrasound through the muscle which are reflected and used to create an image which can be viewed and recorded on a computer. The images of your muscles are in monochrome (black and white), and just show features within your muscle. Individual people cannot be identified from these images.

Recording EMG involves inserting a needle into the muscle, which will detect the electrical activity in the muscle which occurs when it contracts or twitches.

While we are collecting the EMG and the images you can sit on a chair or lie on a couch, depending on the muscle being scanned. You will not need to do anything else. We want to take recordings of the naturally occurring, involuntary twitches which occur in healthy muscles. We will take three recordings from each muscle, each lasting 30 – 40 seconds.

You will only need to participate once and in total it will take no more than 2 hours to collect all the ultrasound images and EMG required.

WHAT ARE THE POSSIBLE BENEFITS OF TAKING PART?

There will be no direct benefits to you for taking part in the study. We hope however that the work will contribute to the development of a new, non-invasive method of diagnosing some degenerative muscle diseases.

WHAT ARE THE POSSIBLE RISKS OF TAKING PART?

There are no risks associated with the ultrasound imaging. It is a minimally invasive technique which is commonly used to assess muscle tissue and unborn babies in pregnant women.

There are small risks associated with the needle EMG. It can cause a degree of pain and can lead to a small amount of bruising. There is also a very low risk of infection occurring at the site the needle was inserted.

WILL MY TAKING PART BE KEPT CONFIDENTIAL?

Yes. We will not need to record any of your personal information for this work. Details of your age, height, weight will be noted but not linked to any information from which you could be identified. All the ultrasound videos and EMG recorded will be saved on a computer with a unique alphanumeric participant identifier, which will not be linked to any of your confidential records.

WHAT IF I CHANGE MY MIND ABOUT TAKING PART?

You are not obligated in any way to take part in this study it is entirely your choice. Once you have signed the consent form you are still free to withdraw at any time and without giving a reason and we will delete any data we had collected from you.

WHO DO I CONTACT IF I FEEL MY RIGHTS HAVE BEEN VIOLATED?

If you feel that your rights as a participant in this study have been violated, you may write to:


The University Secretary and Clerk to the Board of Governors,
Manchester Metropolitan University,
Ormond Building,
Manchester,
M15 6BX
Tel: 0161 247 3400

Contact details for further information

Kate Bibbings
School of Healthcare Science
Manchester Metropolitan University
Oxford Road
Manchester, M1 5GD

Email: kate.bibbings@stu.mmu.ac.uk

9.10 Appendix 10: Poster from the MND Association International Symposium



Computational approaches to fasciculation detection in ultrasound images

Kate Bibbings¹, Peter J. Harding¹, Ian D. Loran¹, Nicholas Combes², and Emma F. Hodson-Tole¹
¹ Cognitive Motor Function Research Group, School of Healthcare Sciences, Manchester Metropolitan University, UK
² Dpt. Neurophysiology, Royal Preston Hospital, Preston, Lancashire, UK

Research Question

How well do different computer vision techniques detect fasciculations in ultrasound images when compared to:

1. Manual identifications compiled by human operators
2. Intramuscular electromyography

Introduction

Electromyography (EMG) is the standard diagnostic technique for the detection of fasciculations (twitches) that present in neuromuscular disorders such as MND. This technique requires the insertion of needle electrodes into a number of the patients' muscles in order to collect electrophysiological data that may indicate the presence and nature of any existing pathology. Due to the unpleasantness of needle insertion, clinicians tend to avoid repeated or prolonged testing, making research into areas such as disease progression difficult.

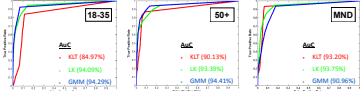
Ultrasound (US) imaging may provide a more sensitive and painless alternative to EMG for detection of fasciculations. However, most research has focused on image analysis using human operators, meaning results will have a certain level of subjectivity to them¹.

Computational techniques have previously been used alongside human operator identifications of fasciculations (ID's), but have not previously been used to objectively identify involuntary tissue displacements in comparison to electrophysiological activity^{2,3}.

Results

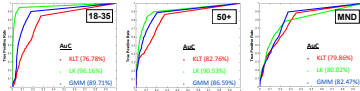
ROC curves for Manual ID Comparisons

Overlays of ROC curves calculated for comparisons between the computational techniques (KLT, LK and GMM) and manual ID's in the medial gastrocnemius. Each plot shows results for participant groups 18-35, 50+ and MND respectively.



ROC curves for IEMG Comparisons

Overlays of ROC curves calculated for comparisons between the computational techniques (KLT, LK and GMM) and intramuscular EMG in the medial gastrocnemius. Each plot shows results for participant groups 18-35, 50+ and MND respectively.



Methods

US images of medial gastrocnemius (MG) and biceps brachii (BB) were collected from:

- Group 1 Healthy 18-35
- Group 2 Healthy 50+
- Group 3 MND Patients

EMG was simultaneously collected from five participants in each group.

Computer vision techniques used for fasciculation detection:

1. Kanade Lucas Tomasi (KLT) tracker with mutual information
2. Lucas Kanade (LK) optical flow
3. Foreground detection using a mixture of Gaussians (GMM)

Agreement between the computational methods and the manual ID's EMG was calculated using Receiver Operator Characteristics (ROC's), which compare the true negatives and true positives of the signal and the ID's EMG at different threshold values. The area under the curve (AUC) was the method used to calculate the accuracy of each method in comparison to the two truth signals.

Conclusions

- The automated technique when compared to ID's, showed very high levels of agreement throughout all test groups and the EMG comparison yielded good agreement, through most test groups.
- Differences in agreement levels between truth signals may be due to complexity of EMG signals, making it harder to extract fasciculation potentials. In addition, the EMG detection volume is also much smaller (approx. 0.07 mm³) than the area assessed by US, with images being collected in 50mm x 50mm slices.
- The KLT algorithm was regularly outperformed by the GMM and the LK optical flow algorithms.
- In relation to the EMG comparisons, the LK algorithm reports higher agreement in healthy muscles, where the muscles are generally quiet. In muscles with voluntary activations and other phenomenon such as complex repetitive discharges the GMM algorithm is superior.
- An analysis technique using a combination of the LK and GMM methods may improve results.

Figure 1: Examples of Fasciculations in an Electromyogram (L) and Motor Units (R)³.

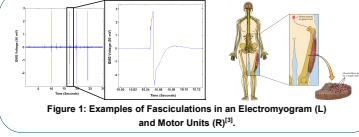
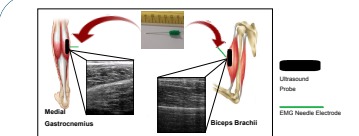


Figure 2: Examples of Data Collection Set – up for Medial Gastrocnemius and Biceps Brachii.




Acknowledgments
 Staff and patients at Preston Royal Hospital, Lancashire Teaching Hospitals.
 All participants taken from the School of Healthcare Sciences, M&M.
 The Motor Neurone Disease Association, who have provided funding for this project. With special thanks to the members of The MND Association Cheshire and Manchester branches.

References

1. Harding, P., Loran, I., Combes, N., Hodson-Tole, E., "Ultrasound Based Detection of Fasciculations in Healthy and Diseased Muscles," in *Biomedical Engineering, IEEE Transactions on*, vol. PP, no. 99, pp. 1-1, doi: 10.1109/1686.2015.2405168.
2. Fiers, S. Skeletal muscle ultrasound. *European Journal of Physiological*, 2014, 2010, ISBN 2037-2403.
3. Purvis, D. *Neuroscience*. Singular Associates, 2012. ISBN 07507933553.

Contact Details: Email: kate.bibbings@mmu.ac.uk



SCAN THIS CODE
 For our YouTube channel and a more in depth look at the techniques used in this poster